SAIMM
THE SOUTHERN AFRICAN INSTITUTE OF MINING AND METALLURGY
VOLUME 125 NO. 11 NOVEMBER 2025

Conducting world-class research and engineering training for South Africa's unique mining challenges

Working to meet FUTURE CHALLENGES

South Africa is home to one of the world's leading mining industries. However, this sector faces widespread sustainability challenges. To revitalise the industry, South Africa must invest in technological advancements to enable safer and more productive mining. Given the unique geological and socio-political position of our mining industry, local solutions must be found to the challenges we face.

OUR VISION

The Department of Mining Engineering at the University of Pretoria positions its teaching and research endeavours to address the country's unique mining challenges. In particular, our researchers form part of a small cohort of scientists seeking to understand the behaviour of the rock mass around the country's deep tabular excavations, and to find solutions to this problem. The Department's vision comprises several key elements:

FOCUSING ON DEVELOPING INNOVATIVE RESEARCH SOLUTIONS IN ROCK ENGINEERING

Our research focuses particularly on aspects such as pillar design for tabular layouts, numerical methods to simulate the geometries, and methods to mechanise the mines and improve their productivity. New problems that will be tackled are multi-reef mining in the Bushveld Complex and the design of barrier pillars in these mines. No in-depth studies have been performed on these aspects in the past.

GROWING EXPERTISE IN MINE PLANNING, OPEN-CAST MINING AND THE OPTIMISATION OF MINING PROCESSES

We are committed to the development of younger staff members in their pursuit of doctoral studies. We are also committed to expanding knowledge capacity through the appointment of industry staff as extraordinary lecturers and extraordinary professors.

PRODUCING THE NEXT GENERATION OF TECH-SAVVY MINING ENGINEERS

The Department engages in the ongoing development of its curriculum and interaction with the industry to determine national needs in terms of graduate skills.

INTERACTING WITH VARIOUS STAKEHOLDERS TO ENSURE AN IMPROVED ENROLMENT OF GOOD STUDENTS

The Department, in collaboration with industry stakeholders, strives to make studies in the mining industry a more attractive option for students. This includes advocating for mining education and the marketing of its importance in schools and universities.

RANKED TOP 41

FOR MINERALS AND MINING ENGINEERING WORLDWIDE IN THE LATEST QS UNIVERSITY RANKINGS BY SUBJECT

www.up.ac.za/mining-engineering

UNIVERSITEIT VAN PRETORIA
UNIVERSITY OF PRETORIA
YUNIBESITHI YA PRETORIA

Faculty of Engineering, Built Environment and Information Technology

Fakulteit Ingenieurswese, Bou-omgewing en Inligtingtegnologie / Lefapha la Boetšenere, Tikologo ya Kago le Theknolotši ya Tshedimošo

Make today matter

www.up.ac.za

OFFICE BEARERS AND COUNCIL FOR THE 2025/2026 SESSION

President
G.R. Lane

President Elect
T.M. Mmola

Senior Vice President
M.H. Solomon

Junior Vice President
S.J. Ntsoelengoe

Incoming Junior Vice President
M.C. Munroe

Immediate Past President
E. Matinde

Honorary Treasurer
W.C. Joughin

Ordinary Members on Council

W. Broodryk	M.A. Mello
A.D. Coetzee	K. Mosebi
Z. Fakhraei	M.J. Mothomogolo
B. Genc	S.M. Naik
F. Lake	G. Njowa
K.M. Letsoalo	S.M. Rupprecht
S.B. Madolo	A.T. van Zyl

Co-opted Council Members
K.W. Banda
M.L. Wertz

Past Presidents Serving on Council

N.A. Barcza	W.C. Joughin
R.D. Beck	C. Musingwini
Z. Botha	J.L. Porter
V.G. Duke	M.H. Rogers
I.J. Geldenhuys	G.L. Smith
R.T. Jones	

M.L. Wertz – TP Mining Chairperson
W. Broodryk – TP Metallurgy Chairperson

C.T. Chijara – YPC Chairperson
T.S. Ndlela – YPC Vice Chairperson

Branch Chairpersons

Botswana	K. Mosebi
DRC	Vacant
Johannesburg	A. Hefer
Limpopo	M.S. Zulu
Namibia	T. Aipanda
Northern Cape	Vacant
North West	T. Nsimbi
Pretoria	P.G.H. Pistorius
Western Cape	M.H. Solomon
Zambia	N.M. Kazembe
Zimbabwe	L. Shamu
Zululand	Vacant

PAST PRESIDENTS

*Deceased

* W. Bettel (1894–1895)
* A.F. Crosse (1895–1896)
* W.R. Feldtmann (1896–1897)
* C. Butters (1897–1898)
* J. Loevy (1898–1899)
* J.R. Williams (1899–1903)
* S.H. Pearce (1903–1904)
* W.A. Caldecott (1904–1905)
* W. Cullen (1905–1906)
* E.H. Johnson (1906–1907)
* J. Yates (1907–1908)
* R.G. Bevington (1908–1909)
* A. McA. Johnston (1909–1910)
* J. Moir (1910–1911)
* C.B. Saner (1911–1912)
* W.R. Dowling (1912–1913)
* A. Richardson (1913–1914)
* G.H. Stanley (1914–1915)
* J.E. Thomas (1915–1916)
* J.A. Wilkinson (1916–1917)
* G. Hildick-Smith (1917–1918)
* H.S. Meyer (1918–1919)
* J. Gray (1919–1920)
* J. Chilton (1920–1921)
* F. Wartenweiler (1921–1922)
* G.A. Watermeyer (1922–1923)
* F.W. Watson (1923–1924)
* C.J. Gray (1924–1925)
* H.A. White (1925–1926)
* H.R. Adam (1926–1927)
* Sir Robert Kotze (1927–1928)
* J.A. Woodburn (1928–1929)
* H. Pirow (1929–1930)
* J. Henderson (1930–1931)
* A. King (1931–1932)
* V. Nimmo-Dewar (1932–1933)
* P.N. Lategan (1933–1934)
* E.C. Ranson (1934–1935)
* R.A. Flugge-De-Smidt (1935–1936)
* T.K. Prentice (1936–1937)
* R.S.G. Stokes (1937–1938)
* P.E. Hall (1938–1939)
* E.H.A. Joseph (1939–1940)
* J.H. Dobson (1940–1941)
* Theo Meyer (1941–1942)
* John V. Muller (1942–1943)
* C. Biccard Jeppe (1943–1944)
* P.J. Louis Bok (1944–1945)
* J.T. McIntyre (1945–1946)
* M. Falcon (1946–1947)
* A. Clemens (1947–1948)
* F.G. Hill (1948–1949)
* O.A.E. Jackson (1949–1950)
* W.E. Gooday (1950–1951)
* C.J. Irving (1951–1952)
* D.D. Stitt (1952–1953)
* M.C.G. Meyer (1953–1954)
* L.A. Bushell (1954–1955)
* H. Britten (1955–1956)
* Wm. Bleloch (1956–1957)
* H. Simon (1957–1958)
* M. Barcza (1958–1959)
* R.J. Adamson (1959–1960)
* W.S. Findlay (1960–1961)
* D.G. Maxwell (1961–1962)
* J. de V. Lambrechts (1962–1963)
* J.F. Reid (1963–1964)
* D.M. Jamieson (1964–1965)
* H.E. Cross (1965–1966)
* D. Gordon Jones (1966–1967)
* P. Lambooy (1967–1968)
* R.C.J. Goode (1968–1969)
* J.K.E. Douglas (1969–1970)
* V.C. Robinson (1970–1971)
* D.D. Howat (1971–1972)
* J.P. Hugo (1972–1973)
* P.W.J. van Rensburg (1973–1974)
* R.P. Plewman (1974–1975)
* R.E. Robinson (1975–1976)
* M.D.G. Salamon (1976–1977)
* P.A. Von Wielligh (1977–1978)
* M.G. Atmore (1978–1979)
* D.A. Viljoen (1979–1980)
* P.R. Jochens (1980–1981)
* G.Y. Nisbet (1981–1982)
A.N. Brown (1982–1983)
* R.P. King (1983–1984)
J.D. Austin (1984–1985)
* H.E. James (1985–1986)
H. Wagner (1986–1987)
* B.C. Alberts (1987–1988)
* C.E. Fivaz (1988–1989)
* O.K.H. Steffen (1989–1990)
* H.G. Mosenthal (1990–1991)
R.D. Beck (1991–1992)
* J.P. Hoffman (1992–1993)
* H. Scott-Russell (1993–1994)
J.A. Cruise (1994–1995)
D.A.J. Ross-Watt (1995–1996)
N.A. Barcza (1996–1997)
* R.P. Mohring (1997–1998)
J.R. Dixon (1998–1999)
M.H. Rogers (1999–2000)
L.A. Cramer (2000–2001)
* A.A.B. Douglas (2001–2002)
* S.J. Ramokgopa (2002-2003)
T.R. Stacey (2003–2004)
F.M.G. Egerton (2004–2005)
W.H. van Niekerk (2005–2006)
R.P.H. Willis (2006–2007)
R.G.B. Pickering (2007–2008)
A.M. Garbers-Craig (2008–2009)
J.C. Ngoma (2009–2010)
G.V.R. Landman (2010–2011)
J.N. van der Merwe (2011–2012)
G.L. Smith (2012–2013)
M. Dworzanowski (2013–2014)
J.L. Porter (2014–2015)
R.T. Jones (2015–2016)
C. Musingwini (2016–2017)
S. Ndlovu (2017–2018)
A.S. Macfarlane (2018–2019)
M.I. Mthenjane (2019–2020)
V.G. Duke (2020–2021)
I.J. Geldenhuys (2021–2022)
Z. Botha (2022-2023)
W.C. Joughin (2023-2024)
E. Matinde (2024-2025)

Typeset and Published by
The Southern African Institute of Mining and Metallurgy
PostNet Suite #212
Private Bag X31
Saxonwold, 2132
E-mail: journal@saimm.co.za

Printed by
Camera Press, Johannesburg

SAIMM
THE SOUTHERN AFRICAN INSTITUTE OF MINING AND METALLURGY
VOLUME 125 NO. 11 NOVEMBER 2025

Contents

Honorary Legal Advisers
M H Attorneys

Auditors
Genesis Chartered Accountants

Secretaries
The Southern African Institute of Mining and Metallurgy
7th Floor, Rosebank Towers, 19 Biermann Avenue,
Rosebank, 2196
PostNet Suite #212, Private Bag X31, Saxonwold, 2132
E-mail: journal@saimm.co.za

ISSN 2225-6253 (print) · ISSN 2411-9717 (online)

AFRIROCK 2025 CONFERENCE PAPERS

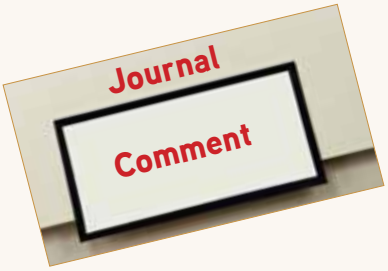

Pioneering progress: The future of rock engineering

It was our great pleasure to welcome delegates to AfriRock 2025, themed "*Pioneering progress: The future of rock engineering*," held at the Sun City Hotel and Casino in Rustenburg from 19 to 23 July 2025. The conference was an absolutely resounding success. This prestigious international event brought together rock engineering professionals, researchers, and industry leaders from across the globe to share knowledge, exchange ideas, and showcase innovations that are shaping the future of mining both on the African continent and worldwide.

Two pre-conference workshops were held ahead of the formal proceedings—one focused on pillar design and the other on stress measurements—setting the tone for an engaging and technically rich event. We were honoured to host distinguished keynote speakers, each contributing unique expertise and insight. In addition to the keynote addresses, the symposium featured a robust programme of technical papers presented by industry professionals, consultants, and researchers. Technical slope stability papers published in the special edition of the *SAIMM Journal (August 2025)* were also presented at the conference, reinforcing the academic and practical depth of AfriRock 2025. Following the formal proceedings, technical visits to gold, platinum, diamond, and copper mines were organised, offering delegates the opportunity to experience innovative rock engineering practices in action. Complementing the technical programme, social events held at the end of each day provided valuable opportunities for attendees to network in an informal and engaging setting.

Conferences like AfriRock 2025 play a vital role in advancing our industry by fostering collaboration, professional growth, and the dissemination of cutting-edge technologies and best practices. The discussions and presentations throughout the event highlighted the importance of continuous learning, sustainable design, and the application of modern geotechnical methods to meet the evolving challenges faced by the mining environment.

We extend our sincere gratitude to everyone who contributed to making this conference a success—our keynote speakers, paper authors, reviewers, exhibitors, and sponsors. Their dedication, time, and expertise formed the foundation of this achievement. A special note of appreciation goes to the Technical Paper Review Committee and the Organising Committee, comprising members of the South African National Institute of Rock Engineering (SANIRE) and the Southern African Institute of Mining and Metallurgy (SAIMM), for their commitment and hard work in delivering an exceptional international conference.

K. Le Bron

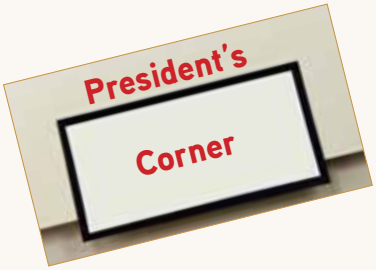

Navigating the Identification of Engineering Work— a call for professional registration

For a while now, I have been aware of the Identification of Engineering Work (IDoEW) being developed by the Engineering Council of South Africa (ECSA). It was only after attending an ECSA presentation recently, engaging in discussions, and conducting further research that I came to appreciate the far-reaching impact this initiative will have on the engineering profession and particularly on the mining industry.

When I graduated as a civil engineer, I understood the importance of registering as a Professional Engineer (Pr. Eng.) with ECSA to be able to take accountability for the design, construction, supervision, and certification of civil engineering projects where failure could result in loss of life or significant damage. This model of professional oversight mirrors other regulated disciplines such as law, medicine, accounting, and architecture, ensuring competence, accountability, and ethical conduct.

The IDoEW framework now formalises these same principles across all branches of engineering.

The IDoEW framework

After many years of consultation, ECSA finalised the IDoEW framework in March 2021 and published the rules in the Government Gazette on 26 March 2021 under Section 26 of the Engineering Profession Act 46 of 2000.

The framework defines which categories of engineering work must be performed or supervised by registered professionals, whether professional engineers (Pr. Eng.), professional engineering technologists (Pr. Tech Eng.), professional engineering technicians (Pr. Techni Eng.), or professional certificated engineers (Pr. Cert Eng.). This applies across all disciplines, including mining, mechanical, civil, electrical, metallurgical, chemical, control and instrumentation, and industrial engineering.

While full implementation was initially planned for March 2024, the compliance deadline was extended to April 2025 to allow industries sufficient time to align their structures, policies, and personnel.

Implications for the mining industry

Compliance is now a legal requirement for anyone performing identified engineering work under the Engineering Profession Act 46 of 2000. Historically, ECSA registration levels in the mining sector have been low, meaning a concerted effort will be required to achieve full alignment.

Typical mining activities falling within "identified engineering work" include:

- Mine design and planning — shafts, slopes, stopes, and ventilation systems.
- Life-of-mine (LoM) planning and production optimisation.
- Mineral project evaluation and valuation.
- Rock engineering and geotechnical design.
- Infrastructure, equipment design, maintenance, and process-plant engineering.

Mining companies must ensure that such work is executed or signed off by registered professionals, and that unregistered staff perform their duties under appropriate supervision. This may require upskilling programmes, policy revisions, and the integration of registration status into recruitment, role descriptions, and career development frameworks.

Non-compliance constitutes a statutory offence. In terms of Section 41 of the Act, offenders may face fines of up to double the professional fee earned, penalties equivalent to three years' imprisonment, or disciplinary action. The message is clear — engineers must be registered and must maintain their registration.

President's Corner (continued)

Alignment with the Mine Health and Safety Act (MHSA)

It is important to note that compliance with the IDoEW does not replace or override the statutory obligations of the Mine Health and Safety Act (MHSA). The two frameworks operate in parallel, each addressing a different but complementary aspect of professional accountability.

Under the MHSA, certain key roles, such as mine manager, section engineer, and rock engineer, require a Certificate of Competency or "ticket" issued by the Department of Mineral Resources and Energy (DMRE). These legal appointments ensure operational safety and compliance with mining legislation.

The IDoEW, on the other hand, governs the professional accountability for engineering design, analysis, and technical decision-making, requiring registration with ECSA. In many cases, both credentials may be necessary, for example, a section engineer responsible for the design, operation, and maintenance of mining systems may need both a DMRE certificate (to satisfy MHSA legal appointment requirements) and ECSA registration (to perform and sign off identified engineering work under the Engineering Profession Act).

In practice, mining companies should assess each role to determine whether a legal appointment, professional registration, or both are required, ensuring that accountability and competence are fully covered across operational and engineering domains.

How SAIMM supports compliance

As a recognised voluntary sssociation (VA) under ECSA, the SAIMM is well positioned to assist the mining industry in managing this transition. Our support includes:

1. Information and awareness – publishing updates, articles, and hosting seminars to clarify IDoEW requirements.
2. Mentorship and facilitation for registration – connecting candidate engineers with experienced mentors through our networks and the Young Professionals Council (YPC) and assisting members with the registration process.
3. Liaison and advocacy – engaging directly with ECSA on behalf of our members to address mining-specific issues and ensure practical implementation.
4. Continuing professional development (CPD) – offering accredited events, conferences, and courses. Registered professionals must accumulate 25 CPD credits every five years; SAIMM membership earns one credit per year, and participation in committees or volunteer activities also qualifies.

Corporate partnership with SAIMM extends these benefits to company professionals, providing access to technical programmes, mentoring support for registration, and structured CPD pathways.

A call to action

Every engineer, technologist, and technician involved in identified work must ensure that they are registered or actively working toward registration. Maintaining professional standing through ongoing CPD will be equally important.

The introduction of the IDoEW marks a major step forward in strengthening South Africa's engineering standards and safeguarding the public interest. The SAIMM remains committed to supporting our members and the broader mining industry through this critical evolution in professional practice.

G.R. Lane
President, SAIMM

Rockbolts in shear

by G. Knox[1], J. Hadjigeorgiou[1]

Affiliation:
[1]University of Toronto, Toronto, Canada

Correspondence to:
G. Knox

Email:
greig.knox@mail.utoronto.ca

Dates:
Received: 26 Jun. 2025
Published: November 2025

How to cite:
Knox, G., Hadjigeorgiou, J. 2025. Rockbolts in shear. *Journal of the Southern African Institute of Mining and Metallurgy*, vol. 125, no. 11, pp. 621–628

DOI ID:
https://doi.org/10.17159/2411-9717/822/2025

This paper is based on a presentation given at the AfriRock Conference 2025, 21-23 July 2025, Sun City Resort, Rustenburg, South Africa

Abstract

There is a considerable wealth of information on the behaviour of rockbolts under axial loading conditions both in situ and under controlled laboratory conditions. However, there is comparably less data on the behaviour of rockbolts in shear. Several authors have contributed to the understanding of the behaviour of conventional rockbolts' performance under shear loading. Much of this data have been gathered through experimental programmes conducted on sections of the rockbolt. Considering the continuous coupling between the rockbolt and borehole interface, the approach is justified. Due to the design premise of energy-absorbing rockbolts with discrete couplings, full scale testing is required to quantify the behaviour of the rockbolts.

This paper reviews published results obtained from two testing facilities, which are the SINTEF rockbolt pull test rig in Trondheim, Norway and the Epiroc Combinations Shear and Tensile test rig in Johannesburg, South Africa, both capable of conducting full scale testing of rockbolts. Based on this high-quality database it was possible to identify three distinct responses of rockbolts in shear. The behaviour under load is controlled by the presence or absence of an encapsulation medium (resin/cement grout), the reinforcement mechanism, and whether the rockbolt is continuously or discretely captured. As a reference the results are compared to the performance in shear of conventional grouted rockbolts.

Keywords

rockbolts, shear loading, conventional fully encapsulated, energy-absorbing, full scale laboratory testing

Introduction

Ground support is routinely used to maintain the integrity of underground excavations in rock for both mining and civil engineering applications. These include providing access to an ore deposit (mining), developing transportation routes, or storage caverns (civil). The design of an effective ground control system considers both the local ground conditions and anticipated loading conditions. In addition, it is important to ensure the compatibility between different ground support elements and aerial coverage. Recognising that there are multiple ground support options, it is convenient to design for "normal" and "challenging or extreme" ground conditions (Hadjigeorgiou, 2023).

From a design perspective it is important to quantify the capacity and demand of ground support elements both as units and as a system. The focus of this paper is on improving our understanding of the load, deformation, and energy capacity of rockbolts subjected to shear loading. In this context the location, direction, and rate of loading are considered as controlled variables.

Early work in trying to understand the behaviour of reinforcement was based on small scale experimental programmes conducted on sections of a reinforcement element (Bjurstrom, 1974; Haas, 1976; Dight, 1982; Ludvig, 1984; Spang, Egger, 1990; Ferrero, 1995; Grasselli, 2005; Jalalifar, Aziz, 2010; Li et al., 2016). Arguably, this approach can be justified for most conventional rockbolts due to the continuous coupling between the rockbolt, chemical anchor, and borehole. In the case of energy-absorbing rockbolts, used in extreme ground conditions, this is clearly inappropriate and any results from small scale partial tests can be misleading. Under these conditions a full-scale test is more appropriate due to the discrete coupling and relationship between the length of the rockbolt and its performance capacity.

Currently, there are two testing facilities, which have the capacity to conduct full scale testing of a rockbolt, that being the SINTEF rockbolt pull tester in Trondheim, Norway (Stjern, 1995) and the Epiroc Combination Shear and Tensile Tester in Johannesburg, South Africa (Knox, Hadjigeorgiou,

2022). Several contributions have been made to demonstrate the effect of both conventional and energy-absorbing rockbolts to shear loading (Stjern, 1995; Chen, Li, 2015a; Hagan et al., 2019; Knox, Hadjigeorgiou, 2022, 2023, 2024a, 2024b; Kouhia et al., 2024).

Li et al. (2014) compared the behaviour of several conventional rockbolts under shear loading. Most of the data, however, were from a single source, the experimental programme conducted by Stjern (1995). Consequently, the shear behaviour of most energy-absorbing rockbolts was not included due to the limited applications at the time of the experimental programme by Stjern (1995).

This paper presents a review of five rockbolt types, comparing the shear and tensile performance using the single shear method. Within the selected five rockbolt types two anchoring methods are represented. Three distinct rockbolt responses were identified within the sample set, providing insight into the behaviour of the rockbolts under shear loading conditions.

Rockbolts in shear

There are several examples where rockbolts are subjected to a combination of shear and tensile loading at multiple points along the length of the rockbolt both under static and dynamic loading, as illustrated in Figure 1. The observed mode of failure highlights the interaction between the rockbolt and the rock mass, resulting in bending of the rockbolt prior to rupture. This phenomenon is difficult to capture in laboratory tests without careful consideration of the boundary conditions (host medium in which the rockbolt is installed).

The interaction between the rock mass and anchoring medium can result in a complex loading mechanism, as per Figure 2. Due to the difference in the mechanical properties of the steel and grout, the shear displacement will result in localised crushing of the anchor medium and rock mass at the collar of the borehole at

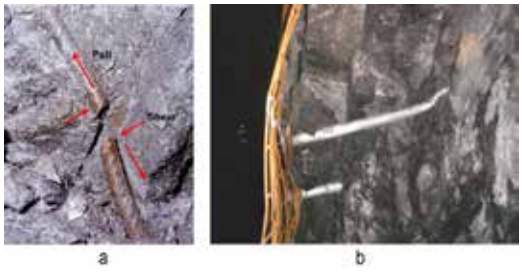

Figure 1—Examples of shear loading of rockbolts. a) conventional rebar rockbolt (Li, 2010), b) bulking of an excavation side wall leading to shearing of the rockbolts, a Ø46 mm friction rock stabiliser (Yao et al. 2014)

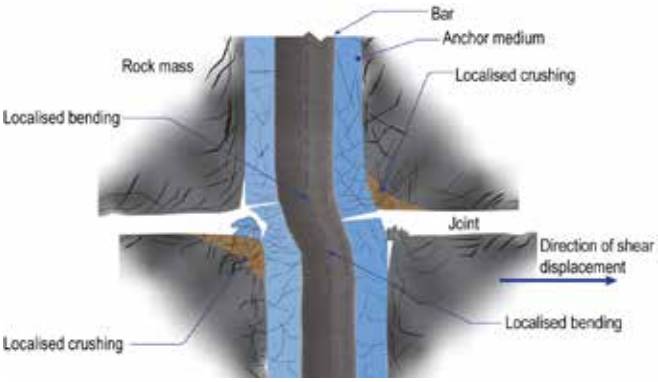

Figure 2— Illustration of the conceptual shear loading mechanism present when loading a rockbolt

the joint (shear interface). A consequence of the localised crushing is that the rockbolt bends, thus aligning the axial of the rockbolt towards the direction of the displacement and resultant loading. The bending of the rockbolt serves to isolate the section of the bar, which is loaded, resulting in the rupture of the bar at the shear interface. This phenomenon was demonstrated in the results presented by Chen and Li (2015b) where strain gauges applied to the rockbolt demonstrated a localised strain concentration of the bar.

The shear loading of rockbolts is often present in field applications. Consequently, it is necessary that laboratory tests replicate the composite loading mechanism for the results to be able to predict the in situ performance of rockbolts.

Laboratory shear loading of rockbolts

The objective of a laboratory testing campaign is to quantify the load and deformation capacity of a rockbolt. Careful consideration of the boundary conditions is required to represent the composite loading witnessed in situ. Axial laboratory load testing of rockbolts is typically conducted in either a steel host tube (chemically anchored rockbolts) or a borehole drilled into concrete core cast within a steel host tube (friction and/or mechanically anchored rockbolts); selection of the configuration is dependent on the anchor mechanism (Li, 2010; Li, 2012; Player, 2012; Bierman et al., 2019). A number of shear loading investigations have been conducted on rockbolts installed within steel host tubes (Ayres, Gardner, 2014; Dube,1995; Punkkinen, Royer, 2022). An alternative method is the method adopted by Stjern (1995), Chen and Li (2015a, 2015b), and Knox and Hadjigeorgiou (2022, 2023, 2024a, 2024b), whereby a rockbolt is installed within two concrete blocks located in a loading frame. The two testing methods were compared by Hagen et al. (2019), demonstrating that the displacement shear capacity of a rockbolt determined within a steel tube is lower than when determined by loading a rockbolt within a concrete block. The effect of the strength of the concrete block/host material was demonstrated by Spang and Egger (1990), with the results within concrete and granite being comparable. Additional displacement was recorded when the rockbolts were installed within sandstone, demonstrating the effect of the host material properties on the rockbolt performance.

There are currently two methods of conducting a shear test within concrete blocks to simulate the boundary conditions, the single shear (Haas, 1976; Spang, Egger, 1990; McHugh, Signer, 1999; Stjern, 1995) or the double shear method (Aziz et al., 2003; Grasselli, 2005). Both techniques are illustrated in Figure 4. It

Figure 3—Comparison between the rupture interface of two of the shear loading methods. a) Within a steel host tube, b) installed within a concrete block (images curtesy of Epiroc)

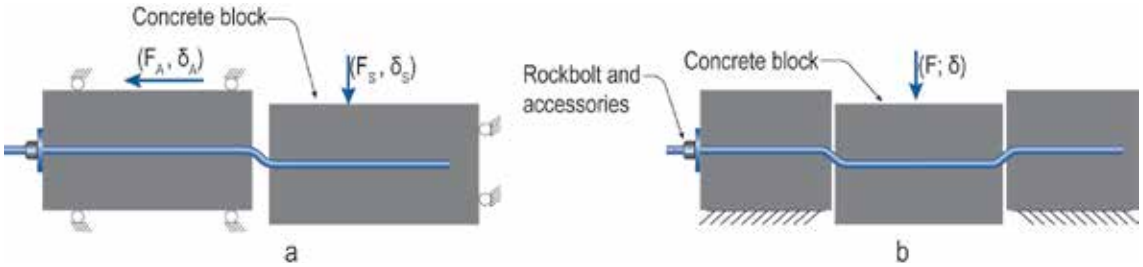

Figure 4—Laboratory-based rockbolt shear loading mechanisms: a) single shear loading, b) double shear loading

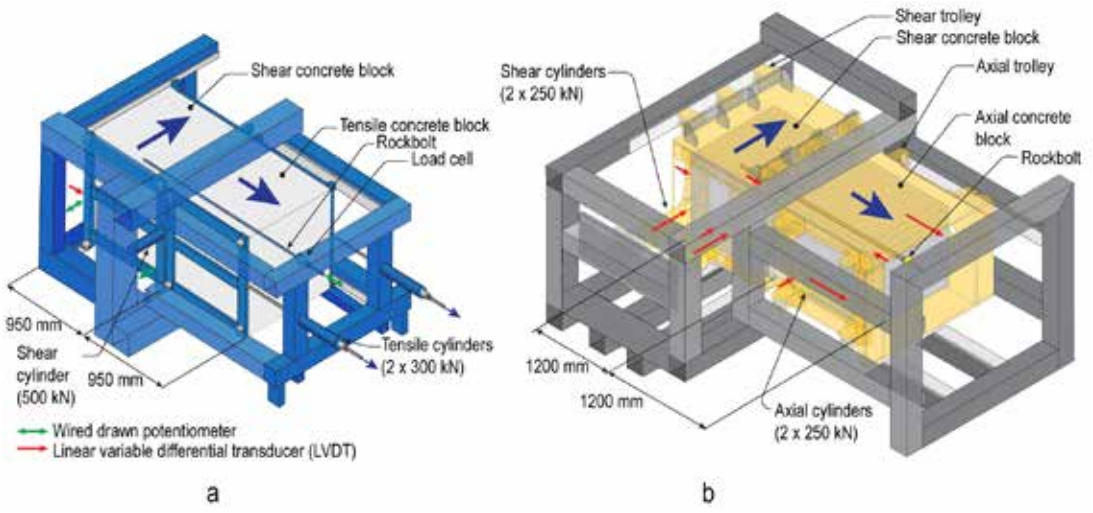

Figure 5—Laboratory testing equipment for conducting full scale shear and tensile testing. a) The SINTEF rig based in Trondheim, Norway (Stjern, 1995), b) the Epiroc Combination Shear and Tensile Tester, Johannesburg, South Africa

should be noted that when the double shear methodology is applied, the applied force is halved to determine the capacity of the loaded element.

To date the double shear method has been used to test sections of conventional rock reinforcement elements: cable bolts, fibre glass reinforced, and rebar rockbolts (Dube, 1995; Aziz et al., 2003; Grasselli, 2005; Li et al., 2016). Due to the continuous coupling between the rockbolt and the anchoring medium, this method can provide representative results for conventional rockbolts. Energy-absorbing rockbolts are discretely coupled along the length of the rockbolt, consequently, testing sections of the rockbolt does not represent the capacity of the rockbolt. Two test rigs have been developed, which can apply shear loads to full scale samples, the SINTEF rockbolt pull test rig and the Epiroc Combination Shear and Tensile (CST) test rig. The two rigs are similar in construction as the latter was developed using the same design premise with improvements to the hydraulic control system and increasing the scale to test 2.4 m long rock reinforcement elements.

The concrete blocks are prepared in moulds prior to installation in the test rig. The boreholes are then drilled into the concrete blocks, which are subsequently installed in the testing rig. A rockbolt is then installed into the borehole, with the interface between the two concrete blocks simulating a joint within the rock mass. When loaded in tension, the load is applied by the two tensile cylinders and the displacement rate is controlled. Prior to applying a shear load to an installed rockbolt, a tensile load is applied to result in a joint separation of 3 mm. This mitigates the potential for a frictional resistance between the two blocks.

Data sources

The review of the shear performance of the rockbolts was conducted on previously published results. Five different types of rockbolt were selected for comparison. Conventional rockbolts, energy-absorbing rockbolts, solid bar rockbolts, hollow bar rockbolts, and hybrid rockbolts are all represented within the dataset. All results considered were from full scale rockbolt tests conducted in approximately 100 MPa concrete blocks employing the single shear method using either the SINTEF rockbolt pull test rig or the Epiroc Combination Shear and Tensile test rig. The final criteria were that the presented result should include both a tensile and shear load and displacement curve, which were to be included in the dataset.

The dataset comprised of two conventional and three energy-absorbing rockbolts. The two conventional rockbolt bolts were the self-drilling rockbolt and the rebar rockbolt, illustrated in Figure 6. It should be noted that the results obtained for the SINTEF rig were for 1.8 m long rockbolts while the results obtained from the Epiroc rig were for rockbolt that were 2.4 m in length. The self-drilling rockbolt results included the R25 produced from a ductile material (Kouhia et al., 2024) tested by using the SINTEF rig, and an R28 self-drilling rockbolt (Knox, Hadjigeorgiou, 2023) tested by using the Epiroc rig. As for the rebar rockbolts (Chen, Li, 2015; Knox, 2022) both were Ø20 mm in diameter and sourced from the same grade of steel. This allowed for a direct comparison between the two testing rigs.

Figure 7 illustrates the paddled energy-absorbing rockbolts, a yielding mechanical hybrid rockbolt and an energy-absorbing self-drilling rockbolt. Two datasets for the paddled energy-absorbing

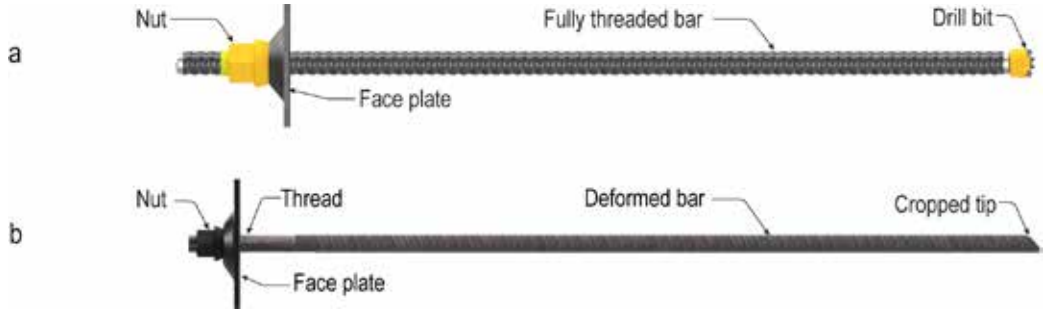

Figure 6—The two conventional rockbolts selected for the experimental programme. a) Self-drilling rockbolt, a hollow fully threaded bar, b) rebar rockbolt, a solid ribbed bar

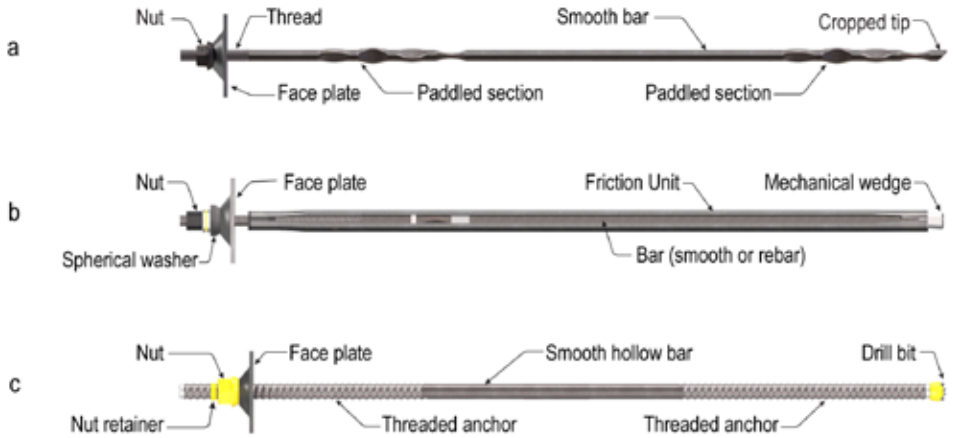

Figure 7— Three types of energy-absorbing rockbolt, which dissipate energy through the plastic deformation of the tendon. a) Paddled energy-absorbing rockbolt, b) yielding mechanical hybrid rockbolt, c) energy-absorbing self-drilling rockbolt

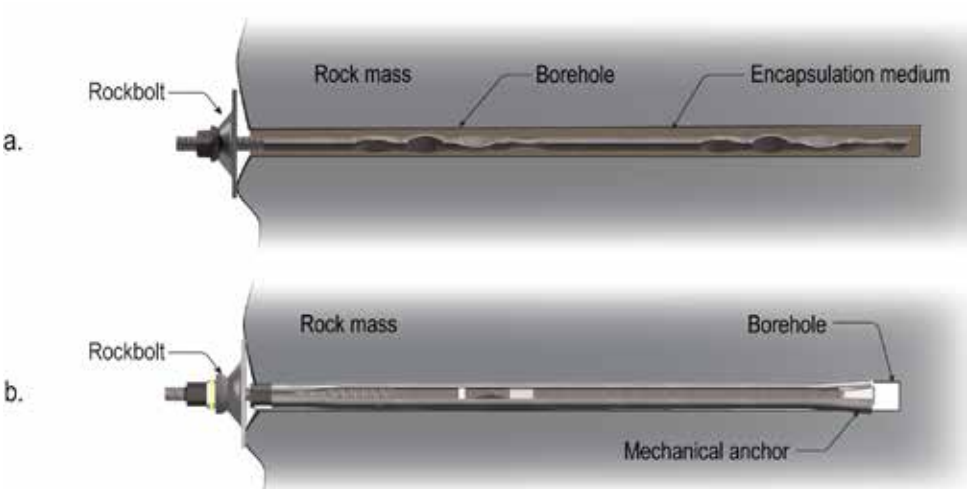

Figure 8— Rockbolt anchoring mechanisms for the experimental programme. a) fully encapsulated rockbolt, b) yielding mechanical hybrid rockbolt

rockbolt, Ø20 mm in diameter were used, however, the length of smooth bar between the paddled sections (anchor points) differed. The paddled energy-absorbing rockbolt used by Knox and Hadjigeorgiou (2024) was 2.4 m in length with a 1.4 m section between the paddled sections. The rockbolt tested by Chen and Li (2015) was 2.0 m in length with a 1.0 m smooth section between the paddled sections. The yielding mechanical hybrid rockbolt was 2.4 m in length with a Ø20 mm bar mechanically anchored within a Ø39 mm friction unit (Knox, Hadjigeorgiou, 2024). Finally, the energy-absorbing self-drilling rockbolt was an R28 variant, 2.4 m in length with a 1.2 m smooth section bounded by the two threaded anchors (Knox, Hadjigeorgiou, 2023).

The rockbolts used in the experimental programme can also be classified based on their anchoring mechanism. As illustrated in Figure 8, fully encapsulated rockbolts are installed with a chemical anchor, which fills the annulus between the rockbolt and the borehole serving as the load transfer interface. The rebar rockbolts and the paddled energy-absorbing rockbolts were installed into a

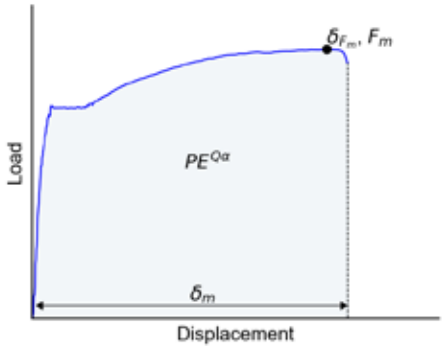

Figure 9—Representation of shear and tensile test result

pre-grouted borehole. The hollow bar rockbolts, and the self-drilling and energy-absorbing self-drilling rockbolts were both installed into the borehole and then post-grouted using a polyurea-silicate resin.

The intent of this analysis was to highlight the shear behaviour of the different rockbolt types. Consequently, all data were sourced from two testing rigs, similar in construction and employing similar shear testing procedures to reduce the risk of testing equipment bias. The similarities in the results for the rebar rockbolts demonstrated that there is limited or no equipment bias between the two testing rigs.

Representation of results

In all tests, the ultimate load (F_m) and the displacement at the ultimate load (δ_{F_m}) were recorded as originally proposed by Stjern (1995), Figure 9. This is reasonable given that beyond the ultimate load the capacity of the rockbolt diminishes to the point of rupture. Consequently, an applied load that exceeded the ultimate load capacity of the rockbolt will likely cause the rock mass strain rate to accelerate as the capacity of the rockbolt diminishes.

For the purposes of this comparative study two additional metrics were used, the displacement at rupture ($\delta\delta_{mm}$) and the total plastic energy at rupture (PE^{Q}). In this configuration the superscript 'Q' denotes that the energy capacity was determined at a quasi-static loading rate and 'α' represents the displacement loading angle. Each dataset was reprocessed to calculate the metrics for each result to facilitate a comparison between the responses of the rockbolts.

Data synthesis

The eight datasets of tensile and shear data for the five rockbolt types were collated from various sources (Chen, Li, 2015; Knox, 2022; Knox, Hadjigeorgiou, 2023; Knox, Hadjigeorgiou, 2024a; Knox, Hadjigeorgiou, 2024b; Kouhia et al., 2025). The average results when loading axially (0°) and in shear (90°) are summarised in Table 1. The response of each rockbolt can be observed in Figure 10. For all five of the rockbolt types a softer loading response is observed when loading the rockbolt in shear. This can be affected by the presence/absence and strength properties of encapsulation/anchoring medium. The installation parameters for each of the seven datasets are summarised in Table 2.

A careful review of the load deformation data for all rockbolt datasets has identified three distinct responses, as depicted in Figure 11. All four rockbolts encapsulated in a chemical anchoring medium dispalyed a reduction in load capacity (F_m) when loaded in shear. The load capacity of the yielding mechanical hybrid rockbolt, however, increased when the rockbolt was loaded in shear. The change in displacement (δ_{F_m}) when loaded in shear was different between conventional and energy absorbing rockbolts. This is illustrated in Figure 12, where results to the left of the dashed diagonal line indicate that the shear displacement capacity is greater than that of the tensile displacement capacity. While the absolute capacity of the energy-absorbing rockbolt is greater than that of the conventional rebar and self-drilling rockbolt, a significant reduction in the shear displacement capacity was recorded when compared to their axial displacement capacity.

The relative capacity of a rockbolt is a method of comparing the capacity of a rockbolt at a given loading angle to the capacity determined through axial testing. This highlights the relationship between the axial and shear response for the rockbolt. The relative capacities for the different rockbolts are summarised in Figure 13.

Table 1

Summary of quasi-static axial and shear loading results for the conventional rockbolts (Chen, Li, 2015; Knox, Hadjigeorgiou, 2023, 2024a, 2024b; Kouhia et al., 2024)

Rockbolt	Nr. samples	α	δ_{F_m}(mm)	F_m (kN)	δ_m (mm)	PE^{Q}(kJ)
Rebar rockbolt (Ø20 mm x 2.4 m)	3	0°	26	189	40	7
	3	90°	51	181	54	6
Rebar rockbolt (Ø20 mm x 1.8 m)	2	0°	21	210	40	7
	2	90°	43	197	48	6
R28 SDA	3	0°	26	273	32	7
	3	90°	44	218	45	6
R25 SDA	2	0°	28	231	35	7
	2	90°	40	215	43	6
Paddled energy-absorbing (Ø20 x 1.4 m)	3	0°	143	215	155	30
	3	90°	58	200	66	9
Paddled energy-absorbing (Ø20 x 1.0 m)	2	0°	117	208	144	26
	2	90°	59	208	71	9
Yielding mechanical hybrid rockbolt	3	0°	246	222	255	47
	5	90°	160	333	167	29
R28 energy-absorbing self- drilling rockbolt	3	0°	182	233	206	44
	3	90°	55	216	60	8

Rockbolts in shear

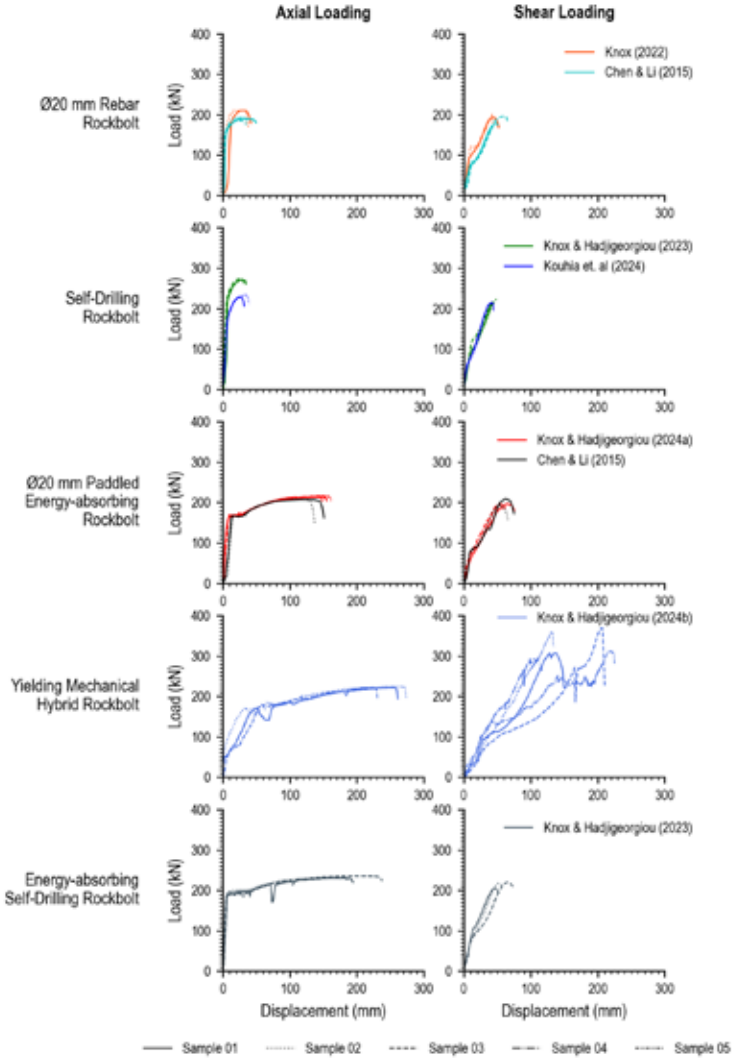

Figure 10—Summary of the load-displacement response for a number of rockbolt types under axial loading (left) and shear loading (right) (Chen, Li, 2015; Knox, Hadjigeorgiou, 2023; Knox, Hadjigeorgiou, 2024a; Knox, Hadjigeorgiou, 2024b, Kouhia et al., 2024)

Table 2

Rockbolt installation properties

Rockbolt	Borehole Ø (mm)	Anchoring Medium
Rebar rockbolt (Ø20 mm x 2.4 m)	33	Grout
Rebar rockbolt (Ø20 mm x 1.8 m)	33	Grout
R28 SDA	36	Polyurea silicate resin
R25 SDA	unknown	Polyurea silicate resin
Paddled energy-absorbing (Ø20 x 1.4 m)	36	Grout
Paddled energy-absorbing (Ø20 x 1.0 m)	33	Grout
Yielding mechanical hybrid rockbolt	38	Friction & mechanical anchor
R28 Energy-absorbing self-drilling rockbolt	36	Polyurea silicate resin

The yielding mechanical hybrid rockbolt was the only bolt to have a relative increase in the load capacity when loaded in shear. This was attributed to the mobilisation of the friction unit when loaded in shear. However, the friction unit borehole interface failed when loaded axially, resulting in the bar providing the primary load bearing and energy-dissipation mechanism (Knox, Hadjigeorgiou, 2023). The relative energy capacity (Rel. PE^{Q}) for all rockbolt types was less than 1, indicating a decrease in the capacity. The reduction in energy capacity was less than 20% across the four conventional rockbolt samples. As a consequence of the significant reduction in displacement capacity, the energy capacity of the fulling encapsulated energy-absorbing rockbolts was greater than 60%.

Of the energy-absorbing rockbolts, the yielding mechanical hybrid rockbolt appears to be the most resilient to shear loading, with an increase in the recorded load capacity and a reduction in displacement and energy capacity of less than 40%. This is due to the absence of an encapsulation medium allowing for greater displacement prior to the induction of bending and pinching of the

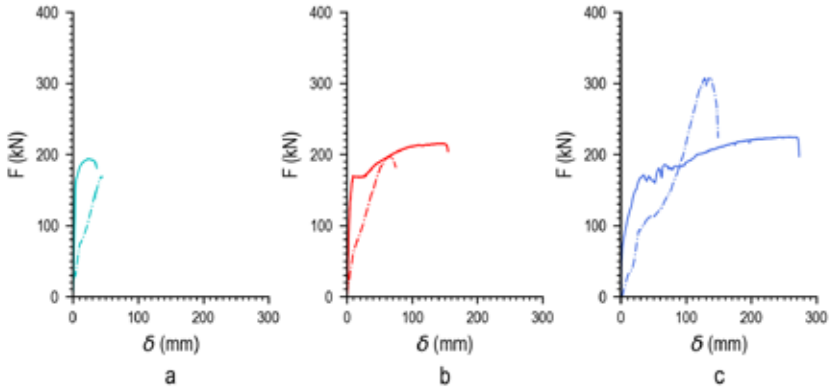

Figure 11—Three types of response observed in the results. a) Conventional encapsulated rockbolts, b) encapsulated energy-absorbing rockbolt, c) yielding mechanical hybrid rockbolt

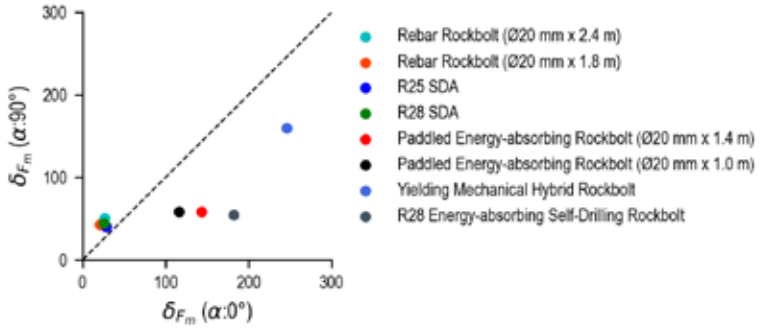

Figure 12—Comparison between the displacement at ultimate load determined through shear and tensile testing

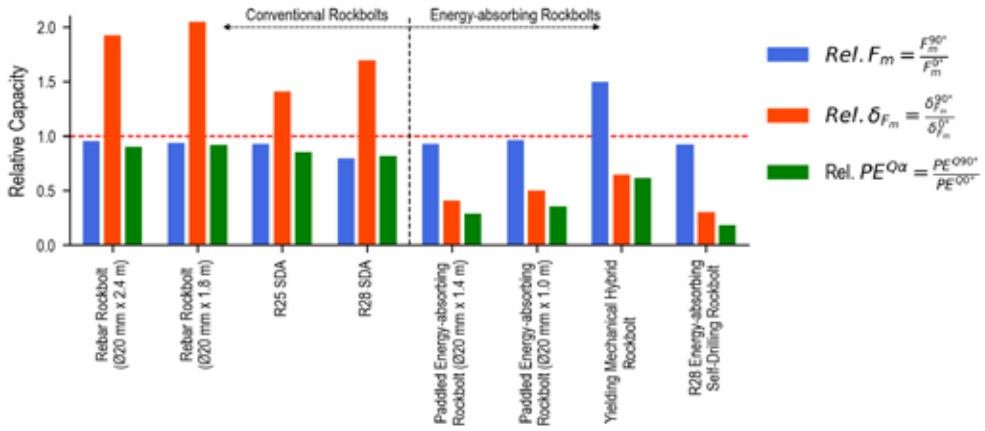

Figure 13—Relative performance capacities for the rockbolts

bar. The trade-off is a reduction in the stiffness of the response of the rockbolt, which may limit its application in certain conditions. In addition, the lack of an encapsulation medium presents a potential concern when the rockbolt is installed in highly corrosive environments for long term applications.

Conclusion

This paper presented a review of the response of five types of rockbolts, conducted using the single shear method on full scale rockbolts. Of the eight datasets included, three were undertaken using the SINTEF rockbolt pull test rig and the remaining five using the Epiroc Combination Shear and Tensile test rig. The inherent similarities in the construction and operation of these two testing rigs allowed for a direct comparison of the published results.

Three responses to shear loading were observed, differentiated by the encapsulation of the rockbolt and design premise, and conventional versus higher energy-absorbing rockbolts. The typical response was that of a decrease in the ultimate load capacity, which ranged between a 3% and a 20% reduction in load capacity, the exception being the yielding mechanical hybrid rockbolt, which recorded a 50% increase in load capacity. The displacement capacity for the conventional rockbolts all increased, however, remained less than the absolute value of the shear displacement capacity of an energy-absorbing rockbolt. This study is a contribution to an improvement in our understanding of rockbolt behaviour under controlled testing conditions.

References

Ayres, N.L., Gardner, L.J. 2014. Testing tendon support units under a combination loading scenario. *Journal of the Southern African Institute of Mining and Metallurgy*, vol. 114, no. 10. pp. 829–834.

Aziz, N., Pratt, D., Williams, R. 2003. Double shear testing of bolts. In. *Proceedings of the Coal Operators Conference*. Wollongong, Australia. pp. 154–161.

Bierman, J.R., Gardner, L., Piper, P. 2019. An evaluation of the bond strength of multiple resin bolt and capsule combinations through laboratory testing and applied methodologies. In Joughin, W (ed). Deep Mining 2019: *Proceedings of the Ninth International Conference on Deep and High Stress Mining*. The Southern African Institute of Mining and Metallurgy. Johannesburg, South Africa. pp. 175–190.

Bjurstorm, S. 1974. Shear strength of hard rock joins reinforced by grouted un-tensioned bolts. In *Proceedings 3rd International Congress on Rock Mechanics*. National Academy of Science: Washington. Denver, Colorado. pp. 1194–1199.

Chen, Y., Li, C. 2015a. Performance of fully encapsulated rebar bolts and D-bolts under combined pull-and-shear loading. *Tunnelling and Underground Space Technology*, vol. 45. pp. 99–106.

Chen, Y., Li, C. 2015b. Experimental and Three-Dimensional Numerical Studies of the Anchorage Performance of Rock Bolts. *Proceedings of the 13th ISRM International Congress of Rock Mechanics*, Montreal, Canada.

Dight, P.M. 1982. A case study of the behaviour of a rock slope reinforced with fully grouted rock bolts. In Proceedings *International Symposium on Rock Bolting*. Balkema. Rotterdam, Netherlands. pp. 523–538.

Dube, S. 1995. A *laboratory study on the behaviour of cable bolts subjected to combined tensile and shear loads* (Masters of Science).

Ferrero, A. 1995. The shear strength of reinforced rock joints. *Journal of Rock Mechanics and Mining Sciences & Geomechanics*, vol. 32, no. 6. pp. 595–605.

Grasselli, G. 2005. 3D behaviour of bolted rock joints: Experimental and numerical study. *International Journal of Rock Mechanics and Mining Sciences*, vol. 42, no. 1. pp. 13–24.

Haas, J. 1976. Shear resistance of rock bolts. *International Journal of Rock Mechanics and Mining Sciences & Geomechanics*, vol. 13, no. 6). A97.

Hagen, S., Larsen, T., Berghorst, A., Knox, G. 2019. Laboratory full-scale rock bolt testing: Analysis of recent results. In Joughin, W (ed). *Deep Mining 2019: Proceedings of the Ninth International Conference on Deep and High Stress Mining*. The Southern African Institute of Mining and Metallurgy. Johannesburg, South Africa. pp. 217–230.

Hadjigeorgiou, J. 2023. Ground Support for Extreme Conditions. In *Proceedings of NRock 2023: The IV Nordic Symposium on Rock Mechanics and Rock Engineering*. pp. 7–24

Jalalifar, H., Aziz, N. 2010. Analytical behaviour of Bolt–Joint intersection under lateral loading conditions. *Rock Mechanics and Rock Engineering*, vol. 43, no. 1. pp. 89–94.

Knox, G. 2022. *Quasi-static comparison between self-drilling support elements*. Report. Johannesburg, South Africa.

Knox, G., Hadjigeorgiou, J. 2022. Shear performance of yielding self-drilling anchors under controlled conditions. In Potvin, Y. (ed.) *Caving 2022: Proceedings of the fifth International Conference on Block and Sublevel Caving. Australian Centre for Geomechanics*. Perth, Australia. pp. 201–212.

Knox, G., Hadjigeorgiou, J. 2023. Performance of conventional and energy-absorbing self- drilling hollow core rockbolts under controlled laboratory conditions. *Rock Mechanics and Rock Engineering*, vol. 56. pp. 4363–4378.

Knox, G., Hadjigeorgiou, J. 2024a. Behaviour of yielding mechanical hybrid rockbolts under complex loading conditions. *International Journal of Rock Mechanics and Mining Sciences*, vol. 182. pp. 1–11

Knox, G., Hadjigeorgiou, J. 2024b. Behaviour of paddled energy-absorbing rockbolts under complex loading laboratory conditions. *Journal of the Southern African Institute of Mining and Metallurgy*, vol. 124, no. 9, pp. 535–545.

Kouhia, A., Penczek, R., Scolari, F. 2024. Integrated solutions based on injectable bulk resin for fast and safe rockbolting. In Andrieux, P. & Cumming-Potvin, D. (eds). *Deep Mining 2024: Proceedings of the 10th International Conference on Deep and High Stress Mining. Australian Centre for Geomechanics*. Perth, Australia. pp. 607–620.

Li, C. 2010a. Field observations of rock bolts in high stress Rock masses. *Rock Mechanics and Rock Engineering*, vol. 43, no. 4. pp. 491–496.

Li, C. 2010b. A new energy-absorbing bolt for rock support in high stress rock masses. *International Journal of Rock Mechanics and Mining Science*, vol. 47, no. 3. pp. 396–404.

Li, C. 2012. Performance of D-bolts under static loading. *Rock Mechanics and Rock Engineering*, vol. 45, no. 2. pp. 183–192.

Li, C., Stjern, G., Myrvang, A. 2014. A review on the performance of conventional and energy- absorbing rockbolts. *Journal of Rock Mechanics and Geotechnical Engineering*, vol. 6, no. 4. pp. 315–327.

Li, X., Aziz, N., Mirzaghorbanali, A., Nemcik, J. 2016. Behavior of Fiber Glass Bolts, Rock Bolts and Cable Bolts in shear. *Rock Mechanics and Rock Engineering*, vol. 49, no. 7. pp. 2723–2735.

Ludvig, B. 1984. Shear tests on rock bolts. *Proceedings of the International Symposium on Rock Bolting*. Abisko. Balkema, Rotterdam, Netherlands. pp. 113–123.

Mchugh, E., Singer, S. 1999. Roof bolt response to shear stress: Laboratory analysis. In *Proceedings 18th International Conference on Ground Control in Mining*. Morgantown, West Virginia. pp. 232–238.

Player, J.R. 2012. *Dynamic testing of rock reinforcement systems* (Doctor of Philosophy).

Punkkinen, A., Royer, R. 2022. Performance of Normet Self Drilling Dynamic Bolt (SDDB®) Types in Dynamic Loading - The Energy Dissipating Hollow Core Rockbolt Installed in Normet's Urea-Silicate Injection Resin. In *RASIM* 2022

Spang, K., Egger, P. 1990. Action of fully-grouted bolts in jointed rock and factors of influence. *Rock Mechanics and Rock Engineering*, vol. 23, no. 3. pp. 201–229.

Stjern, G. 1995. *Practical performance of rockbolts* (PhD).

Yao, M., Sampson-Forsythe, A., Punkkinen, A.R. 2014. Examples of ground support practice in challenging ground conditions at vale's deep operations in Sudbury. In Hudyma, M. and Potvin, Y. (eds). *Deep Mining 2014: Proceedings of the seventh International Conference on Deep and High Stress Mining*. Australian Centre for Geomechanics. Perth, Australia. pp. 291–304. ◆

The role of stress and geology on the design of block cave mining sequences and layouts - a case study

by T. Mtshali[1], N.M. Chiloane[2], B. Makgate[1], T. Chauke[2], F.K. Mulenga[2], V.C. Madanda[2], T. Moyane[1], R.B. Khumalo[1]

Affiliation:
[1]Palabora Mining Company, Limpopo, South Africa
[2]University of South Africa, Johannesburg, South Africa

Correspondence to:
N.M. Chiloane

Email:
chilonm@unisa.ac.za

Dates:
Received: 26 Jun. 2025
Published: November 2025

How to cite:
Mtshali, T., Chiloane, N.M., Makgate, B., Chauke, T., Mulenga, F.K., Madanda, V.C., Moyane, T., Khumalo, R.B. 2025. The role of stress and geology on the design of block cave mining sequences and layouts - a case study. *Journal of the Southern African Institute of Mining and Metallurgy*, vol. 125, no. 11, pp. 629–636

DOI ID:
https://doi.org/10.17159/2411-9717/827/2025

This paper is based on a presentation given at the AfriRock Conference 2025, 21-23 July 2025, Sun City Resort, Rustenburg, South Africa

Abstract

While high production rates are important for the profitability of a mine, the influence of geotechnical engineering cannot be ignored. In block caving, a high-stress level is required for cave propagation; this is one of the core elements for ore recovery. Therefore, stress distribution and geological structures play a major role in the planning and layout design of the mine. This paper explores the influence of stress and geological features on the design of the mine from the feasibility study phase. The geology and stress measurement of the mine were determined through logging and overcoring, respectively. This study found that while production rate is the primary operational consideration, the long-term layout design of the undercut face advance, face angle, drawpoint spacing, and undercutting sequence is mainly governed by the stress orientation and major geological structures. Moreover, widely spaced drawpoints result in isolated draw zones, consequently, resulting in ore loss and early dilution whereas closely spaced drawpoints affect the stability of the major apex pillar. This paper also provides insight into how operations can leverage stress distribution to optimise mine layout and safety in massive mining methods.

Keywords

block caving, advanced undercut, drawpoint spacing, leads and lags, isolated draw zones

Introduction

Block caving is a large-scale underground mining method primarily used for extracting low-grade, massive ore bodies, as shown in Figure 1. The bottom of the orebody is undercut by blasting to initiate the caving of the rock mass through gravity (Diaz et al., 2024; Melati et al., 2023). The undercutting process generates mine-induced stress distribution, contributing to the progressive caving of the rock mass. Moreover, deep mining is characterised by rock fractures and unstable hangingwalls that challenge the safety of mine workers and equipment (Wagner, 2019). Considering this, strategic management of mining-induced stress, seismicity, and air blast should be the core of mine design and planning in block caving operations (Cuello, Newcombe, 2018). This paper aims to evaluate the role of stress distribution and geological structures on block cave mining sequence and the mine layout. That is, the face shape, drawpoint spacing, and the vertical distance between the production and undercut level. A thorough knowledge of the geological structures of the mine in all three dimensions, in conjunction with the geotechnical properties of the rock mass, dramatically impacts the long-term design of the mine (Murphy et al., 2016). This is because the undercut and production tunnels intersect the weaker zones, whereas the mine design and sequence must remain open for the life of the production level (Tukker et al., 2016).

Several studies have examined the influence of geotechnical parameters on block-cave mining operations. Morales et al. (2024) reviewed several studies on the challenges of orebody cavability prediction in block caving. These authors were able to argue that rock mass characterisation is the foundation for reliable estimations of the rock mass quality for design applications. On the other hand, Hadjigeorgiou (2012) stressed that there is a lack of quality data in underground mines due to mapping difficulties caused by limited access, walls covered with shotcrete, and poor visibility On the other hand, poor visibility significantly impacts the reliable estimation of rock mass strength. Massive mining methods such as block caving often result in conditions of high-strain energy stored in the rock. Mining activities can result in the release of stored strain energy, consequently leading to dynamic rock failure (Bewick, 2021; Roy et al., 2023).

Bartlett and Nesbitt (2000) studied how stress-induced damage in tunnels in a cave mining environment can influence mine planning. The study reveals that high-stress levels are set up in the

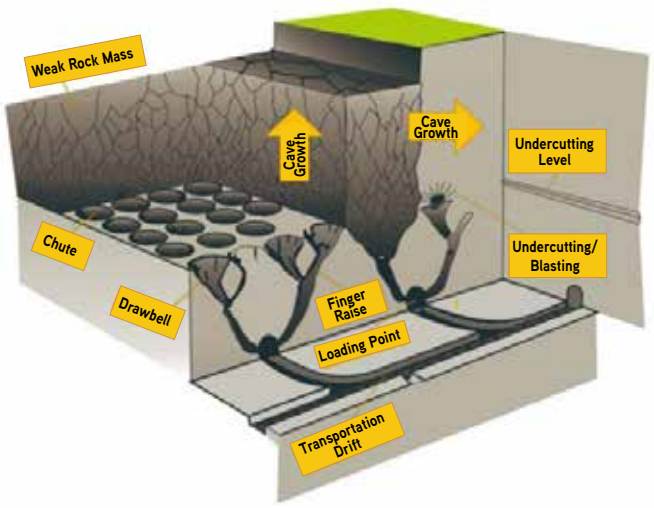

Figure 1—Block caving layout (Melati et al., 2022)

abutment zone around the perimeter of the caving area, which can affect tunnel stability at 20 m from the cave front. The authors add that the most stable face shape is concave or V-shaped towards the cave. This face shape has the advantage of allowing low abutment stresses to develop at the apex on both the undercut and extraction levels. High abutment stresses develop towards the edge of the cave. A straight-face shape is often more challenging to control than the V-shape and does not provide the low-stress area that the V-shape does (Bartlett, Nesbitt, 2000). The V-shaped cave front has a shorter face length compared to a straight-face geometry. In contrast, longer straight faces tend to advance more slowly, leading to higher stress concentrations along the face due to limited relief of abutment stresses. In support of the previous statement, Van As and Guest (2020) also add that cave design aims to engineer control over the cave's behaviour and performance. Therefore, a good understanding of the geotechnical domains, their spatial distribution, their rock mass characteristics, and their response to the stress regimes induced during the various stages of caving is required. Although there are several great studies on the effect of stress on the mining layout in block caving, there is a lack of studies holistically integrating geotechnical analysis with mine design in block cave operations. Therefore, the main objective of this study is to investigate the role of stress and geological structures on the design of mining sequences and layouts in block cave mining.

Geological setting

This study was conducted at Palabora Mining Company (PMC) in South Africa, Limpopo Province, Phalaborwa. The Palabora Copper Igneous Complex is a foskorite-carbonatite pipe complex with an area of 20 km2 that resulted from an alkaline intrusive cycle into a host Archaean granite. The copper ore body is an elliptically shaped vertical pipe with an area of 1 km2. The pipe intruded at a late stage into the central core of the PMC Igneous Complex. The pipe, as illustrated by Figure 2, consists of foskorite, banded carbonatite, and transgressive carbonatite. The composition features iron and copper mineralisation, especially magnetite, bornite, and chalcopyrite. Considerably later in the formation of the complex, the area was crossed by numerous dolerite dykes (Dixon, 1979). The central core is crossed by dolerite dykes trending NE-SW. The same basic arrangement persists for the full depth of the known deposit, although there is much local variation in all units. The dykes dip steeply to the west, as such move with increasing depth. The dolerite dykes intruded at a much later time than the other units and it appears that this occurred at a much shallower depth, when the wall rocks behaved in a brittle manner, giving the dykes their relatively regular thickness and form. Due to the declining ore grade in the first cave (Lift I), PMC is developing the Lift II project, which is a continuation of the block cave below the existing Lift I cave.

During the initial development of Lift II, the mining direction was configured perpendicular to the prevailing dyke orientations. This configuration was informed by early numerical modelling of Lift II, where stress assumptions were based on a back-analysis of the in situ stress field undertaken by Itasca Consulting in 2009. This back-analysis suggested that the stress regime was not hydrostatic but that the major principal stress is likely sub-horizontal, with

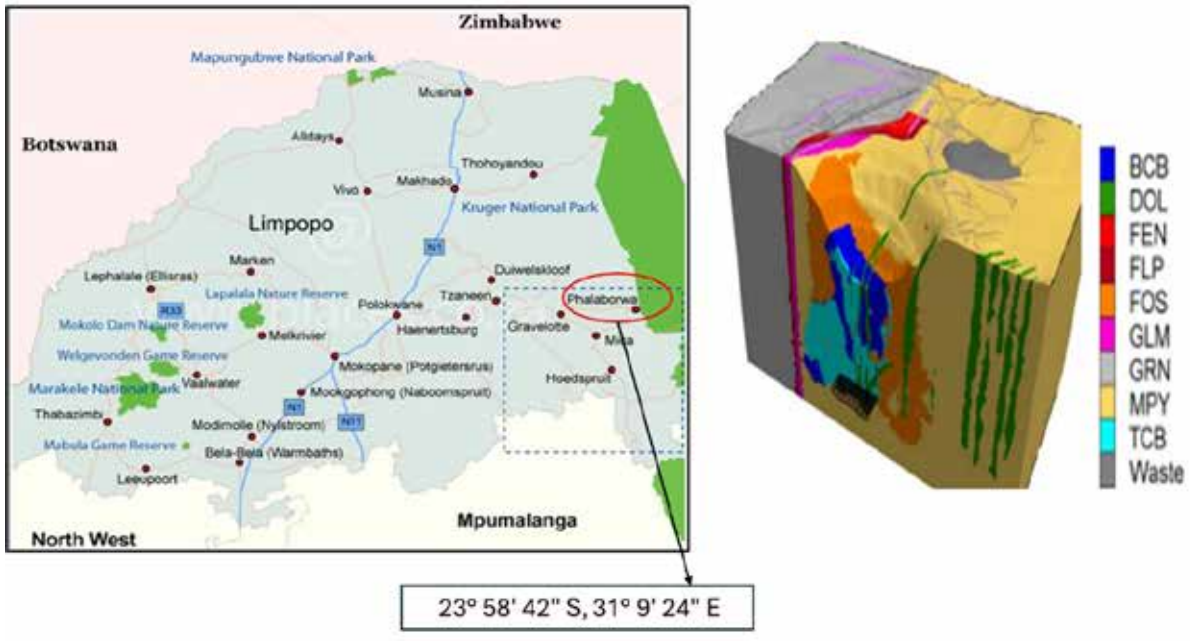

Figure 2—A map showing the location of PMC and the sectional view of the PMC's orebody

major principal horizontal stress (σH) = 2σz and minor principal horizontal stress (σh) =1.5σz (Van As, 2014). However, this orientation of the mining face, perpendicular to major geological structures (i.e., dykes and parallel to a fault), subsequently presented significant stability challenges. Dykes, due to their distinct mechanical properties, are known to absorb and release strain energy, which can result in rock bursts when disturbed. Consistent with this, stress-induced damage was observed throughout the Lift I infrastructure and during the early development of the Lift II infrastructure. Consequently, these observations necessitated further investigations to explore alternative face directions. Following these findings, a revised lower in situ stress regime, with a horizontal to vertical stress ratio (K) of 1.2:1, was subsequently adopted for the Lift II analysis (Sainsbury, 2016). The application and implications of this revised stress regime will be elaborated further in the Methodology section.

Methodology

This section discusses the steps followed in collecting raw data used during the mine planning process. The data from exploration drilling, cover drilling, and field observations were used to investigate the effect of stress and geological structures on the orientation of large excavations, mining sequences, and mine layout.

Geotechnical domains

The rock mass properties of the underground mine were initially determined through the mapping of the previous open pit before underground mining could start. The pre-feasibility study for Lift II was informed by extensive geotechnical data, derived from logging over 150 drill holes, totaling more than 57,500 m. Complementary geotechnical characterisation was provided by a geophysical survey that incorporated an acoustic televiewer (ATV) and other down-hole logging tools. This work was aimed at subdividing the total rock mass into geotechnically similar zones of similar characteristics in what is known as geotechnical domaining (Laubscher, 1994). This was done with the understanding that all the rocks within a domain exhibit similar engineering characteristics. However, the parameter/s used to subdivide an orebody (or any rock mass) into domains vary. In any type of rock, these variables might be the lithological composition (including alteration), the type or intensity of fracturing, the orientation of fractures, the strength of the rock material, or any combination of these parameters.

For the Lift I cave, the orebody within the zone of influence of the cave was divided into 3 structural domains, namely, the East, the Ramp Dyke, and the West Zones. These domains were further subdivided into "well jointed" and "less jointed" zones based on the joint spacings derived from the open pit mapping and drill core logging (where a joint spacing of 2 m separates the zones). The sub-domaining into "well jointed" and "less jointed" zones was to improve the accuracy of the fragmentation predictions. Various analyses established a 30:70 ratio between the "less jointed" and "well jointed" zones. The geotechnical domains for Lift II are based on lithology, namely, the branded carbonatite (BCB), dolerite (DOL), foskorite (FOS), micaceous pyroxenite (MPY), and transgressive carbonatite (TCB). The properties of the geotechnical domains are summarised in Table 1.

Table 1

Hoek-brown failure properties of the geotechnical domains (Van As, 2014)

Geotechnical domain	σ_{ci} (MPa)	mi	GSI	m_b
BCB	22.9	22.9	22.9	22.9
DOL	24.1	24.1	24.1	24.1
FOS	25.2	25.2	25.2	25.2
MPY	17.4	17.4	17.4	17.4
TCB	28.0	28.0	28.0	28.0

Stress distribution/orientation

The stress orientation of the rock mass for Lift II was determined through overcoring in foskorite on the Lift II production level. It stands out in rock mechanics since it is the only method capable of obtaining the magnitude and direction of the full three-dimensional stress from a single OC test (Li et al., 2024). Specifically, a revised in situ stress regime was proposed based on the stress measurements that were conducted. A summary of both the initial (as discussed in the background section) and the revised Lift II stress conditions, which informed the present analysis, is presented in Figure 3.

The modelling input values are summarised in Table 2.

The revised stress regime differs from the initial Lift II regime in the following aspects:

- The σ_1 and σ_3 orientations have been swapped. In other words, σ1 was previously striking NW-SE, but it is now vertical. Conversely, σ_3 was previously vertical, but it is now striking NW-SE.

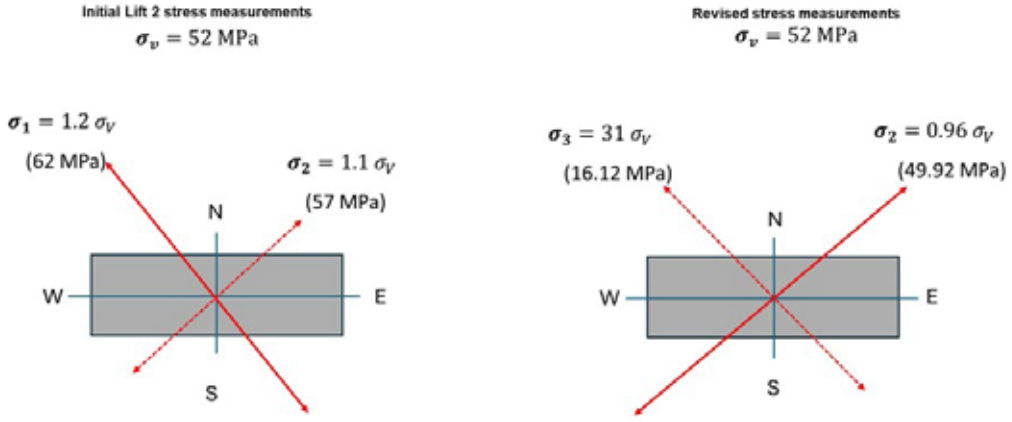

Figure 3—Initial Lift II and revised Lift II in situ stress conditions (Sainsbury, 2023)

Table 2
Simulated in situ stress regime (Sainsbury, 2023)

Stress	Magnitude (MPa)	Dip (o)	Dip direction (0)
σ_1	ρgH	90	0
σ_2	0.96*σ_1	0	058
σ_3	0.31*σ_1	0	148

- The horizontal stress magnitudes are lower. Indeed, striking NW-SE, the stress magnitude has now decreased from 62 MPa to 16 MPa at the Lift II production level. However, the deviatoric stress (difference between σ1 and other stresses) is higher at 0.96 and 0.31, as opposed to 1.2 and 1.1). Stress measurements indicated that both horizontal principal stresses are lower than the vertical stress, identifying the vertical stress as the major principal stress.

The initial response of the Lift II production level and cave initiation supports the revised stress regime (Sainsbury, 2023).

Results and discussion

Mining method

This section discusses the influence of the measured stress on the mining layout of Lift II. The layout specifically refers to the undercutting method, the face advance rate, the face angle, and the face length.

Advanced undercut

To minimise stress damage and increase rehabilitation requirements in extraction levels, PMC opted for advanced undercutting techniques. In simple terms, the advanced undercut method (see Figure 4) was selected to ensure the stability of the extraction level for the mine's life. The advantage of advanced undercut over post-undercut is that large unsupported drawbell excavations are not subjected to high abutment stresses, and less support rehabilitation is required in areas where undercutting precedes production-level development. On the other hand, post-undercutting results in stress-induced damage to the draw horizon level, therefore, it would be prudent that the undercut should be advanced first, and the draw horizon should be developed in de-stressed conditions. This approach aligns with established principles in block caving, as Butcher (1999) and Laubscher (2000) concur that stress increase associated with undercutting is a significant factor that influences the stability of the production level. Indeed, a fundamental principle for mitigating draw horizon damage, articulated by Butcher (1999), is the implementation of advanced undercutting within the block cave. Figure 4 differentiates the two methods.

Undercut face advance rate

The rate at which the undercut face is advanced is critical as the rock mass ahead of the undercut face is subject to high abutment stresses. The slower the undercut advances, the greater the deterioration of the rock mass, and the more difficult it is to successfully blast the face. To put it another way, slower advances result in creep damage due to stress build-up, which then increases the probability of seismicity (Sun et al., 2022). Conversely, rapid undercut face advance, where the face is greater than 50 m–60 m ahead of the last line of drawbells, leads to the formation of a stress shadow. This acts as an abutment stress concentrator, which typically results in large drive deformations and rockbursts.

Before development, the average advance rate of the Lift II undercut was initially planned at around 3,400 m²/month, equating to approximately 11 m/month. The current advance rate is 10 m–15 m/month, which still complies with standard practice (Crook, Prince, 2018). It is important to adhere to the standard advance rate since a slower advance rate increases the stress-induced damage. This phenomenon is supported by Butcher (1999), who adds that stress-induced damage increases with a reduction in the rate of advance of the cave line. The undercut abutment stresses reach the maximum magnitude when the undercut area equates to the required hydraulic radius of the block.

Undercut face angle

The initial undercut face was designed based on the initial stress orientation of the Lift II model to be initiated from the SE to NW, with an undercutting face striking NE-SW. However, based on the groundwork stress measurement done in 2017, the initial undercut long face orientation would have been parallel to the major

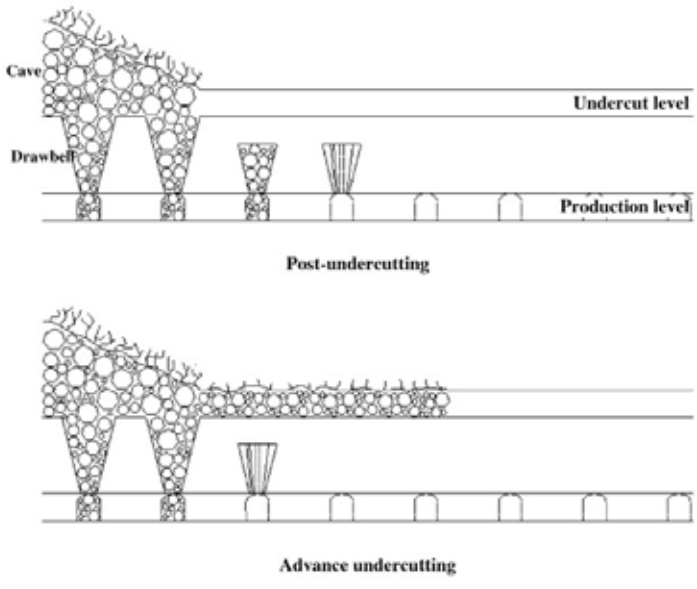

Figure 4—Development sequence of post and advance undercut (after Trueman et al., 2002)

principal stress and the major dolerite dykes (Groundworks, 2017). This would have had the potential to cause large slip failures posing a risk of unsuccessful execution of the undercutting. Dolerite dykes display brittle behaviour, making them susceptible to sudden failure under high-stress conditions (Ledwaba, 2012).To mitigate against the potential for large seismic risk, an undercut face design change was implemented to ensure that the long-undercut face advance is perpendicular to the major principal stress and dolerite dykes. The current mining direction in Lift II is from NE to SW, where the major geological features (dykes) are approached perpendicularly. The current face shape and undercut advance are depicted in Figure 5.

The initial angle of the undercut face advance was governed by the major horizontal stress based on the initial stress measurement. This angle was predominantly orthogonal, which was the best practice for reducing abutment stresses in the undercut face. However, following the updated stress regime orientation, it became apparent that the eastern face of the initial undercut wedge, as initially planned, would advance parallel to both the major horizontal stress and major dykes. Consequently, the direction of the face was changed to avoid this unfavourable condition. Fortunately, the extent of the NE advancing undercut face was limited, which helped to minimise its exposure to these problematic dykes during this transition.

Undercut leads and lags

The differential distances between adjacent faces (drill drives) are known as the leading and lagging distances. The greater the leads or lags between adjacent faces, the greater the stress differential. The objective is generally to minimise the lead and lag distances so that the tangential stresses are maintained in the undercut face while aiding in its stability by adding confinement to the rock mass. In practice, the operating lead-lag distance is between 10 m to 15 m (maximum) and ideally no more than 2 to 3 rings. Note here that blasting rings are spaced 2 m apart around the Lift II cave. As such, the lead-lag distance of the mine is currently at 6 m–12 m (see Figure 6). It is worth highlighting that the rock mass conditions of each mine differ, therefore, the lead-lag pattern is not always one-size-fits-all. Thus, the lead-lag distance was chosen based on the depth and stress conditions of the surrounding rock. As mining depth increases, the corresponding stress conditions also increase. Therefore, lead–lag pattern helps to spread out the abutment stress zones, lowering their magnitude and reducing the potential for large stress build-ups.

Undercut face length

The length of the undercut face is a function of the undercut face angle. The longer the face, the more difficult it is to construct a sufficient number of drawbells behind the face to allow it to keep moving. Practical empirical evidence suggests that an undercut face length of over 450 m is impossible to advance at a reasonable rate (Ross, 2018), as the construction rate for drawbells behind the face cannot be achieved. Typically, an average construction rate of 5-6 drawbells/month is the norm for drawbells (Pascoe et al., 2008). The maximum undercut face length planned for Lift II was 250 m. This is considered manageable, and the mine is still maintaining a face length of not more than 240 m. Long-face shapes over 300 m are difficult to manage from the point of view of ground stability control. These shapes also affect the advancement rate that can be achieved in a particular time. Consequently, a slow advance rate results in excessive abutment build-up, which in turn leads to the deterioration of undercut drives. This is because when undercutting is not advancing as quickly as planned, some areas in the cave will not cave as expected. As a result, this causes some localised stress on the abutments that will become difficult to successfully undercut.

Extraction level

The extraction level is designed to maximise ore reserves. As such, it should remain stable for the life of the mine to ensure maximum ore reserve recovery. The stability of the extraction level is often affected by the ore extraction activities, resulting in tunnel convergence, concrete slabbing at the walls, and sometimes closure (Castro et al., 2020). In granular material, such as caved rock ore, vertical stresses are significantly lower than total column weight because of the arching effect generated by shear stresses due to the rock friction. When the granular material is underflowing (flowing beneath the broken mass), at least two main zones, the movement zone and the stagnant zone, can be identified. In the movement zone (or draw zone), porosity increases, and vertical stresses decrease due to flow, while in the stagnant zone (or non-draw zone), vertical stresses increase. Castro (2006), through his experimental studies, has demonstrated that stresses can be transferred from the movement

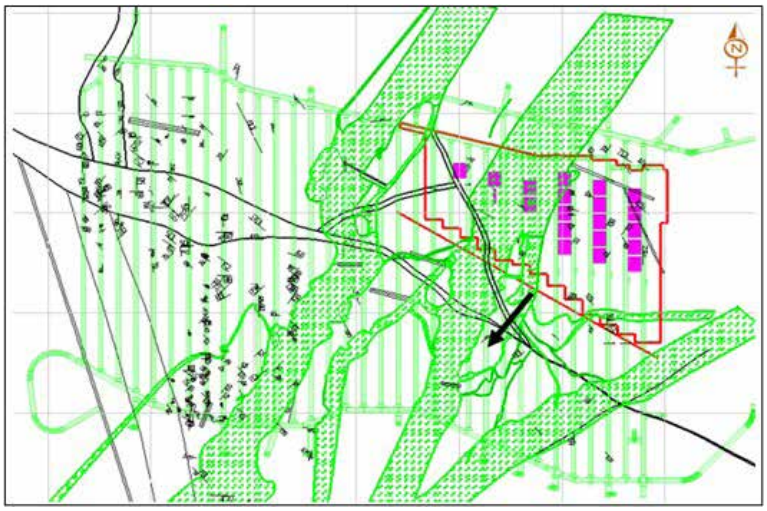

Figure 5—Revised Lift II undercut face advance direction; the green structures crossing through diagonally are the dolerite dykes (Sainsbury, 2016)

Figure 6—PMC Lift II undercut face and leads/lags (Sainsbury, 2016)

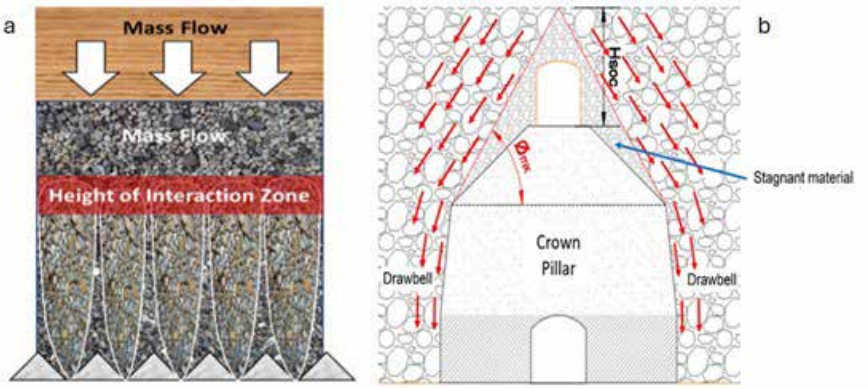

Figure—7(a) Illustration of interacting draw zones (after Laubscher, 1994); (b) Illustration of stagnant material (after Morales et al., 2024)

zone to the stagnant zone during flow. Then, induced vertical stresses over the production level depend on the movement of the gravity flow. Ngidi and Pretorius (2010) also emphasised that good draw control prevents stress concentration damage on the extraction horizon. Palabora Mine is currently using Gemcom's Personal Computer Block Cave (PCBC) systems for the draw strategy. Even draw is applied, ensuring maximum ore extraction from the reserves.

Drawpoint spacing

Drawpoint spacing is governed by the interaction of adjacent draw zones, amongst others. The interaction of adjacent draw zones refers to the point where the draw zones of two adjacent drawpoints meet (Figure 7a). It is worth noting that ore flow will occur when adjacent flow zones are spaced to allow interaction at a given height (Castro et al., 2020). The size of the ore fragmentation also dictates the draw-cone diameter. According to Laubscher (2000), the standard guideline is that finer fragmentation requires smaller drawpoint spacing whereas coarse fragmentation requires bigger draw zone spacing. Most importantly, drawpoint spacing must be related to the draw zone spacing, instead of being dictated by the size of the load haul dump (LHD) trucks. The isolated draw zone (IDZ) diameters for the averages of all rock types are approximately 12 m–13 m. This suggests an optimal drawpoint spacing of 32 m (drive centres) by 16 m (drawbell centres) to ensure an interactive draw. This design choice was primarily driven by two critical factors: the operational requirement to accommodate large load-haul-dump (LHD) equipment, and the geotechnical objective of improving the stability of the extraction level.

The drawpoints at Lift II are spaced 17 m apart centre to centre. From a business point of view, drawpoint spacing determines the ore reserve recovery of the mine. That is, as the spacing between drawpoints increases, there is a greater amount of non-recoverable ore (marked as "stagnant material" in Figure 6b). This is due to the increased separation along the major apex, generating an increase in the height of the interactive zone (HIZ) and leaving more ore between the drawpoints. It should be noted that the Lift I drawpoints are spaced too widely to facilitate an interactive draw, and this has ultimately led to higher heights of draw, early dilution entry, and loss of reserve (Van As, 2014). When individual drawpoints are drawn in isolation or drawpoints are spaced too wide for draw interaction to occur, then isolated draw predominates. As a result of this, the height of interaction increases, and even the flow of material is lost. In other words, the higher the interaction zone, the earlier the dilution will be encountered at the extraction level (Van As, Guest, 2020). Laubscher (1994) recommends that drawpoints should be spaced at 1.5 times the diameter of the isolated draw zone, whereas other studies (Kvapil, 1965) suggested that isolated movement zones must overlap. A follow-up investigation is being conducted to determine the optimal spacing.

From a safety point of view, widely spaced drawpoints with poor interaction resulted in overloading of vertical stress on the major apex due to the extra stagnant material and weight of the

mass from the cave. The findings by Van As and Guest (2020) concur that the loading (weight) of the overlying stagnant and compacted ore has a major impact on the stability of the apex pillar. The over-concentrated vertical stress can cause a potential shear failure between the major apex and the extraction drive underneath. Additionally, in coarse fragmentation, the stagnant material forms a barrier that prevents the lateral growth of the isolated movement zone, thus resulting in a narrow-isolated movement zone (Pierce, 2009). The argument of widely spaced drawpoints is that they improve the strength of the extraction level by creating large apex pillars that can withstand higher loads from the ore column above.

Conclusion

This study described the effect of stress, geological structures and stability of the undercut and production level on the layout design of a block cave mine. The findings of the study are summarised as follows:

- The standard guidelines for mine design cannot be given, as the rock mass properties of each mine are unique.
- Face advances perpendicular to the major principal stress and parallel to the dolerite dyke were found to be preferable.
- The mine found that a 45° lead/lag face shape of the undercut minimised abutment damage to the undercut level.
- The mine opt for widely spaced drawpoints to accommodate large LHDs, in contrast to theory, which suggests isolated draw zones, ore loss and early dilution.
- The optimal drawpoint spacing between production and ideal extraction is unknown for the geotechnical conditions at the mine.

References

Bartlett, P.J., Nesbitt, K. 2000. Stress induced damage in tunnels in a cave mining environment in kimberlite. *Journal of the Southern African Institute of Mining and Metallurgy*, vol. 100, no. 6, pp. 341–346.

Bewick, R.P. 2021. The strength of massive to moderately jointed rock and its application to cave mining. *Rock Mechanics and Rock Engineering*, vol. 54, pp. 3629–3661. https://doi.org/10.1007/s00603-021-02466-3

Butcher, R.J. 1999. Design rules for avoiding draw horizon damage in deep level block caves. *Journal of the Southern African Institute of Mining and Metallurgy*, vol. 99, no. 3, pp. 151–156.

Castro, R. 2006. Study of the mechanisms of gravity flow for block caving. PhD thesis, University of Queensland, Australia.

Castro, R., Gomez, R., Pierce, M., Canales, J., Juan, J. 2020. Experimental quantification of vertical stresses during gravity flow in block caving. *International Journal of Rock Mechanics and Mining Sciences*, 127, 104237. https://doi.org/10.1016/j.ijrmms.2020.104237

Crook, K., Prince, F. 2018. Development planning for the Oyu Tolgoi panel cave mine. In Potvin, Y. and Jakubec, J. (eds.). *Caving: Proceedings of the Fourth International Symposium on Block and Sublevel Caving*. Australian Centre for Geomechanics, Perth. https://doi.org/10.36487/ACG_rep/1815_30_Crook

Cuello, D., Newcombe, G. 2018. Key geotechnical knowledge and practical mine planning guidelines in deep, high-stress, hard rock conditions for block and panel cave mining. In Potvin, Y. and Jakubec, J. (eds.). *Caving: Proceedings of the Fourth International Symposium on Block and Sublevel Caving*. Australian Centre for Geomechanics, Perth. pp. 17–36.

Díaz, R., Gomez, R., Vidal, R., Hekmat, A., Oyarzo, D. 2024. Combining geomechanical and hydrogeological modeling for drainage analysis in block caving mine development. *International Journal of Rock Mechanics and Mining Sciences*, 173, 105606. https://doi.org/10.1016/j.ijrmms.2023.105606

Dixon, C.J. 1979. The Palabora Complex — South Africa. In: *Atlas of Economic Mineral Deposits*. Springer, Dordrecht. https://doi.org/10.1007/978-94-011-6511-2_52

Groundworks. 2017. Palabora Stress Measurement Report – Sites 1B and 2A, June 2017.

Hadjigeorgiou, J. 2012. Where do the data come from?. Mining Technology, vol. 121, no. 4, pp. 236–247. https://doi.org/10.1179/1743286312Y.0000000

Kvapil, R. 1965. Gravity flow of granular material in hoppers and bins – Part 1. *International Journal of Rock Mechanics and Mining Sciences*, vol. 2, pp. 35–41. https://doi.org/10.1016/0148-9062(65)90020-3

Laubscher, D.H. 1994. Cave mining – the state of the art. *Journal of the Southern African Institute of Mining and Metallurgy*, vol. 94, no. 10, pp. 279–293.

Laubscher, D. 2000. Block caving manual. *Report for the International Caving Study*, Brisbane, Australia. 525 pp.

Ledwaba, L.S. 2012. Seismic damage mechanism at Impala Platinum Mine. MSc dissertation, University of the Witwatersrand, Johannesburg.

Li, P., Cai, M., Miao, S., Miao, S., Li, Y., Sun, L., Wang, J., Gorjian, M. 2024. Accurate measurement techniques and prediction approaches for the in-situ rock stress. *Scientific Reports*, 14, 13226. https://doi.org/10.1038/s41598-024-64030-7

Melati, S., Wattimena, R.K., Sahara, D.P., Syafrizal, Simangunsong, G.M., Hidayat, W., Riyanto, E., Felisia, R.R.S. 2023. Block caving mining method: Transformation and its potency in Indonesia. *Energies*, vol. 16, no. 1, p. 9. https://doi.org/10.3390/en16010009

Morales, D., Castro, R., Gómez, R. 2024. A methodology to determine undercutting height in block/panel caving. *Mining*, vol. 4, no. 2, pp. 417–428. https://doi.org/10.3390/mining4020024

Morales, S.K., Suorineni, F.T., Hebblewhite, B. 2024. Orebody cavability prediction challenges in block caving mining — a review. *Bulletin of Engineering Geology and the Environment*, 83, 23. https://doi.org/10.1007/s10064-023-03516-6

Murphy, T., Webster, A., Chitombo, G. 2016. Beyond rock mass characterisation – the impact of geology on block cave mining. MassMin 2016: *Seventh International Conference & Exhibition on Mass Mining*, 9–11 May 2016, Sydney, Australia.

Ngidi, S.N., Pretorius, D.D. 2010. Impact of poor fragmentation on cave management. In Potvin, Y. (ed.). *Proceedings of Caving 2010*, Australian Centre for Geomechanics, 20–22 April 2010, Perth, Australia.

Pascoe, C., Oddie, M., Edgar, I. 2008. Panel caving at the Resolution copper project. *5th International Conference and Exhibition on Mass Mining*, 9–11 June 2008, Luleå, Sweden. pp. 35–42.

Pierce, M.E. 2009. A model for gravity flow of fragmented rock in block caving mines. PhD thesis, University of Queensland, Australia.

Ross, I.T. 2018. Benchmarking and its application for caving projects. *The Fourth International Symposium on Block and Sublevel Caving*, 15–17 October, Vancouver, Canada.

Roy, J.M., Eberhardt, E., Bewick, R.P., Campbell, R. 2023. Application of data analysis techniques to identify rockburst mechanisms, triggers, and contributing factors in cave mining. *Rock Mechanics and Rock Engineering*, vol. 56, pp. 2967–3002. https://link.springer.com/article/10.1007/s00603-022-03206-x

Sainsbury, B. 2016. Palabora Block Cave - Lift II Cave and Subsidence Analysis. Mining One report for Palabora Mining Company. 3813v2.

Sainsbury, B. 2023. Updated Assessment of Lift II Production Level & Cave Propagation Performance. 23003v3.

Sun, C., Jin, C., Wang, L., Ao, Y., Zhang, J. 2022. Creep damage characteristics and local fracture time effects of deep granite. *Bulletin of Engineering Geology and the Environment*, 81, 79. https://doi.org/10.1007/s10064-022-02578-2

Trueman, R., Pierce, M., Wattimena, R. 2002. Quantifying stresses and support requirements in the undercut and production level drifts of block and panel caving mines. *International Journal of Rock Mechanics and Mining Sciences*, vol. 39, no. 5, pp. 617–632. https://doi.org/10.1016/s1365-1609(02)00060-6

Tukker, H., Holder, A., Swarts, B., van Strijp, T., Grobler, E. 2016. The CCUT block cave design for Cullinan Diamond Mine. Journal of the Southern African Institute of Mining and Metallurgy, 116(8), 715–722. http://dx.doi.org/10.17159/2411-9717/2016/v116n8a2

Van As, R.A. 2014. Feasibility study Lift II – New base case.

Van As, A. and Guest, A. 2020. The design and operating philosophies of panel vs block caving. In Castro, R., Báez, F. and Suzuki, K. (eds.). Proceedings of the Eighth International Conference & Exhibition on Mass Mining, MassMin 2020, 9–12 December, University of Chile, Santiago. pp. 207–220. https://doi.org/10.36487/ACG_repo/2063_10

Wagner, H. 2019. Deep mining: A rock engineering challenge. Rock Mechanics and Rock Engineering, 52, 1417–1446. https://doi.org/10.1007/s00603-019-01799-4 ◆

Review of quality assurance methods for hydro-powered resin bolting

by J.P. Gouvea[1], W. Geel[2]

Affiliation:
[1]Glencore, South Africa
[2]Notham Platinum Holdings Ltd, South Africa

Correspondence to:
J.P. Gouvea

Email:
jean-pierre.gouvea@kamotocopper.com

Dates:
Received: 30 Jun. 2025
Published: November 2025

How to cite:
Gouvea, J.P., Geel, W. 2025. Review of quality assurance methods for hydro-powered resin bolting. *Journal of the Southern African Institute of Mining and Metallurgy*, vol. 125, no. 11, pp. 637–648

DOI ID:
https://doi.org/10.17159/2411-9717/860/2025

This paper is based on a presentation given at the AfriRock Conference 2025, 21-23 July 2025, Sun City Resort, Rustenburg, South Africa

Abstract

Resin bolting in South Africa has been developed and refined in underground coal mines (i.e., soft rock) since the late 1940s. The extension of resin bolting to hard rock mines started in 2003 and has required significant adaptations, challenging the status quo from both a supplier and applicator perspective. As far as resin bolting is concerned, the most affected aspect in coal mining and hard rock mining environments, is the rock drills or machinery used for installation. Hard rock mines mostly use hand-held airlegs with limited thrust, low torque, and rotation speed, relative to coal mine mechanised bolters. Resin bolt development for hard rock mines was, and still is today, predominantly focussed on compensating for the 'shortfalls' of using hand-held airlegs.

At face value, hydro-powered rock drills, which are more powerful than traditional hand-held equipment, provided hard rock mines with a means to attain more consistent and reliable resin bolt installations. This paper assesses the quality and performance of hydro-powered resin bolting at an intermediate to deep level platinum mine in South Africa and its potential contribution to rock-related instabilities when applied erroneously. The findings of this paper necessitate a revision of current quality control and quality assurance measures related to resin bolting for underground support.

Keywords

hydro power, underground support, resin bolting, pull test, encapsulation, load transfer

Introduction

Since its earliest application in the late 1940s (Ferreira, Franklin, 2008), South Africa has developed a rich history of resin bolting in underground coal mines. From 2003, the application of resin bolting extended to other underground commodities, including the platinum mining industry. The transition to underground hard rock mines, using airleg installations in larger diameter support holes, was particularly challenging as the performance and reliability of resin bolts were tested beyond their typical benchmarks and limits. More than 20 years later, resin bolting remains one of the most researched topics in underground mine support, focused on delivering consistent and dependable support solutions.

This paper presents a practical assessment of the quality and performance of hydro powered resin bolting at an intermediate to deep-level hard rock platinum mine in South Africa.

Background

The study site is located on the northern end of the western limb of the Bushveld Igneous Complex in South Africa, operating at depths up to 2400 m below surface. Conventional drill-and-blasting techniques are used to access and extract platinum group metals from both UG2 and Merensky reef deposits. Multi-reef mining strategies are deployed with de-stressing taking place on the Merensky Reef horizon, situated approximately 20 m to 40 m above the UG2 Reef horizon. Given the relatively low middling between the UG2 and Merensky Reefs, both ore bodies are extracted using the same primary tunnel development. Both orebodies dip at approximately 20° towards the south-east.

Haulages, orientated along the strike of the ore body, are typically off reef and situated in the footwall of the UG2 Reef horizon. Crosscuts, orientated along the dip of the ore body, are broken away from haulages and are for the most part off-reef. These crosscuts are developed up to Merensky and/or UG2 reef intersections, followed by the development of on-reef raises to the level above. A layered sequence of these access ways (~63 m vertical middling) is repeated to expose the entirety of the ore body.

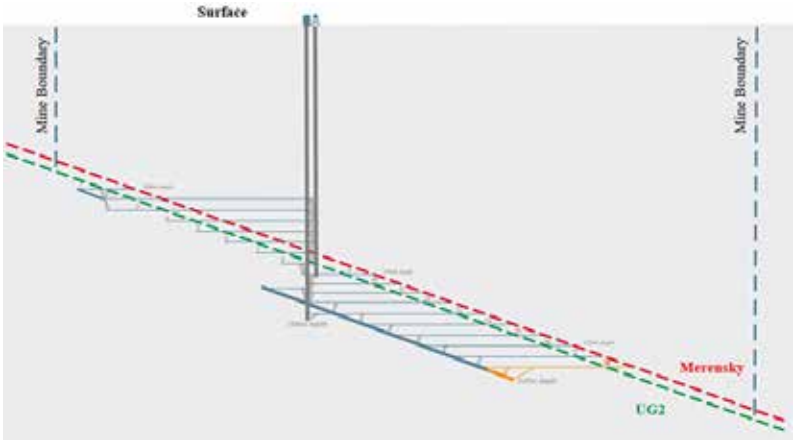

Figure 1—Dip cross-section of the case study mine

Considering the inter-level distance between haulages or crosscuts and the dip of the ore body, raise lengths up to 180 m can be effectively established, allowing for six stoping panels on each side of the raise at an average face length of 30 m.

Resin bolts are installed as primary and secondary support at the case study mine. Primary support implies that it is installed to secure the immediate stability of an excavation as it is being developed or mined, whereas secondary support is installed to secure the long-term stability of an excavation. Resin bolts, as primary support, are installed along the hangingwall of stoping centre gullies, stoping strike gullies, as well as the hangingwall and sidewalls of tunnels during development. Resin bolts, as secondary support, are installed in crosscuts and haulages where initially installed support has corroded (i.e., rehabilitation).

The case study mine experienced several rockfalls where resin bolts were installed, especially near the skin of the excavation. Once fallout has taken place and the fractured zone around the excavation has unravelled, the section of the resin bolt towards the collar of the support hole was exposed (refer to Figure 2). Of concern was that the bottom section of the resin bolts was not encapsulated in resin. In addition, most resin bolt installations were not tensioned (i.e., shear pins still intact), resin capsules were gloving inside support holes, and resin bolt installations were not centred inside support holes.

Rock mass behaviour

To better understand the role and performance of resin bolting at the mine, it was necessary to study the geotechnical environment in which the resin bolts are installed. The principle of resin bolting at the mine is a combination between suspension and rock reinforcement. Resin bolts are long enough to penetrate the natural pressure arch and densely spaced to establish an artificial pressure arch within the fractured zone around the skin of the excavation (refer to Figure 3).

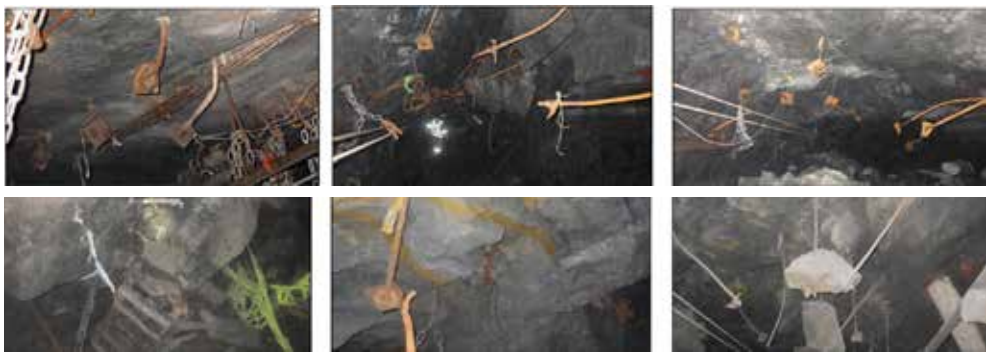

Figure 2—Instabilities recorded close to the skin of the excavation, exposing the proximal end of the resin bolt

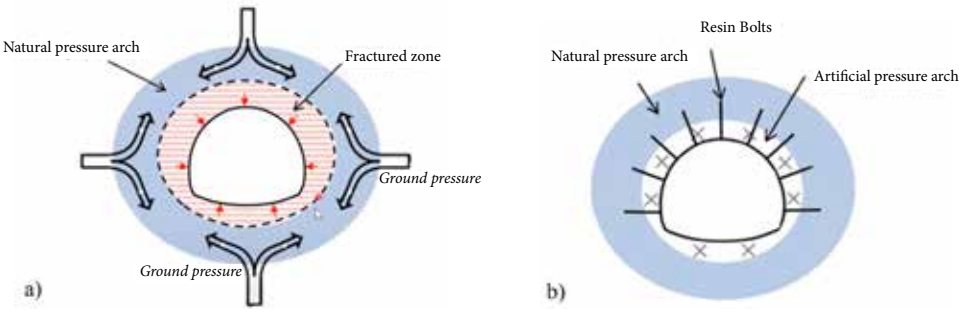

Figure 3—The principle of creating an artificial pressure arch using rock bolting (after Li, 2017)

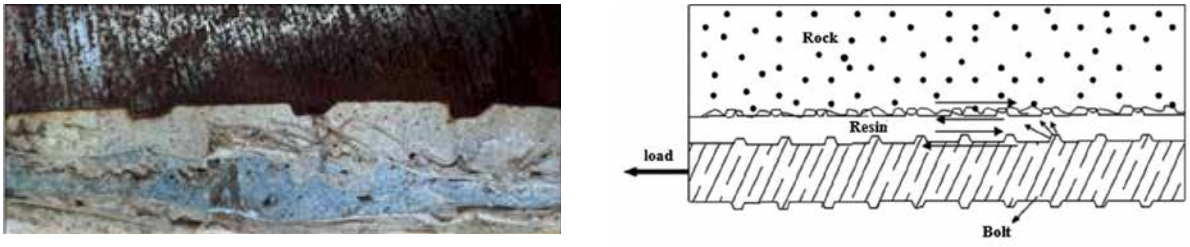

Figure 4—Partially over-cored resin bolt indicating the principle of load transfer through mechanical interlocking of surface irregularities

Figure 5—Transversal ribs are visibly still intact following unravelling of the surrounding rock mass

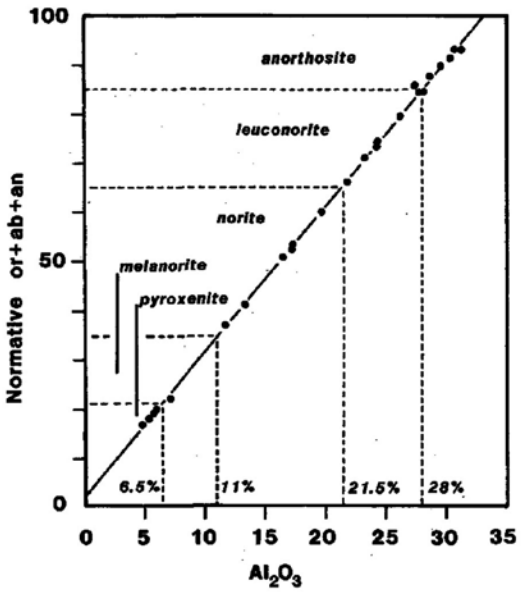

Figure 6—Terminology adopted for orthopyroxene-plagioclase rocks (after Eales et al., 1988)

During rock movement, predominantly from the fractured zone, resin bolts are dependent on the mechanical interlocking of surface irregularities between the resin, the bar, and the rock to successfully transfer load (refer to Figure 4). Load is transferred from the unstable or fractured rock mass to the resin bolt and then into the stable ground.

Load transfer capabilities are particularly inhibited when rock movement is not laterally constrained, e.g., when unravelling ensues following an initial rockfall, with little to no interlocking taking place between the surface irregularities of the resin, bar, and rock (see Figure 5).

Haulages are predominantly situated in norite, which is a type of igneous rock (layered intrusion), composed of plagioclase feldspar and pyroxene. This rock type has a uniaxial compressive strength ranging between 124 MPa and 173 MPa (Vogler, 1990). Uncontrolled rock falls in these areas are rare, despite challenges related to the installation quality of resin bolts.

Crosscut breakaways are also situated in norite, however, the tunnel transitions through different classes of norite as it develops up to the UG1 reef marker. The mine has different distinctions or field terms for norite depending on its content ratio and distribution of pyroxene to plagioclase feldspar (refer to Figure 6). The transition from norite to leuconorite is distinguished by feldspar distributed in a network of lighter colour veins, commonly referred to as 'Streepies' norite (shown in Figure 7). The transition from leuconorite to anorthosite is abrupt with distinct contacts.

Norite, supported by a strong network of plagioclase feldspar, is known to be prone to rock bursting due to its higher stiffness (Malki et al., 2024). To this end, rock drill operators have reported localised strain bursting at tunnel faces when 'Streepies' norite, leuconorite and anorthosite are exposed. The strain bursts are not severe, and no instances of typical rockburst damage have been recorded, however, strain bursting is followed by a notable regression in the condition of the excavation rock walls (comparing Figure 8 and Figure 9). Densely spaced fractures develop in the tunnel hangingwall, and when it is inadequately supported, especially close to the skin of the excavation, it can lead to fallout. Initially, potentially high

Figure 7—Plagioclase feldspar veins

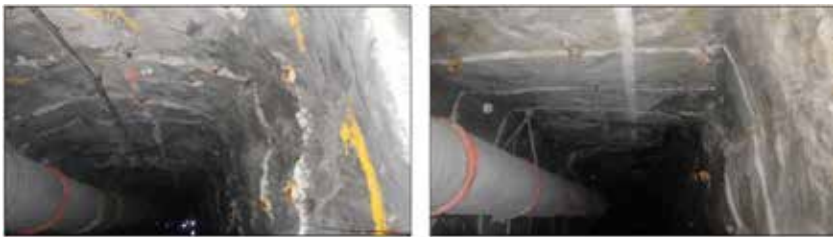

Figure 8—Good and competent hangingwall – crosscut situated in mela norite

Figure 9—Densely fractured hangingwall – crosscut situated in 'Streepies' norite

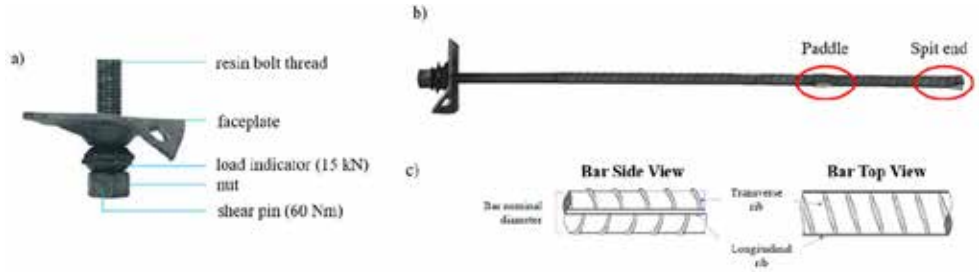

Figure 10—(a, b) Schematic of the proximal and distal ends of the resin bolt with (c) transverse and longitudinal ribs

horizontal stresses were considered as a contributing factor as fracturing was predominantly along the hangingwall of the tunnel, such as gothic arching described by Johnson et al. (2009), however, the effects were too localised and unaffected by regional mining abutments or major geological structures. It is rather suggested that the natural fracture initiation and propagation surrounding tunnels are adversely affected by the abundance of plagioclase feldspar. Rock masses dominated by plagioclase feldspar exhibit brittle behaviour, fracturing quasi-dynamically at depth and causing micro seismicity as fracturing propagates. At shallower depths, fracturing of these rocks occur over an extended period (quasi-statically), and its manifestation is curbed by the timeous installation of support (Nyungu et al., 2014).

Underground observations indicated that crosscuts broken away in a south-easterly direction experienced more ground control difficulties transitioning through 'Streepies' norite, leuconorite, and anorthosite than crosscuts broken away in a south-westerly direction. This phenomenon was attributed to stress-induced anisotropy considering that major and minor principal stresses (σ_1 and σ_3) act on crosscuts broken away in a south-easterly direction, whereas major and intermediate principal stresses (σ_1 and σ_2) act on crosscuts broken away in a south-westerly direction.

Actual underground observations provided valuable insights into the rock mass' behaviour and understanding the perceived underperformance of resin bolt installations.

Hydro powered resin bolting

There are several factors that can contribute to the under-performance of resin bolts. In 2005, Canbulat et al. tabled extensive quality control guidelines for underground resin bolting. This paper will focus on direct controllables impacting the performance of resin bolting at the case study mine.

Rock bolt parameters

Resin bolts or bars were originally produced according to SABS 920, now SANS 920:2011, which is still the national specification covering the physical and mechanical requirements for steel bars used in concrete reinforcement. As resin bolting became more prominent in underground mining support, mainstream manufacturing companies started developing improved resin bars in partnership with steel mills for more repeatable and consistent underground resin bolt installations. The latest version of SANS 920:2011 Edition 2.3 was released in 2022. SANS 1408 was also revised in 2019, stipulating the requirements and testing methods for resin bolt components.

The nominal diameter of a resin bolt used at the case study mine is 20 mm. It has a uniform and continuous rib that is parallel to the long axis of the bar (i.e., longitudinal rib) with several ribs across the long axis of the bar (i.e., transverse ribs), as indicated in Figure 10c. The ribs are geometrically controlled and designed to aid in the mixing of resin capsules, subsequently enhancing the load transfer capabilities of resin bolt installations.

The resin bolt has a modified section or paddle set, 40 cm long, situated at the distal end of the bar (refer to Figure 10b). The paddle set consists of three deformities, where the bar was pinched or compressed perpendicularly to the long axis of the bar, to effectively

Table 1

Resin capsule specifications

Property	Resin A	Resin B
Colour	Blue	Yellow
Capsule length	900 mm	900 mm
Capsule diameter	32 mm	32 mm
Resin mastic content	80,1%	80,5%
Pipeline viscosity	283 N	432 N
Set time	90 sec	280 sec
Punch shear strength	>23 MPa	>19 MPa

increase its diameter. Also situated at the distal end of the bar was an open split end. The bolt diameter at these modifications is 24 mm.

The resin bar has an ultimate tensile strength of 195 kN and a yield load in the range of 150 kN. The physical and mechanical properties of the bar are comparable to what is generally used in the rest of the South African mining industry.

Resin parameters

Resin cartridges or capsules are made up of two parts, that being resin and catalyst, separated by a thin plastic film. When a rock bolt is inserted and spun into a support hole, the plastic film is torn, and the two components mix, causing a chemical reaction and curing the resin mastic within a predetermined period. After curing has taken place, the resin is usually more rigid than the surrounding rock mass.

The case study mine utilises two different resin capsules for each support hole. Firstly, a blue resin capsule ('Resin A') is inserted into a support hole, followed by a yellow resin capsule ('Resin B').

Resin capsules are contained in water-resistant packaging and typically stored in humid conditions with temperatures up to 32 °C. Little consideration is given to the storage temperature and subsequent shelf life at the mine (refer to SANS 1534:2018), however, this does not imply that the resin capsules are not usable.

Rock drill parameters

Hydro-powered equipment was not commercially available when the mine started narrow tabular stoping in the late 1990s (Kendall et al., 2000). In partnership with the Chamber of Mines Research Organisation, the mine started to develop and adjust equipment

Figure 11—Comparison between the Novatek and Sulzer hydro power rock drills

to cater for the water powered system (i.e., hydro power). The primary benefit of the cooled water system was its ability to reduce the heat in underground workings as the geothermal gradient of the Bushveld Complex was higher than other deep level mines in the Witwatersrand Basin (Fraser, 2010). However, hydro power also provided the operation with the means to improve drilling efficiencies and productivity, which has indirectly benefitted resin bolt installations. The principle of hydro power, as far as drilling is concerned, is delivering more power to a rock drill in a pipe or hose than what is possible with compressed air (higher pressure).

The loaded rotation speed of the rock drill was measured during the spinning process using a tachometer (refer to Figure 12). When a rock drill is loaded, frictional forces resist the free and synchronous rotation of the spinning adapter. In practise, rotation speeds decreased by up to 50% from the specified unloaded rotation speeds.

Installation process

The installation process outlined in the following is based on the mine's safe operating procedure and over inspection/verification of actual installation practices (work-as-prescribed versus work-as-imagined versus work-as-done):

- Entry examination and safe declaration (including the application of a Trigger Action Response Plan) is conducted before any work takes place.
- Once the area has been dressed and declared safe, temporary support (e.g., mechanical jacks) and areal support (e.g., safety netting or mesh sheets) are installed.

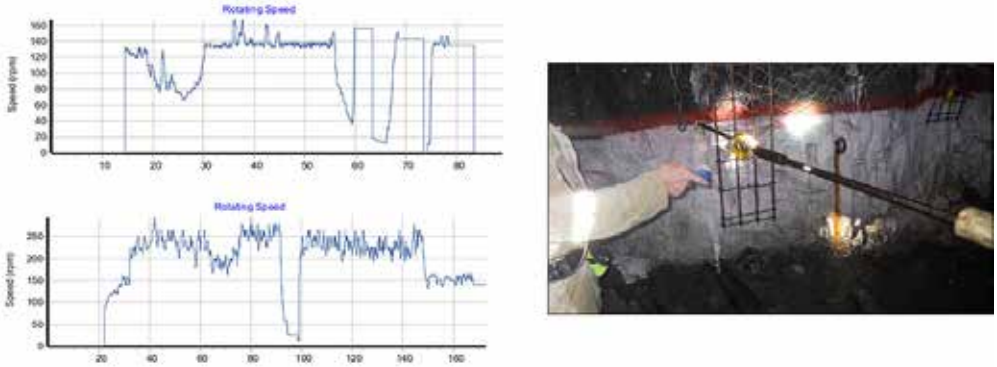

Figure 12—Unloaded and loaded rotation speeds

- From a safe and supported position, the responsible competent person demarcates the position where resin bolts need to be installed.
- Support holes are drilled to their required length, not less than 70º to excavation rock surfaces. All support holes are drilled under the cover of areal support.
- As soon as the support holes are flushed, resin capsules are inserted into the support holes. The quick set (i.e., blue cartridge) capsule is inserted, followed by the slow set (i.e., yellow cartridge) capsule.
- To retain resin capsules inside support holes, top hats are supplied with each container or box. Operators dislike using top hats and instead use cut-offs from resin containers as a wedge at the collar of support holes.
- Once the resin capsules are secured, the resin bolt is pushed into the support hole by hand, far enough so that the bar can be placed in the rock drill's bolt tensioning socket (spinning adaptor).
- Using the rock drill, the bar is pushed further into the support hole with aid from the thrust leg, as deep as practically possible.
- The rock drill valve is completely opened allowing for maximum potential thrust and torque, mixing for at least 15 seconds. During the spinning cycle, the inner barrier sheath and outer sheath are torn by the bar, allowing both the catalyst and resin mastic to mix. The spinning process also generates heat, which aids the chemical process taking place (polymerisation). Considering the rotation speed of the rock drills, the bar will rotate between 22 and 32 times inside the support hole.
- After the spinning cycle, a hold time of 120 seconds is observed. During the holding period, the mixed resin mastic is curing to build up strength. The operator keeps the resin bolt in place with the rock drill, followed by the tensioning process, however, most installations are left un-tensioned.

Support hole length and annulus

The bond strength of resin bolts is often constrained by the relationship between the resin bolt and support hole diameter, known as the annulus (Hagan, 2003). Effective mixing of the resin is typically achieved by ensuring the resin annulus does not exceed a specified maximum limit. The intention of modifications (e.g., paddles and split-end) to the resin bar is to increase the diameter of the resin bolt over the modified section, which decreases the annulus between the bolt and rock interface. This fundamentally increases the bond strength of the installation by providing improved mixing of the resin and catalyst up to the boundary of the support hole. However, this only applies to the section of the bolt that includes modifications.

In 2019, Bierman et al. conducted a large-scale evaluation on resin bolt installations. The paper indicated that Ø 38 mm support holes were possible using Ø 34 mm drill bits, which was initially confirmed by Tadolini (1998). Many factors can impact the hole diameter, such as the condition of the rock drill, available water pressure, age and wear on the drill bit, as well as adherence to drill bit discard criteria. Similar to the findings by Bierman (2019) and Tadolini (1998), Ø 42 mm support holes were measured at the mine where Ø 38 mm drill bits were used. Geotechnical designs rarely consider this phenomenon, resulting in hole annuluses exceeding design limits and a reduction in resin encapsulation (refer to Figure 14).

The diameter and length of resin capsules inside a support hole are important because of the resin requirements for full encapsulation. Equally important is the length of support holes when they are drilled. Maepa and Zvarivadza (2017) recorded 'under- and over-' drilling of support holes during a study that was conducted in the Bushveld Complex. In the study, support holes were within 0.1 m of the designed length. Similarly, support hole lengths at the case study mine ranged between 1.7 m and 1.9 m against the designed length of 1.8 m. The deviance may not be considered extreme; however, it directly impacts the extent of resin encapsulation inside the support hole. The correct resin bar diameter and support hole diameter are critical to ensure that sufficient resin is used to form a fully bonded or full encapsulated installation.

Gloving

Resin mastic and catalyst need to be properly mixed for it to be

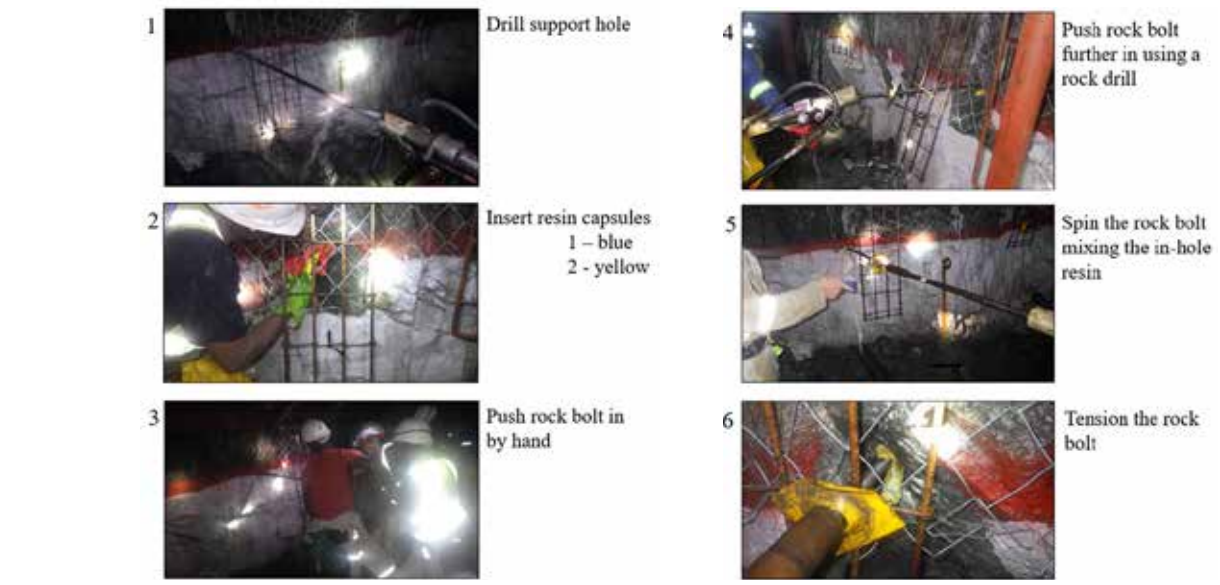

Figure 13—Simplified resin bolt installation process. A holding period of 120 seconds is observed between the mixing and tensioning processes

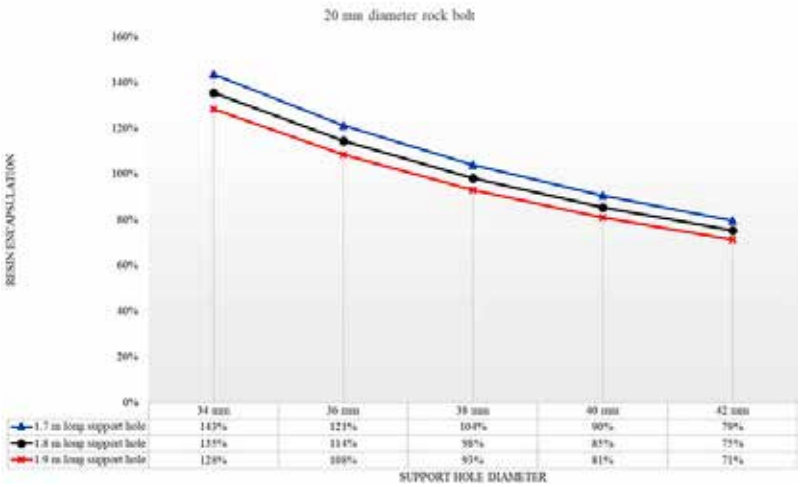

Figure 14—Percentage resin encapsulation as a function of the support hole diameter and length

effective. Installations with large annuli are more prone to be compromised resulting in gloving. Gloving occurs when the resin mastic and/or catalyst film was not pierced during the spinning process, preventing the components from mixing and ultimately the resin from curing (Pastars et al, 2005).

The installation procedure of the mine dictates that resin bolts should be driven halfway into support holes before spinning takes place. In practise, another variation was found where operators drive resin bolts to the back of support holes before spinning. As a result, the mixing of the slow set capsule was questionable, considering that the modified resin bolts used at the mine only had one set of paddles at the distal end of the bar (last 40 cm). In principle, the 'unmodified' portion of the 20 mm diameter bar was solely responsible for mixing the slow set resin for annuli up to 11 mm. Overspinning of resin capsules was not prevalent at the mine, however, the under-spinning of capsules did indicate a trend resulting in gloving and inadequate mixing.

During the investigation process into gloving, it was also discovered that the condition of the installation tool played an important role in the mixing of the resin capsules. When the installation tool was worn, on either side, the rock drill was unable to grip the resin bar. In these cases, the resin bolt was merely hammered into the support hole and no mixing took place, as shown in Figure 16. Visually, these defects are difficult to identify. Historical pull test data gathered from development tunnels indicated that significant gloving led to a reduction in bond strength, with pullout loads as low as 57% of their designed strength.

Annulus is typically not a concern at underground coal mines as these operations are accustomed to using small diameter drill bits (Campbell et al., 2004). However, for many underground hard rock mines using conventional equipment, an additional set of drill bits is required. This inadvertently introduces a safety risk as human behaviour (i.e., discipline) directly impacts the reliability and performance of the support system.

Centralisation

Crompton and Sheppard (2019) reported that the centralisation of a resin bolt inside a support hole encouraged the consistent mixing of resin, maximised the corrosion protection provided by resin, and

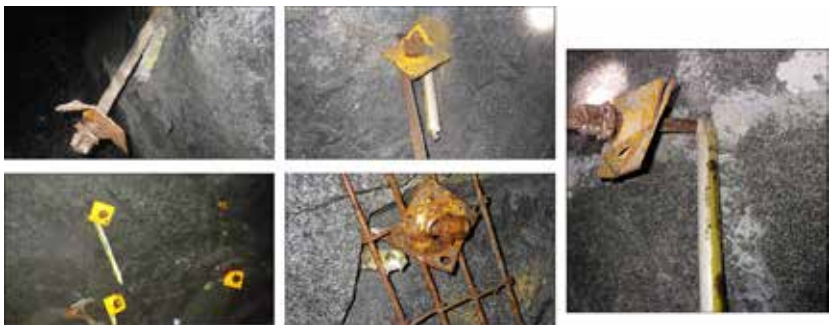

Figure 15—Gloving resin bolt installations

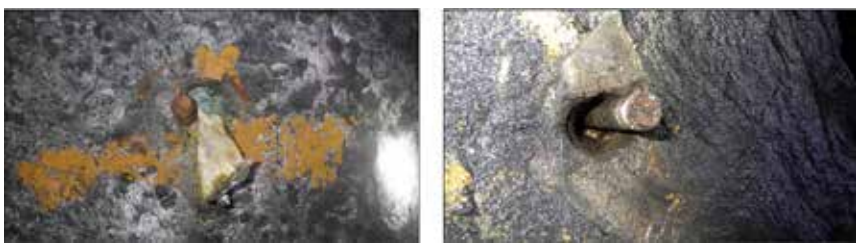

Figure 16—Wear and tear on both ends of the installation tool

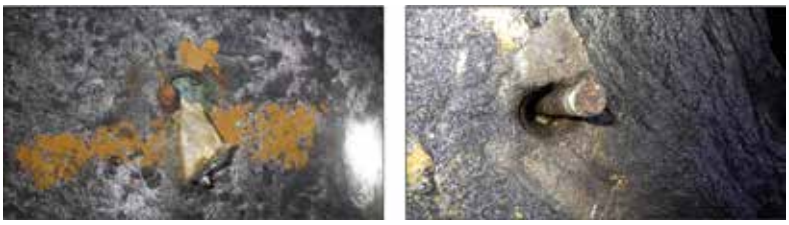

Figure 17—Off-centre resin bolt installations

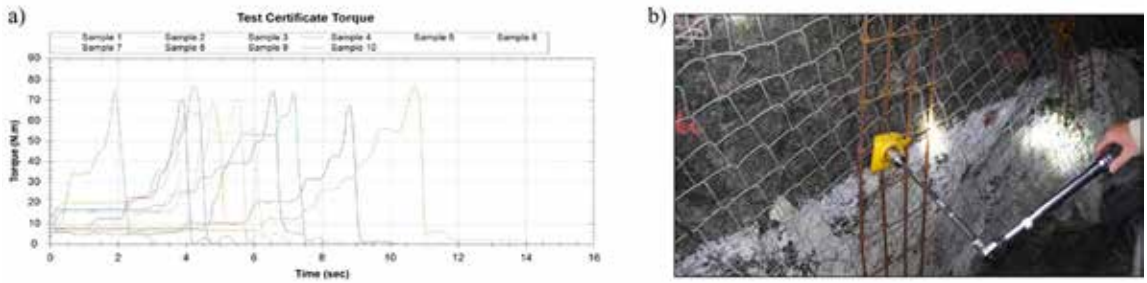

Figure 18—(a) Torque – time performance of shear pins, and (b) a torque wrench used to determine the load at which the shear pins break

ensured the even distribution of stresses during tensile loading. Resin bolt installations that were off-centre had an increased likelihood of gloving, unmixed resin, and voids. Numerous resin bolt installations at the case study mine were off-centre to the critical determinant of support capacity (see Figure 17).

Shear pin

Shear pins connect the rotating nut and bar at their threaded end. These pins are mechanically designed to break when a predetermined force/load is exceeded. The case study mine utilises a 4.5 mm shear pin that fails between 60 kN and 90 kN, illustrating that the resin inside the support hole has cured and that the tensioning process has been initiated.

Spanner tests were conducted on underground installations to verify that the shear pins in the nuts failed at their designed torque (refer to Figure 18b). A total of 40 tests were conducted, 20 tests on 30-day old installations and an additional 20 tests on the same day of installation. Shear pins on 30-day old installations failed at an average torque of 118 N.m (standard deviation of 15 N.m), whereas shear pins tested on the same day of installation failed at an average torque of 73 N.m (standard deviation of 5 N.m). It is believed that corrosion may have contributed to the increase in failure load of shear pins on the 30-day old installations.

Load indicator

Load indicator washers have been around since the early 1960s. These washers are situated between the nut and faceplate to visually represent the clamping force or preload during the tensioning process. Tensioning of resin bolts provide clamping forces into the surrounding rock mass, critical to rock reinforcement and effective skin control. The case study mine utilises a 40 mm x 2 mm load indicator that collapses at 15 kN, illustrating the tension applied between the rock bolt faceplate and nut.

Corrosiveness

The prevalence of gloving not only impacts the bond strength of resin bolt installations, but it also detrimentally affects the corrosion protection of the resin bar. Fully encapsulated resin bolts offer excellent protection from corrosion, however, poor mixing during resin bolt installations and resultant voids expose the bar to corrosive elements.

Resin bolting applications in hard rock mines tend to undervalue the importance of faceplates. Faceplates typically have smaller dimensions compared to other rock bolting applications, and based on industry practices or norms, do not require replacement or re-tensioning after the resin mastic has cured. The need to re-tension or replace faceplates is one of the most discussed topics in resin bolting. It is thought that if the resin inside a support hole is properly mixed, cured and the bar is fully encapsulated in resin, the resin bolt installation can transfer load along its entire length. Unfortunately, these underlying assumptions cannot be verified unless the resin bolt installation was personally inspected, which is not practically feasible. Observations at the case study mine strongly suggest that faceplates are a vital component for effective

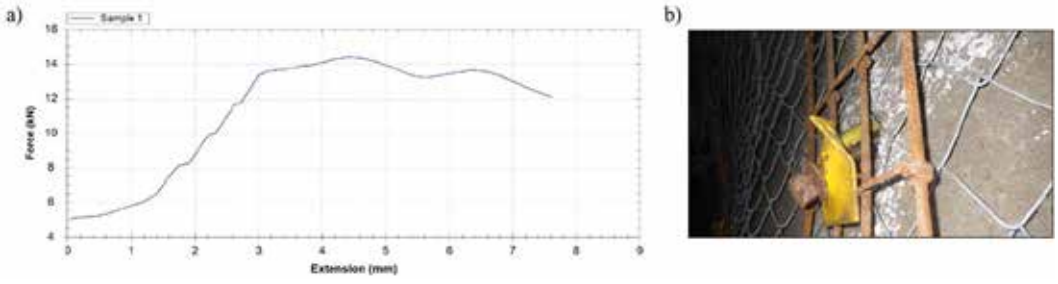

Figure 19—(a) Load – deformation graph of load indicators, and (b) a collapsed load indicator against a mesh strap

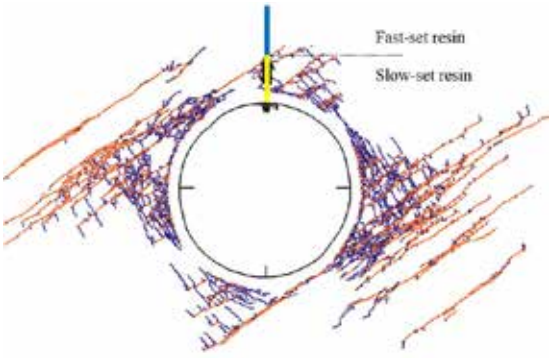

Figure 20—Simplified cross-section showing the slow set resin capsule (i.e., yellow capsule) in the fractured zone around an underground tunnel

skin control, especially in highly discontinuous rock masses. In addition, the faceplate should not be analysed in isolation, as in most cases, it forms part of a greater support system. For example, resin bolt faceplates are integral to the overall performance of the greater support system where interaction with areal support elements is prevalent, such as mesh and/or shotcrete (Gouvea, Du Plessis, 2022).

Underground testing

Rock falls recorded at the mine were predominantly close to the excavation surface. As a result, full-scale underground testing was conducted to determine the ability of resin bolts to transfer load close to the skin of the excavation.

Methodology

Based on the depth of fracturing and historical fallouts recorded at the mine, it was evident that the yellow cartridge or slow set resin capsule was situated in the 'unstable' fractured zone surrounding excavations (refer to Figure 20). It is therefore crucial that the proximal end of the resin bolt is encapsulated in resin and tensioned for effective skin control and load transfer. Underground pull testing was conducted to quantify the load transfer capabilities of resin bolts for the section of the bar encapsulated in slow set resin.

Considering that fallout heights were limited and close to the skin of the excavation, in addition to the configuration of the resin bolt favouring mixing at the distal end of the bar, there was no evidence to question the encapsulation or performance of the fast-setting resin.

Test setup and parameters

The Novatek MK5 rock drill was used to drill support holes and install resin bolts at the underground test site. The performance and specifications of the Novatek rock drill were comparable to those of the Sulzer, hence only one rock drill was used during testing. Support holes were 1.8 m long, drilled using both Ø 34 mm and Ø 38 mm drill bits.

A 900 mm x 32 mm inert resin capsule was inserted into the support hole, followed by a 900 mm x 32 mm slow set resin capsule (refer to Figure 21). Inert resin capsules are chemically inactive as their catalyst component has been removed. As a result, the bonding strength of the resin bolt installations relied entirely on the section of the bar encapsulated by slow set resin. Inert resin capsules were specially manufactured for these tests, as removing the catalyst from existing cartridges reduced their rigidity, causing them to bend or flop.

Two different installation practices were observed at the mine where resin bolts were driven halfway into support holes before spinning took place, and where resin bolts were driven to the back of support holes before spinning. In addition to these practices, a third variation was tested where resin bolts were mixed starting from the collar of the support hole (see Figure 22). The spinning cycle of 15 seconds was measured from the point at which the resin bolt came into contact with the inert resin capsule (during spinning).

Five resin bolts were installed and tested per variation. Pull testing was conducted on the installed resin bolts 24 hours after they were installed, amounting to a total of 30 tests. Pull tests were

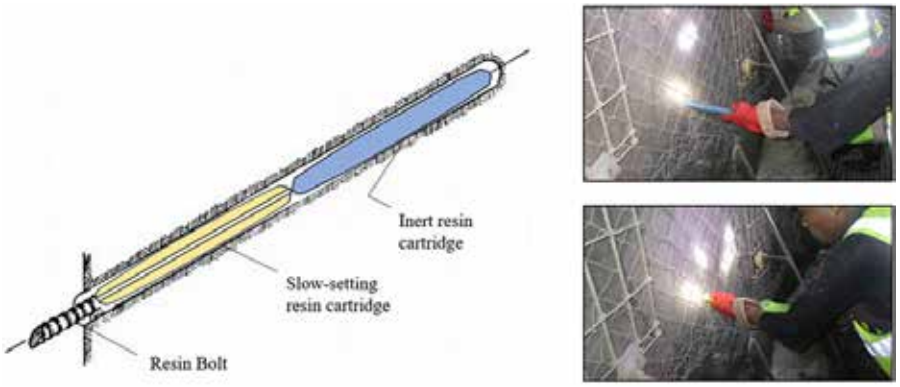

Figure 21—Resin sequence and setup during testing

Figure 22—Testing process map

Figure 23—Underground pull testing

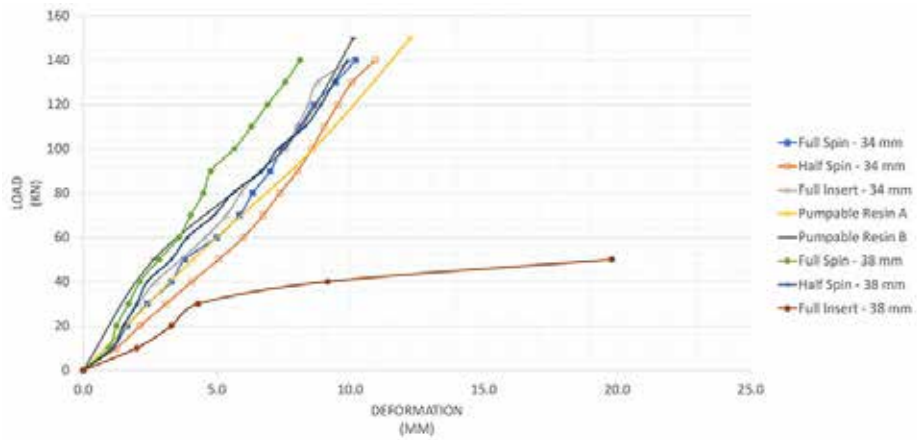

Figure 24—Load vs. displacement graph (mean of five tests per combination)

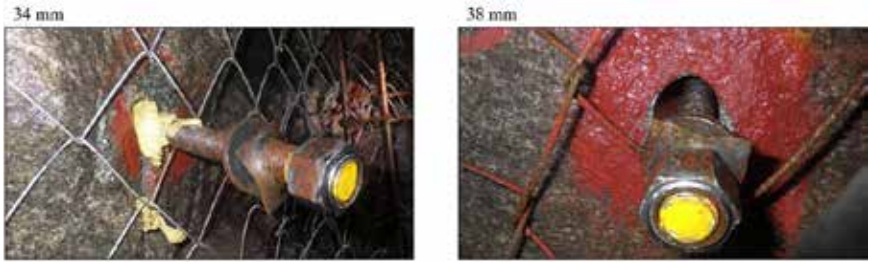

Figure 25—Resin outflow comparison between a Ø 34 mm and Ø 38 mm support hole

conducted up to 140 kN, as the resin bolt yield load was 150 kN, measuring deformation at 10 kN intervals. Measuring deformation with a vernier in this application was challenging due to the confined space between the pull test frame and the hydraulic ram.

Test results

Figure 24 shows the results of the pull tests that were conducted. 'Pumpable Resin A' and 'Pumpable Resin B' were added to the graph for comparative purposes. These two variations were tested at a deep-level gold mine using pumpable resin with similar hole annuli.

Test results indicated that the bond strength of resin bolt installations was mostly unaffected for hole annuli up to 11 mm. The only records of premature pullout were recorded where a Ø 38 mm drill bit was used, and the bar was inserted up to the back of the support hole before spinning. The stiffness of the resin bond was strikingly high for all stable results, indicating the resin's ability to prevent the opening of discontinuities.

Visually, resin was flowing from the support hole collar where a Ø 34 mm drill bit was used (see Figure 25). On average, the bottom 35 cm of the support hole towards the excavation skin was not encapsulated in resin when a Ø 38 mm drill bit was used (81% of the bar encapsulated in resin). While the effects of gloved but mixed resin inside most Ø 38 mm support holes may be minimal on bond strength, the debonded section of the resin bar close to the excavation surface offers no reinforcement or support and exposes the resin bar to possible corrosion.

Test results showed that resin bolt installations using Ø 38 mm drill bits were not fully encapsulated in resin and were therefore entirely reliant on the face plate for load transfer near the skin of the excavation. Considering that most resin bolt installations at the mine used Ø 38 mm drill bits, a comprehensive strategy is required to address the loss of load transfer capabilities and clamping in the fractured zone surrounding excavations.

Traditional pull testing, which is the primary underground quality control method for South African mines, failed to identify that resin bolt installations using Ø 38 mm drill bits were defective (i.e., not fully encapsulated in resin). This is an inherent flaw in current quality assurance systems across the country that poses a significant fall of ground risk, as evidenced by actual uncontrolled rockfalls between resin bolts at the case study mine. In its current state, defects related to encapsulation and load transfer capabilities are unfortunately only detected after a fall of ground has taken

place. Additional quality control or quality assurance measures are needed to determine the extent of resin encapsulation in a support hole to effectively identify defective resin bolt installations.

Non-destructive testing

There has been an increase in research efforts in the field of non-destructive testing to assess the encapsulation of underground resin bolts. Bačić et al. (2019) provided a useful overview of non-destructive testing methods available in the industry, indicating that rock bolt testing has taken a direction towards instrumentation with sensors. Many acoustics-based or vibration-based methods take advantage of modern sensor types such as piezoelectric sensors, optic fibres, etc. Additionally, modern signal processing tools, as well as other advanced computing systems such as neural networks, further open doors to the continuous development of non-destructive methods.

Hassell et al. (2019) conducted a series of non-destructive tests using a hammer blow to create a seismic source and a transducer to detect the resultant vibrations. These recordings were then interpreted to provide an estimate of bolt length and a qualitative assessment of encapsulation quality.

A total of 56 cable bolts and 58 solid bar bolts were tested at an underground site in Australia to validate the testing technique. The diagnosis of void spaces (regions of lack of bonding) was seen as crucial and was successfully trialled. A similar non-destructive testing method was presented by Godfrey et al. (1977). The historical testing method measured the vibration response of a rock bolt to broadband axial and/or transverse vibrations induced by striking the collar end of a rock bolt. The resonant frequencies of a partially encapsulated rock bolt were different from those of a fully encapsulated rock bolt and were interpreted to give the degree of bonding between the resin and rock bolt and the axial extent of a void.

In 2023, Staniek also reported on an experimental non-destructive method to test for the full encapsulation of rock bolt installations. The method, which uses modal analysis procedures, is based on impact excitation (i.e., impact hammer) where the natural frequency of rock bolts is compared to rock bolts installed underground. The method was successfully applied over two years, having tested 70 rock bolts with a length up to 2.5 m.

Destructive testing techniques, such as overcoring, are predominantly used in the mining industry to assess the encapsulation of resin bolts (Craig, 2012), however, these methods are relatively expensive and laborious. Notwithstanding the challenges associated with non-destructive testing techniques, it provides vital insights into the encapsulation of resin bolts.

Conclusions

The data presented in this paper illustrate the limitations that pull testing has, as the primary quality control or quality assurance testing method, to identify defective resin bolt installations. Traditional pull testing is a measure of bond strength; however, it fails to quantify or qualify resin encapsulation along the entire length of the resin bolt. Load transfer capabilities of resin bolts are primarily dictated by encapsulation and are critical to the success of a resin bolting support system. Non-destructive test methods need to supplement traditional pull testing to determine the extent of resin encapsulation and effectively identify defective resin bolt installations.

Despite the use of hydro-powered equipment, the installation quality of resin bolts was overdependent on the practices and actions of underground operators. The fundamental reliance on human behaviour to install resin bolts that are free from defects or significant variations is unfitting. Elimination, substitutive, and engineering controls (i.e., hierarchy of controls) should be considered to reduce the probability or impact of potential rock falls. The expected quality of resin bolt installations must be considered in their design to ensure robust support. The paper further signifies the importance of purposeful monitoring and over inspection of actual underground support installations (e.g., planned task observations and visible field leadership), ensuring that support products used at the mine are designed and operated in a manner that enhances health and safety (Mine Health and Safety Act, 1996).

Acknowledgements

The authors would like to thank Mr N Fernandes (Northam), Mr J Jordaan (Minova), Mr P Henning (Videx Mining Products), Mr A Piroddi (RSC Ekusasa Mining) and Mr M Pieterse (New Concept Mining) for providing the material and equipment in this study as well as for their valuable insights.

References

Bačić, M., Gavin, K., Kovačević, M.S. 2019. Trends in non-destructive testing of rock bolt. *Građevinar*. vol. 10, pp. 823–831.

Bierman, I.R., Gardner, L., Piper, P. 2019. An evaluation of the bond strength of multiple resin bolt and capsule combinations through laboratory testing and applied methodologies, *The Southern African Institute of Mining and Metallurgy. Deep Mining Conference*, Muldersdrift, South Africa.

Campbell, R., Mould, R., MacGregor, S. 2004. Investigation into the Extent and Mechanisms of Gloving and Un-mixed Resin in Fully Encapsulated Roof Bolts. *Coal 2004: Coal Operators' Conference, University of Wollongong & the Australasian Institute of Mining and Metallurgy*, pp. 203–214.

Canbulat, I., Wilkinson, A., Prohaska, G., Mnisi, M., Singh, N. 2005. An investigation into the support systems in South African collieries, *Safety in Mines Research Advisory Committee*. SIM 020205, pp. 180–193.

Craig, P. 2012. Addressing Resin Loss and Gloving Issues at a Mine with Coal Roof. *Proceedings of the Coal Operators' Conference,* pp. 121–129.

Crompton, B., Sheppard, J. 2019. A practical design approach for an improved resin-anchored tendon, *The Southern African Institute of Mining and Metallurgy. Deep Mining Conference*, Muldersdrift, South Africa.

Eales, H.V., Fields, M., De Klerk, W.J., Scoon, R.N. 1988. Regional trends of chemical variation and thermal erosion in the Upper Critical Zone, Western Bushveld Complex, *Mineralogical Magazine*. vol. 52, pp. 63–79.

Ferreira, P.H., Franklin, D. 2008. Resin bolting in South Africa platinum mines with a focus on development and stoping operations, *The 3rd International Platinum Conference*, pp. 113–122. The Southern African Institute of Mining and Metallurgy.

Fraser, P. 2010. Hydropower: Achievements, Opportunities and Challenges, Rise of the Machines - The 'State of the Art' in Mining Mechanisation, Automation, Hydraulic Transportation and Communications. *The South African Institute of Mining and Metallurgy*.

Godfrey, D.E., Kuchar, N.R. 1977. Method of testing the integrity of installed rock bolts. United States Patent US4062229A.

Gouvea, J.P., Du Plessis, M. 2022. Establishing a testing criterion to relate the in-situ performance of static and dynamic capable mesh. *Proc. RaSim 2022*, Tucson, USA.

Hagan, P.C. 2003. The effect of resin annulus on anchorage performance of fully encapsulated rock bolts, P*roceedings of the 10th Congress of the International Society of Rock Mechanics.* Sandton, South Africa.

Hassell, R., Ji Gang, Z., Ming, Z., Hawkes, M. 2019. Quantifying the Quality of Cable Bolt Installation by Acoustic Testing. *The Australasian Institute of Mining and Metallurgy*, Melbourne.

Johnson, R.A., Priest, G., Singh, S. 2009. Shotcrete as an integral component of the excavation and support of flat arch profiled tunnels in high horizontal stress conditions in Bushveld Complex Mines, *Shotcrete for Africa Conference.* pp. 221–236.

Kendall, R.J., Gericke, M. 2000. Mechanization in stoping narrow tabular orebodies, *The Journal of the South African Institute of Mining and Metallurgy*.

Li, C.C. 2017. Rock bolting: Principles and Applications. ISBN 978-0-12-804401-8. Butterworth – Heinemann, *Elsevier*, pp 286.

Maepa, T.G., Zvarivadza, T. 2017. Installation of resin-grouted rock bolts in hard rock mining: challenges and solutions for improved safety. *The Journal of the Southern African Institute of Mining and Metallurgy*, vol. 117, pp. 334.

Malki, J., Vennes, I., Rowe, C.D., Mitri, H.S. 2024. Evaluation of Rock Burstability with Mechanical Property Testing and Microscopic Image Analysis, *Journal of Rock Mechanics, and Rock Engineering.*

Nyungu, D., Stacey, T.R. 2014. Time-dependent tensile strengths of Bushveld Complex rocks and implications for rock failure around mining excavations, *The Journal of The Southern African Institute of Mining and Metallurgy*. vol. 114, pp. 765–772.

Pastars, D., MacGregor, S.A. 2005. Determination of load transfer characteristics of gloved resin bolts from laboratory and in situ field testing. I*n Proceedings of the 24th International Conference on Ground Control in Mining.*

Staniek, A. 2023. Technical problems and non-destructive testing of rock bolt support systems in mines. *International Journal of Coal Science and Technology.*

Tadolini, S. 1998. The Effects of Reduced Annulus in Roof Bolting Performance, *International Conference on Ground Control in Mining*. pp. 230– 236. ◆

Rockburst risk management in deep hard rock mines: A multi-tiered approach with dynamic ground support as the last line of defense

by B. Simser[1]

Affiliation:
[1]Glencore Sudbury Operations, Canada

Correspondence to:
B. Simser

Email:
Brad.Simser@glencore.ca

Dates:
Received: 30 Jun. 2025
Published: November 2025

How to cite:
Simser, B. 2025. Rockburst risk managment in deep hard rock mines: A Multi-tiered approach with dynamic ground support as the last line of defense. *Journal of the Southern African Institute of Mining and Metallurgy*, vol. 125, no. 11, pp. 649–660

DOI ID:
https://doi.org/10.17159/2411-9717/KN05/2025

This paper is based on a presentation given at the AfriRock Conference 2025, 21-23 July 2025, Sun City Resort, Rustenburg, South Africa

Abstract

Rockbursting around underground excavations continues to be a core risk for many deep mining operations. Numerous advancements in mine design, preconditioning, monitoring, mining equipment, exclusion zones, and ground support have significantly lowered the risk to mine workers. As mining continues in deeper, more challenging environments, a multi-tiered approach to rockburst risk mitigation, starting with mine design, is required. Both the overall mine sequence, for example, avoiding converging mining fronts, and local design "stick handling" can play an important role in risk reduction.

Rockburst case studies dating back to the late 1990s up until 2024 are used to highlight risk factors and risk mitigation (tactical and strategic). Examples from several deep hard rock mines are used, generally in high horizontal stress fields (k ratios 1.5 to 2), and strong brittle rock (> 200 MPa unconfined compressive strength). Mining induced stresses as well as high in situ stress due to depth are discussed. The context is Canadian mining, which typically has highly mechanised operations, large openings and equipment. Examples from a narrow vein mine and shaft sinking are also given because neither environment is simple to mechanise, highlighting the need for other risk mitigations.

A "sieve" analysis based on mine incident reports is used to show how a multi-tiered risk management plan can lower exposure to violent ground failures. A few incidents still make their way through the "sieve," indicating a need for further improvements. Thoughts on future/current developments, and their strategic importance are given.

Ground support is the last line of defence. The proliferation of multiple styles of yielding tendons and support systems has made many choices available to rock engineering professionals. Despite the increased availability of dynamic ground support components, there are still difficulties getting clean load transfer to bolts, determining support demand, monitoring loss of capacity over time/mining, and evaluating true system capacity.

Virgin development in deep high stress brittle rock can result in high strainburst exposure prior to any stoping operations. The mining process must reduce worker exposure to unsupported rockmasses. Successful preconditioning in a shaft sinking operation, the use of high early strength shotcrete, and mechanised equipment are also discussed.

Keywords

rockburst, rockburst risk management, deep mining, dynamic ground support

Introduction

Rockbursts in mining have resulted in safety and production challenges over the last century. As orebodies go deeper, and mining occurs in higher risk environments, mitigations for dynamic rockmass failures become increasingly important. Large magnitude seismic events (Counter, 2014; Jalbout, 2024; Mawson et al., 2022) continue to be difficult to manage. Their source mechanisms are often complex, and damage can be widespread. Many improvements have been made with respect to dynamic ground support systems, mechanised equipment, and mine design. Seismic monitoring systems are becoming better as computing technology improves, and implementation of longhole sensors (Butler, Simser, 2017) allows for early deployment and improved 3D coverage. The focus of this paper is on rockburst risk mitigation and its effectiveness. Robust ground support, and best practice mine design will limit the collateral damage from large seismic events.

The examples shown are from mines that typically record a few events greater than moment magnitude 2 per year, with variable rockburst damage from a few tonnes to a few hundred tonnes.

Mining methods varied from narrow vein cut and fill (underhand, overhand, drift and fill), narrow vein blasthole (upholes or downholes), and sub level open stoping with delayed backfill. Although the specific risk mitigations may not directly apply to all mining methods (for example caving, or narrow reef tabular mining), the principals of using mining strategies both on the global and local scale, reduced exposure, and robust ground support apply to all rockburst prone mines. Tunnel and shaft development examples are also used, which tend to be independent of the local mining method.

A multi-tiered risk mitigation strategy is required for deep mining. For example, even if a dynamic ground support system successfully contains rockburst damage, it is still much better not to have a worker in the area when it occurs. Conversely, even if workers can reliably be kept out of an elevated rockburst risk area, say by tele-remote equipment, the access is still required for removal of ore, or ventilation or other purposes. The exclusion protocol does not negate the need for rockburst resilient ground support.

Mine design is the first line of defence. It is well known that risk increases as mining fronts converge, whether on the scale of two tunnels approaching one another or independent mining fronts used for early ramp up of productive capacity. Underhand mining (top down with accesses under backfill) can create an independent mining front without converging on an existing one. Most of the man entry requirements are in the drilling/loading horizon of a stope; placing the access under engineered material that does not burst (cemented tailings backfill) can dramatically reduce exposure. Section 3 of this paper briefly shows a successful example of a sill pillar extraction between 1320 m and 1355 m below surface at a hard rock mine. Table 1 demonstrates a non-exhaustive list of strategies and tactics for rockburst risk mitigation and several of the items listed have specific examples in the body of the paper.

A simple rockburst model

Although there are many diverse types of rockburst mechanisms (Ortlepp, 1997), the simple model shown in Figure 1 is useful for both understanding risk and risk mitigation. The model represents homogeneous rock in a high horizontal stress field. A zone of stress-fractured material around the excavation is represented by the low stress contours, whereas stored strain energy is represented by the hot colours.

Table 1

Some rockburst mitigation strategies/tactics

Global Mine Design (some factors, not an exhaustive list)
- Overall design impacts risk profile
  - Converging mining fronts (e.g. sill pillars)
  - Yielding pillars (e.g. Primary/Secondary layouts at depth, mine 50% of reserve in low stress)
  - Chevron shape, leads/lags, bad geometries
  - Blast hole/bulk mining (more remote equipment) versus jumbo/hand-held mining (e.g. cut and fill)
- Local Mine Design
  - Mining under backfill
  - Developing through yielded and/or stress shadowed ground
  - Developing in less burst prone rock types, avoiding faults/dykes or crossing at shortest distance
  - Smaller openings less vulnerable than large openings

Exclusion
- Barricading old areas
- Seismic re-entry protocols
- Remotely operated equipment

Pre-conditioning
- Local scale (jumbo holes around development)
- Larger rockmass scale
  - Hydraulic fracturing
  - Choke blast patterns

Last line of defense – Ground Support
- Dynamic capacity
- Timing of installation
  - Earlier generally more effective
  - What portion of the cycle does it protect?
    - E.g. Face screening often only protects loading cycle

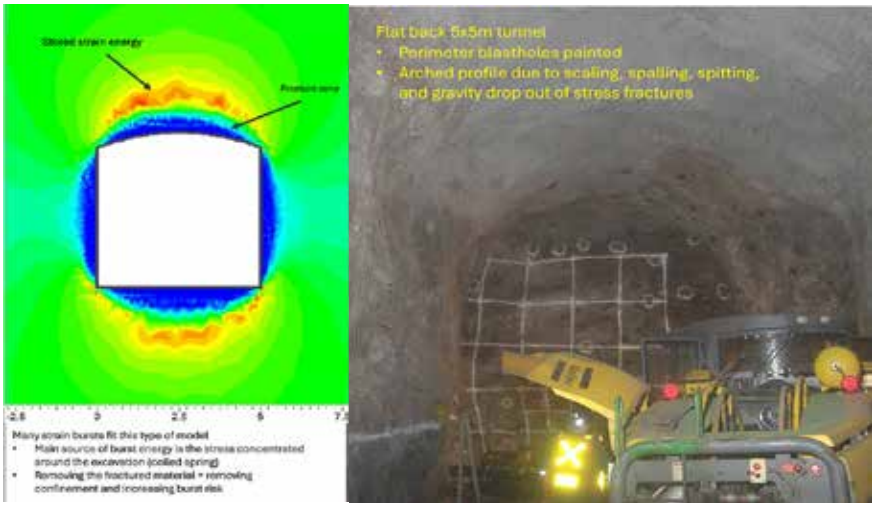

Figure 1—A simple model for strain bursts around tunnels. The locally stored energy/stress concentration around the excavation is often the source of the strain burst energy

Figure 2—Left: deep level (2490 m) shaft station excavation. The back was sprayed with rapid set shotcrete shortly after removing the blasted material. Right: view of intense stress fractures that were ahead of the previous advances face, exposed by the next advance (1400 m)

A dilemma for deep mining is that scaling or removal of the stress fractured material, reduces confinement and heads towards high stress concentration. In most cases this leads to more fractures forming, but in some cases, it may lead to violent bursting. The photo shown in Figure 1 initially had a flat back drilled profile, with gravity and bolter scaling resulting in a more stable arched shape. Strainburst risk increases as the confinement is reduced, so the trade-off becomes more dead weight (fractured material) on the ground support versus stored strain energy closer to the skin of the opening. Numerous factors affect the risk level: stronger rock can store more energy; deeper, increased extraction, and converging mining fronts all increase stress; standup time allows the fracture zone to dilate, loosen and more material is likely to fall out or be scaled out. Conversely ground support inhibits dilation, preserves confinement and lowers the strainburst potential.

The depth of fracturing around openings is a function of stress/strength. In strong, hard brittle rock (Figures 1 and 2), the process is time dependent. On the left side of Figure 2, the back was sprayed with rapid set shotcrete prior to bolting and screening. The early application of shotcrete provides confinement to the stress fractures forming around the opening (high horizontal stress, so fractures preferentially form in the back). In many shaft sinking operations, early development off the shaft barrel is completed by hand-held bolting and drilling. If the operator is spending time scaling out loose material, then exposure time increases, and the loss of confinement by removing the fractured ground increases strainburst risk. Although the shotcrete may not be sufficient for final excavation stability, it can contain the stress fractured material and preserve confinement. Field observations also show that if the heading gets hit later by dynamic loading, the shotcrete helps the outer layer of mesh and bolts by spreading the impulse load more evenly.

Although time-dependent failure in soft rock is well known (e.g., salt or potash), there can also be a significant impact in hard brittle rock when under high stress conditions. The right side of Figure 2 shows very intense stress fracturing that was ahead of the previous advances face. The depth and intensity of fracturing becomes more prominent the longer the face sits. In this example, that face was not advanced for approximately ten days 1400 m below surface with rock unconfined compressive strength of 250 MPa, and high stress conditions. Typical observations show limited face fracturing at this depth in similar rock types if the next advance occurs within a few shifts. At greater depths (~2500 m) in similar rock masses, observing increased stress fracture intensity and depth is common when development headings are not advanced for several days (Figure 3).

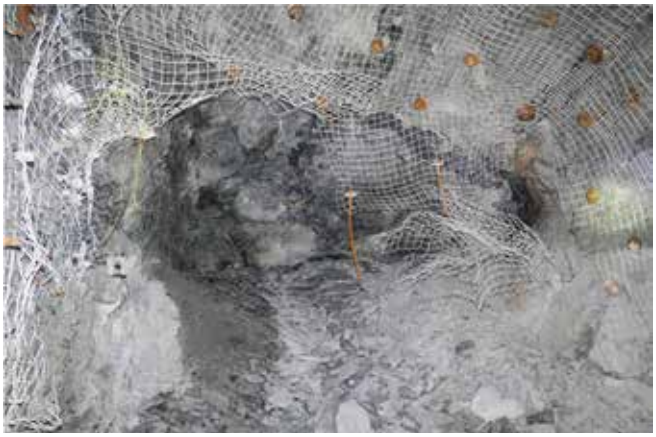

Figure 3—Fresh development round at 2490 m below surface in high horizontal stress (~1.5 x weight of overburden). Stress fractures from the back have dropped via gravity onto the blasted muck pile. The hanging mesh/friction sets were used to support the face prior to blasting

The case study of the shaft station in Figure 2 was successful because the schedule of shaft sinking is always very tight. The rapid set shotcrete was applied soon after the blasted material had been removed and could be bolted within one hour of application. Lateral development in the same rock types at the same depth has highly variable back overbreak and bolting times. In general, the longer the operators leave the new blast unsupported, the higher the overbreak and the longer the bolting time.

For precondition blasting, a similar model to that of Figure 1 is useful to target the "destress" zone. Hall et al. (2024) used precondition holes ahead of the planned break of a deep shaft sink. The intent was to target the stored strain energy based on the depth of fracturing observations. In the shaft sinking application, observed seismic activity increased as the blasted material was removed. The loss of confinement caused increased frequency of strainburst incidents (Figure 4). With the preconditioning holes and ensuring that the operator did not remove material past the planned break (no excessive scaling), the risk was reduced. The blasting pattern had to be customised for different rock types, as the depth of fracturing increases with weaker rock. Stemming of vertical holes is simple, and effective (gravity + gravel). This is not necessarily the case for lateral development where a lot of the preconditioning blast energy tends to rifle out the hole collar.

Reducing the "coiled spring" of stored energy near the skin of the opening is key to reducing the strainburst potential (Figure 5). However, this only partially addresses other rockburst risks such as fault slip or large-scale pillar bursts. By having an increased

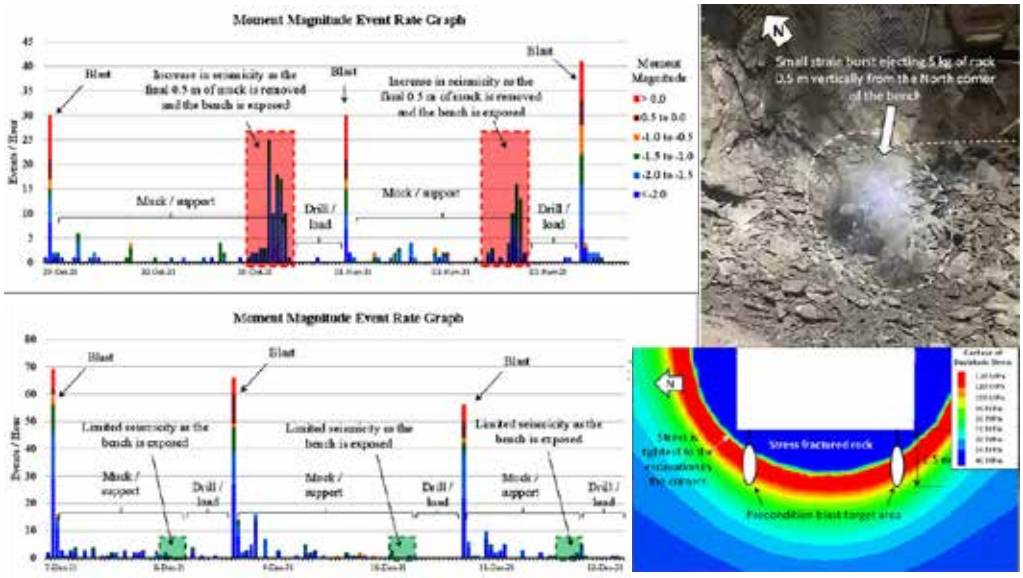

Figure 4—Top left shows seismic monitoring records for a deep shaft development cycle. Small magnitude events increase in frequency when the blasted rock is removed from the bench face (loss of confinement). This is when workers are normally checking for misfires and prepping for the next advance. By adding preconditioning blast holes, targeting the high stress zone ahead of the bench, and by NOT over scaling/mucking, the situation was alleviated. The lower left seismic records show no increased activity after the blasted muck was removed indicating successful preconditioning (Hall et al., 2024)

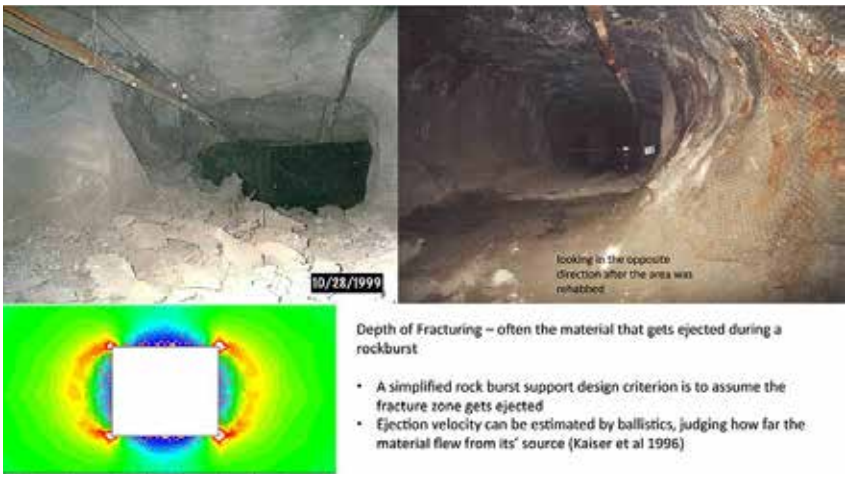

Figure 5—Left: wall burst material consisting of brittle rock, shotcrete and rebar. Shotcrete as the outer later has low deformation capacity. Right: same area after rehabilitation. This wall burst fits the simple model of the strain energy beyond the fracture zone being suddenly released (Simser, 2017)

"cushion" around the opening, knitted together by ground support, the impact of far field events may be dampened, but not necessarily eliminated. The far field event is often a good trigger to release the coiled spring (Simser, 2019).

Underhand mining

The use of excavations in backfill does not fit the simple model used in the aforementioned section. Backfill simply cannot store enough strain energy to generate rockbursts. Well engineered fill can be a safe place to be in the event of large magnitude seismicity (no coiled springs). The practice of underhand mining has been around for a long time (Pigott, Hall, 1961) and remains an effective risk mitigation for high stress mining.

Following, an example is shown from a sill pillar extraction at 1355 m below surface. The orebody was wide enough for three panels in the transverse direction (90 m total), with floor to floor spacing of 30 m. The original crosscut from the overhand mining was re-accessed by benching the floor and coming under cemented tailings backfill (hydraulic fill with unconfined compressive strength of about 2 MPa). Ground support consisted of fibre reinforced shotcrete, welded wire mesh, and expandable rockbolts.

During the mining of the third panel below the backfill, a large (moment magnitude 1.5) seismic event occurred in the stope crown after the first blast was taken. The standard practise at the mine was to take a ~30 000 tonne stope in two blasts using a 1.2 m raisebore as a slot. The first blast ("toe shot") trims the bottom of enough holes to get sufficient void for a final stope blast. For deep mining, the in-stope blasting sequence may need to be further altered to avoid shrinking an in-stope pillar, by daylighting to the overcut and slashing into the void for the final blast. This example highlights why that is a better method. Fewer blasting steps equate to lower worker exposure and better fragmentation. In this case the toes of the holes were fired first, creating a pillar between the overcut and the undercut (Figure 6).

The narrow span of the overcut (5 m) combined with ground support, and the ground motion dampening/attenuation role of the backfill reduced the potential rockburst damage. Some lower

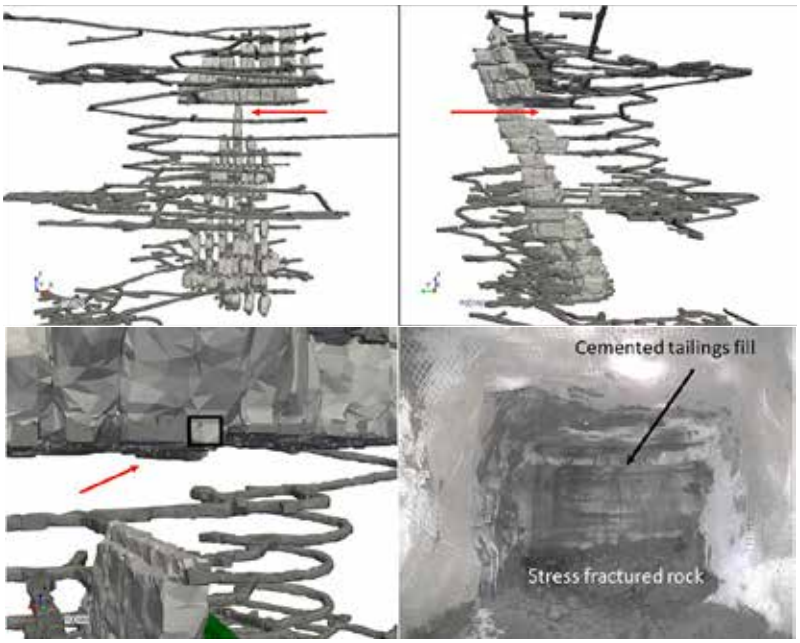

Figure 6—Sill pillar extracted 1355 m below surface (red arrow). The mined-out stopes above were filled with cemented hydraulic tailings. The sill pillar overcut was established by benching under/through the fill about 5 years after the original stope above was mined. The tunnel profile is 5 m x 5 m and mine sub level spacing was 30 m

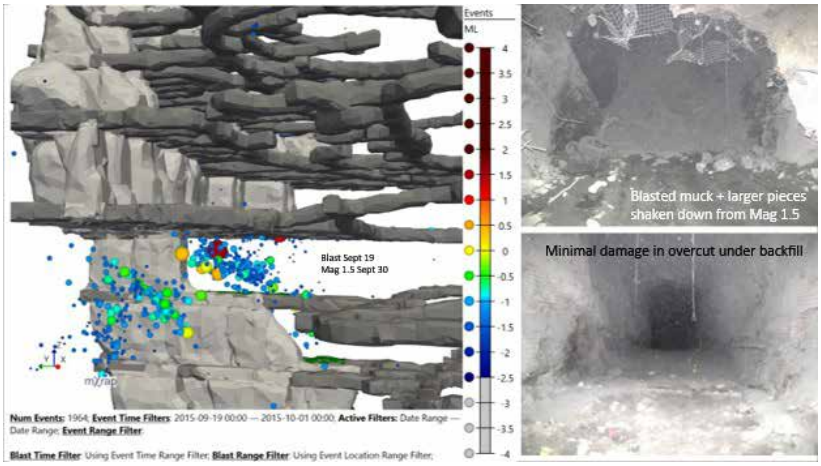

Figure 7—Left: Cross-section of stoping area showing seismicity in the crown (top portion) of the stope after the void blast (lower portion or "toes" of the blastholes fired). A moment magnitude 1.5 event occurred eleven days after the blast. Damage consisted of open stope slough onto the original blasted material. The overcut under backfill had minimal damage

wall shakedown occurred (Figure 7) but only required minor cleanup and check scaling. Fill undercut on the scale of a mined-out stope (12.5 m W x 30 m L in this example) can be prone to failure, however this stage is an open stope with no personnel access allowed.

Hierarchy of controls/control effectiveness

At great depth, in hard brittle rock, there may be sufficient high stress to make every development round a bursting risk. From experience, most advances do not burst but are prone to spalling and small magnitude seismic activity. This seismicity is a record of inelastic rockmass damage. The safety implications of a rockburst require that protection be in place, because even if a small percentage of rounds experience more violent failure, the consequences can be severe. In this type of environment, a robust process is required, because the uncertainty of which round might burst can not be easily resolved. High areal coverage, high deformation capacity (mesh on the outside), and dynamic bolts are applied. Equally important is the selection of mechanised equipment, to lower worker exposure to unsupported ground. There are several choices available such as the Australian style jumbo bolting, platform bolters with robotic arms, and Scandinavian style boom bolters (Figure 8).

Mine design plays a significant role in controlling rockburst risk, especially for larger seismic events. Simser et al. (2024) describe how overall increasing mine extraction leads to increased abutment stresses, and more seismicity, as well as faults becoming more mobile with time/extraction. Fault resistance to slip breaks down as asperities and/or rock bridges break down by repeated seismic activity and fault creep (inelastic deformation). As mining advances, the structures are pierced by more stopes, giving them increased freedom to displace. Ideally the mining advance would be away from the fault zone, however this is not always possible when there are multiple faults. Recognising the stress trapping between the fault and the mining front is also important. Appendix 1 shows an example of elevated seismicity under these circumstances.

Figure 8—Mechanised bolting with hollow core dynamic bolts and pumpable resin. The machine has a mesh handling arm and carousel/drill boom so that all ground support can be completed with the operator in the enclosed cab Left image is a close-up view of the bolting carousel/drill, right image is the same machine with the mesh transportation holder in the foreground

The figures depict a high stress abutment mining area with an underhand mining configuration, primary/secondary stopes and a seismically active fault zone. There were several design "stick handling" manoeuvres that were required to safely extract the area, which are alluded to in the image.

Converging mining fronts are well known stress raisers and elevate rockburst risk. Pillar failures, both on the converging mining front scale and local scale (e.g., draw point pillars, stope pillars, etc.), are also a well-known seismic source. In the mining layout shown in Figure 6, primary/secondary stopes were used. The secondary stopes are ore pillars that are mined after the adjacent primary stopes are extracted/backfilled. The pillars are left with slender width/height ratios (Jalbout et al., 2014) so that they do not build excessive confinement in the core and yield out benignly. The exact width/height ratio will be a function of both rockmass strength and stress. Slender pillars need to have an approximate W/H < 2/3 for hard rockmasses. Pillars that start to have W/H ratios > 1 will tend to build up enough confinement that the core of the pillar still carries load. Irrespective of the exact ratio, in narrow tabular deposits and narrow vein deposits it is difficult to design yielding pillars, as most mining geometries will result in squat pillars, and low W/H ratio pillars are likely to spall excessively (Andrews et al., 2019).

The following Figures 9a to 9j show a progression of annual mining steps in a narrow vein copper mine. The veins have an overall dip of about 45º but locally range from flat to near 90º. Most of the mining was done by cut and fill, with some longhole extraction in converging mining fronts to reduce man entry requirements. The longhole method was optimised for stopes to be extracted in two steps: slot (void blast) and final blast. The final mucking access was typically positioned midway along strike, perpendicular to the vein. This process requires camera mucking left/right but keeps the remote stand outside of the plane of high stress, shadowed by the veins' extraction. Cut and fill mining practise varied to account for local dip, flat areas using drift and fill (mine a cut, cemented tailings backfill, mine adjacent to the backfill), overhand cut and fill (work on top of previous cuts backfill), and underhand (work below previous cuts backfill).

The mining progression shown was from 2015 to 2024, however historic extraction in the general area started in 1983. Rockburst incidents are shown with a "sieve" analysis (Table 1), indicating the effectiveness of controls. A few incidents were not controlled (leak through the sieve). No injuries occurred in any of the examples, but the potential existed. The complex network of veins created many geotechnical risks:

- Converging mining fronts (sill pillars).
- "Island pillars" where isolated waste blocks were formed by surrounding cut and fill mining.
- Mining towards a major fault zone. In this case the fault zone acted as a stress flow barrier, pinching stress between the mining front and the fault.

Typical cut dimensions were 3 m x 3 m or 4 m x 4 m, so most pillars left behind have high W/H ratio (squat). For converging mining fronts, empirical experience at the mine required a minimum of four cuts left (12 m) to safely switch to longhole mining. Numerical model back analysis thresholds were also determined, but in general the rule of thumb worked well. Some flatter dip areas could not be mined via longhole methods, and the last few cuts in a convergence zone were left unrecovered.

Figures 9a to 9j represent a small volume of the mine, approximately 300 m x 350 m x 150 m and 1400 m below surface.

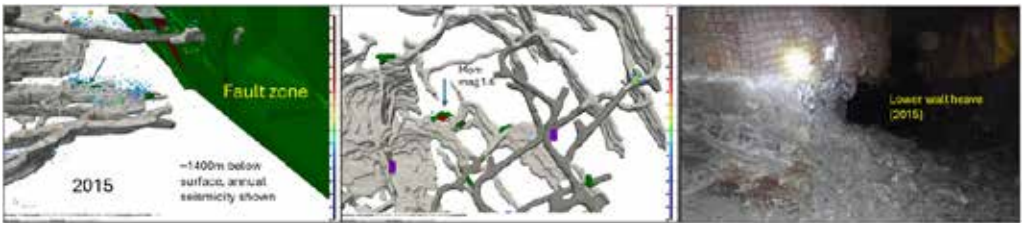

Figure 9a—Series of annual seismicity plots for a portion of an underground copper mine. Left image shows a long sectional view where drift and fill mining gradually approached a prominent fault zone, advancing from left to right in the image. The central image is a plan view of the same general area, where both converging mining fronts and isolated "island" pillars form. Right photo shows damage observed from the seismic event highlighted in the centre image

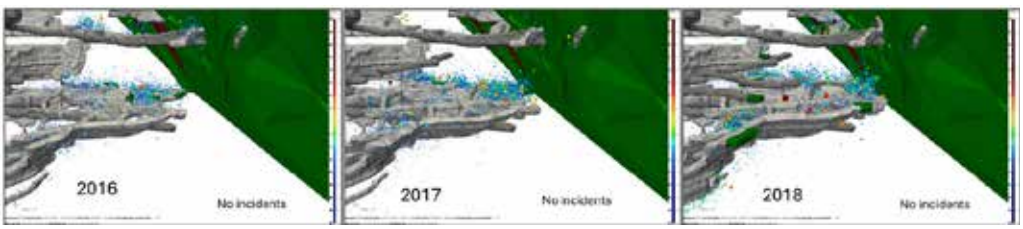

Figure 9b—Continuation from figure 9a left, showing annual seismicity plots as the drift and fill mining of a relatively flat vein advances toward the fault zone. The curvature of the vein in plan view meant that some portions were closer to the fault, the grey tunnels are 3 m x 3 m for scale

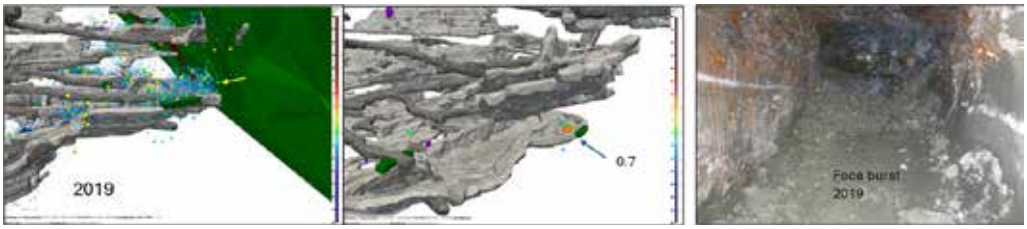

Figure 9c—By 2019 the outer flank of the curving vein was close enough to the fault zone that increased seismicity occurred. A strainburst happened prior to the face ground support being installed (seismic event associated with the burst indicated in the central image)

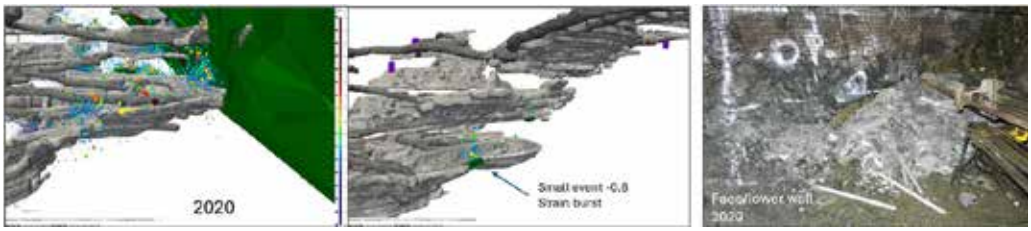

Figure 9d—The seismicity spread more vertically in line with the fault zone trapping stress between the mining front and the fault. Another strainburst incident occurred

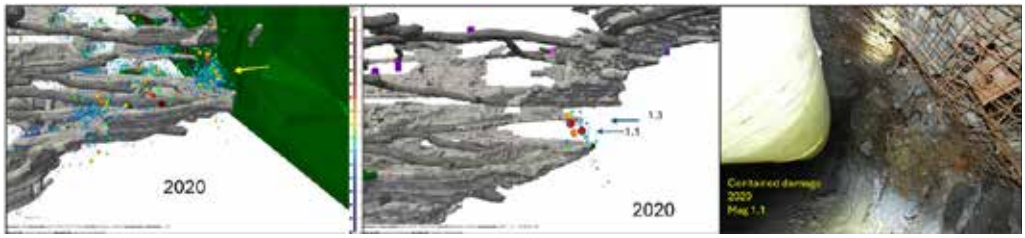

Figure 9e—The drift and fill mining was also approaching the mined-out vein above. Relatively large seismic events shown in the central figure (moment magnitude) had contained rockburst damage as shown on the photo

Figure 9f— The sill pillar vertically below the one forming in figure 9e experienced a moment magnitude 1.8 seismic event with some face and lower wall heave as well as contained damage, as shown in the photographs

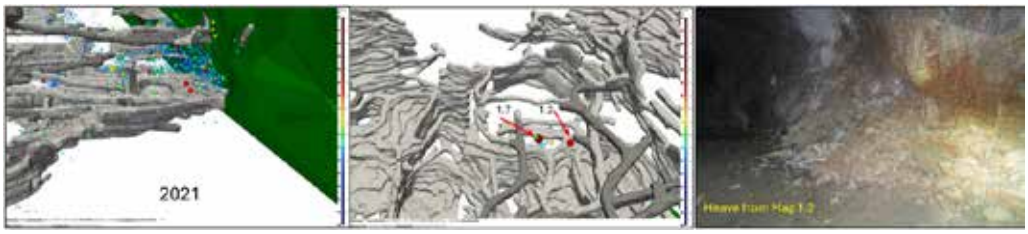

Figure 9g—An interior "island" pillar, which formed in the general region had two large events, damage shown was from the moment magnitude 1.2 event while the magnitude 1.7 event only caused local shotcrete cracking/mesh bagging

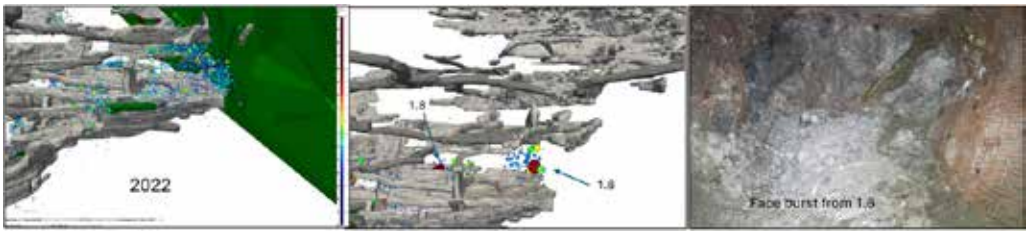

Figure 9h—A moment magnitude 1.6 seismic event caused a face rockburst in the drift and fill heading, again before the face bolts and screen could be installed

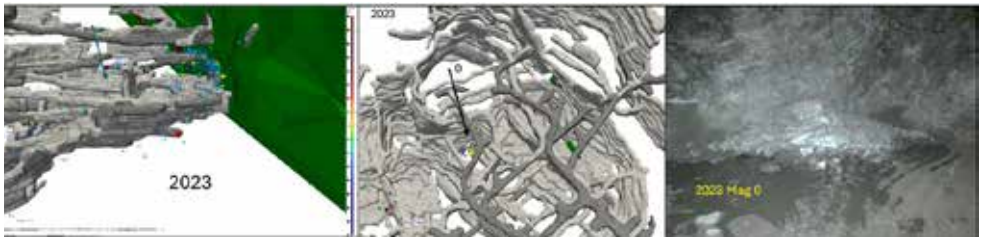

Figure 9i—A local interior "island" pillar experienced a moderate magnitude seismic event (magnitude 0 shown in the central figure) causing damage to the unsupported area in a longhole overcut heading

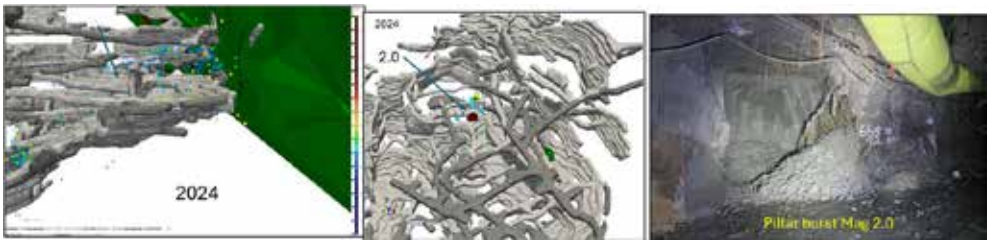

Figure 9j—The same "island" pillar shown in Figure 9g experienced another large seismic event (moment magnitude 2 shown in the central image), which had significant damage (photo)

Table 2

Summary of the 9 incidents shown in Figure 9. Although no injuries occurred, the red text highlights where the risk was not fully mitigated. This can be seen as a sort of "sieve" analysis to determine where controls that were in place were not sufficient to eliminate risk to workers

Incident	Mining geometry	Precursory seismic activity	Blast within 48 hours	Hindsight remedial measure
1	Island pillar	none	no	Support to floor
2	Sill pillar	Normal local seismicity	no	Remote load/wire/fire
3	Sill pillar	Normal local seismicity	26 hours	Re-entry worked
4	Sill pillar	Large event 1 hour before	8 hours	Re-entry worked
5	Sill pillar	none	no	contained by support
6	Island pillar	Large event 3 hours before	no	contained by support
7	Sill pillar	Large event 20 hours before	27 hours	Re-entry worked
8	Island pillar	Normal local seismicity	41 hours	Re-entry worked
9	Island pillar	none	no	Heavier support

The host rocks are granitic with high strength and complexity (breccias, gneisses > 250 MPa unconfined compressive strength). The copper veins are much weaker (~100 MPa u.c.s.) and the large strength contrast was a contributing factor to observed ground conditions. All seismic events are coloured/sized according to moment magnitude.

An exhaustive study of each incident is not included here but the overall summary in Table 2 that follows can be thought of as a "sieve", where multiple controls were in place. Seismic re-entry, rockburst prone support, and equipment selection were all part of the controls. Limited ability to predict the incidents in exact time and space was present, although risk factors, converging mining fronts, approaching the fault zone, and "island" pillars were all present. Narrow vein mining has fewer mechanised equipment options than say, bulk mining, which typically has 5 m x 5 m tunnels, allowing for larger jumbos, bolters, LHDs and other equipment. The early mining in the area used handheld drills for bolting (jacklegs and stopers) and was later switched to mechanised bolting. The mechanised bolter was a scissor deck style rig that required cut and fill profiles to increase from 3 m x 3 m to 4 m x 4 m for operating clearances.

Ground support varied from older rebar/mesh systems to yielding bolts and straps over mesh (75 mm aperture with 4.1 mm wire sheets and mesh strapping with 100 mm aperture and 8.4 mm wire stands). Development faces were supported by mesh and 1.8 m friction sets. An important aspect of that is areal coverage and timing of the face support. The advancing face is going to be blasted, so the temporary face support only protects a portion of the development cycle (loading). The practise at the mine was to bolt and mesh the walls and back first, then install face support. Several face bursts occurred before the face support was fully installed.

This specific area had high overall extraction, and several converging mining fronts. Removing one sill pillar would add load to other sills in the region. A blanket 48-hour seismic re-entry protocol was used after all longhole blasts. This, in principle, could be replaced by tele-remote equipment, eliminating risk to workers by accepting potential equipment damage.

Ground support (the last line of defense)

There are many inconvenient truths about rockburst resistant ground support (Hadjigeorgiou, 2024). Most support testing is based on axial loading, whereas a significant amount of shear loading exists in the field, load transfer to small cross sectional area tendons can be difficult, especially if fly rock is from small fragments. The source region of a large seismic event may not be supportable. Fortunately, the source region of most large fault slip events is often offset some distance from excavations. Despite limitations, there have been many improvements since the pioneering work and guidance of people like Ortlepp and Stacey (1997). The following section uses a few sample photographs to illustrate a few key points regarding dynamic ground support. In the authors' opinion there is still room for improvement despite the proliferation of multiple yielding bolt types available to industry (Simser, 2018).

It is useful to visualise the effect of catching a fast ball or a line drive off a cricket bat. This is best done by giving a little, rather than using a stiff arm. Shotcrete on the outside does not have sufficient deformation capacity, even if reinforced with mesh or fibres, it can only deform a few centimetres, whereas a few decimetres are required for strong bursts (Figures 5, and last visual in Figure 9).

Differential displacement occurs as large magnitude low frequency seismic waves pass through. The shotcrete post in Figure 10 failed during a Richter magnitude 3.7 event, the floor and back momentarily came closer, the stiff post in between did not survive unscathed. Falls of ground can also occur where the wave passing through momentarily interrupts clamping stress, for example, a steep wedge in high horizontal static stress.

A major design dilemma is what capacity to use for any individual tendon. Dynamic testing in the lab usually represents excellent load transfer, and maximum dynamic capacity (Li et al., 2024). Li et al. (2021) also highlighted the fact that an individual testing rig may have repeatable results for a specific bolt type, but there are inconsistencies between different test facilities. In situ it is difficult to get clean load transfer to the tendon, and many rock bolts do not fail during a burst or simply have a thread failure/plate tearing off, which occurs at lower loads than a split tube lab test.

In contrast to Figure 12, where joint dilation improved load transfer to the tendons and accommodated significant displacement during the seismic loading, the examples from Figures 5, 10, and 11 are more like the "simple model" that was discussed earlier on. Strain energy being suddenly released around the opening can eject the stress fracture zone into small fragments, which can easily fly out around the tendon.

Conclusions/discussion

The examples used in this paper are biased by experience in hard, brittle rock in high horizontal stress conditions. Other bursting types exist in mines, buckling of thin stiff layers, coal outbursts, dykes exploding, and faults/joints slipping. Ground support is the last line of defense, if possible no one wants to experience the trauma of a large ground motion close by. Exclusion, either by remotely operated equipment, barricading off old areas, central blasting, or seismic re-entry protocols should always be part of the risk mitigation strategy.

Mine design improvements clearly are required as more challenging conditions are encountered. For example, it is common practise to work multiple mining fronts to improve overall productive capacity. The later convergence of these mining fronts invariably increases stress, and rock bursting risk. At shallow depths this may be fine, at great depth the use of diverging mining fronts such as overhand/underhand lowers risk.

Some mining environments have inherently high strain burst risk due to depth/rock types. Focus on the process, keeping workers away from unsupported ground, becomes a critical control. Future

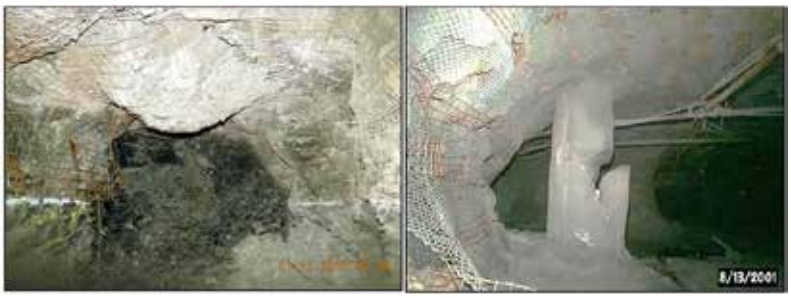

Figure 10—Deformation capacity is required to contain significant rockbursting. Mesh (left) can deform several decimetres if a weak link does not fail. Common weak links are sharp edged plates guillotining the wire strands, and seams between sheets peeling open. Bigger, stronger, more capacity does not work if there is insufficient deformation capacity (right shotcrete post with capacity > 1000 tonnes crunched by a seismic wave passing through the area)

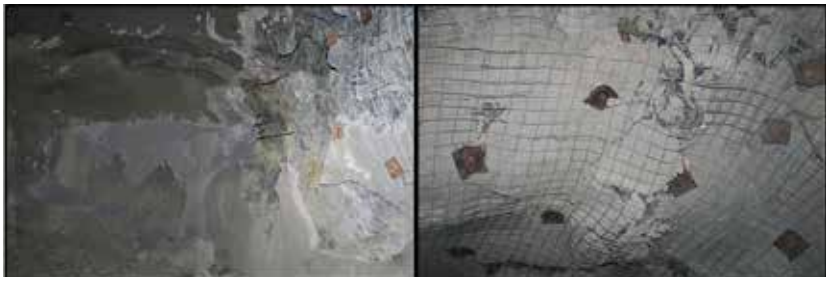

Figure 11—Left: "naked tendons", a phrase coined by Ortlepp (1997) where the rockbolt does not break but the rock unravels around it, sometimes tearing of the face plate, sometimes leaving the bolt intact. Right: successful containment of a strain burst, the shotcrete on the inner layer promotes more even loading to the outer layer mesh. Despite using yielding tendons, there is still a deformation incompatibility between the highly compliant mesh and the stiff bolts. Rubber conveyor belt pieces were used to back the steel face plates to prevent guillotining

Figure 12—Blocky ground fares better than massive ground during a burst. The area shown had a seismic episode including moment magnitude 1.4, 1.8., and 1.9 seismic events. A substantial amount of deformation was absorbed by joint dilation, and dilating joints with smooth steel bars between them achieved good load transfer, allowing the yielding tendon to work closer to the lab testing result. See also Simser (2018)

improvements would include remote load/wire/fire. The practise of face screening in development is limited by the use of temporary support capacity and only protects the loading cycle. The ensuing blast-damaged face mesh and bolts are difficult to dispose of in new mining projects with limited development.

The simple model of stored strain energy around the opening as being the main source of rockburst energy is not universally applicable. It does apply in many instances and shows the need to target preconditioning holes to where the stored strain energy is. This seems obvious, but many preconditioning patterns are designed around where future bolt holes might intersect potentially unexploded powder. The model also explains why over-scaling at depth can create a hazard by removing confinement, and why rapid application of shotcrete to lock in stress fractures can be effective.

Acknowledgements

As I pass 37 years in the mining industry, there are too many people to properly thank. Knowledge sharing by Dave Ortlepp, William Joughin, John Hadjigeorgiou, Tony Butler, Alex Hall, Patrick Andrieux, Veronique Falmagne, Rob Mercer, Mark Board, Richard Brummer, Wilson Blake, Graham Swan, Scott Carlisle, Ali Jalbout, Dave Counter, Peter Kaiser, Pranay Yadav, Rick Deredin, and many others, is greatly appreciated!

References

Andrews, P.G., Butcher, R.J., Ekkerd, J. 2019. The geotechnical evolution of deep level mechanised destress mining at South Deep. *Deep Mining 2019 Conference*. Muldersdrift, 24-25 June 2019. The Southern African Institute of Mining and Metallurgy.

Butler, T., Simser, B. 2017. Microseismic Monitoring Strategy for Glencores's Nickel Rim Deep and Onaping Depth Projects. *Rasim9. 9th International Symposium on Rockbursts and Seismicity in Mines*. Santiago, Chile.

Counter, D.B. 2014. Kidd Mine – dealing with the issues of deep and high stress mining – past, present and future. *Deep Mining 2014* – M. Hudyma and Y Potvin (eds). Australian Centre for Geomechanics, Perth.

Hadjigeorgiou, J. 2024. Inconvenient truths about ground support in deep and high-stress mines. *Deep Mining 2024* – P. Andrieux and D. Cumming-Potvin (eds). Australian Centre for Geomechanics, Perth.

Hall, A., Simser, B., Cai, M., Lindsay, J. 2024. Preconditioning blasting for rockburst control in a deep shaft sink. *International Journal of Rock Mechanics and Mining Sciences*, vol. 181, 105841.

Jalbout, A. 2024. Geotechnical strategies to resume mining at Westwood mine following a Mn3.7 seismic event: part 1 – the investigation. *Deep Mining 2024: Proceedings of the 10th International Conference on Deep and High Stress Mining*.

Jalbout, A. 2024. Geotechnical strategies to resume mining at Westwood mine following a Mn3.7 seismic event: part 2 – the mitigation plan. *Deep Mining 2024: Proceedings of the 10th International Conference on Deep and High Stress Mining*.

Jalbout, A., Simser, B. 2014. Rock Mechanics tools for mining in high stress ground conditions at Nickel Rim South Mine. *Deep Mining 2014* – M Hudyma and Y Potvin (eds). Australian Centre for Geomechanics.

Kaiser, P.K., Tannant, D.D., McCreath, D.R. 1996. *Canadian Rockburst Support Handbook*. Geomechanics Research Centre, Laurentian University, Sudbury, Ontario.

Li, C., Hadjigeorgiou, J., Mikula, P., Know, G., Darlington, B., Royer, R, Pytlik, A., Hosp, M. 2021. Performance of identical rockbolts tested on four dynamic testing rigs employing the direct impact method. *Journal of Rock Mechanics and Geotechnical Engineering*.

Li, C., Mikula, P., Hadjigeorgiou, J., Simser, B., He, M. Canbulat, I, Joughin, W. 2024. I*SRM* Suggested Method for Determining the Properties of Rock Bolt Assemblies by Mass Freefall Impact Testing in the Laboratory. *Rock Mechanics and Rock Engineering*. 2024.

Mawson, M. Dahner-Lindkvist, C.R., Anderson, U.B., Thomas, A, Backstrom, A. 2022. The Kiruna seismic event: important insights from the geotechnical model. Caving 2022 – Y. Potvin (ed.). *Australian Centre for Geomechanics*.

Ortlepp, W.D., Stacey, T.R. 1997. Testing of Tunnel Support: Dynamic Load Testing of Rock Support containment systems. SIMRAC GAP Project 221. South Africa.

Ortlepp, W.D. 1997. *Rock* Fracture and Rockbursts, an illustrative study. *The South African Institute of Mining and Metallurgy*, Johannesburg, Monograph Series M9.

Pigott, J.A., Hall, R.J. 1961. Undercut-and-fill mining at the Frood-Stobie Mine of the International Nickel Company of Canada, Limited. Canadian Institute of Mining, annual General Meeting, Quebec City.

Simser, B. 2019. Rockburst Management in Canadian Hard Rock Mines. *Journal of Rock Mechanics and Geotechnical Engineering*. Jrmge. 2019.07.005

Simser, B. 2017. Design of Rockburst Support Systems for Deep Hard Rock mines. *Rock Mechanics and Engineering Volume 4: Excavation, Support and Monitoring*. CRC Press, April 2017.

Simser, B., Yadav, P., Butler, T. 2024. Evolution of fault-related seismic behaviour at Nickel Rim South Mine. Deep Mining 2024 – P. Andrieux and D. Cumming-Potvin (eds). *Australian Centre for Geomechanics*, Perth.

Simser, B. 2018. Rock burst Observations from hard rock mines: failures, successes, lessons learned. Rock Dynamics – Experiments, Theories and Applications – C. Li, X. Li, & Z-X Zhang (eds). 2018 Taylor & Francis Group, London. ◆

Rockburst risk management in deep hard rock mines: A multi-tiered approach

Appendix 1

Example of mine design lowering rockburst risk, overall approach and local "stick handling"

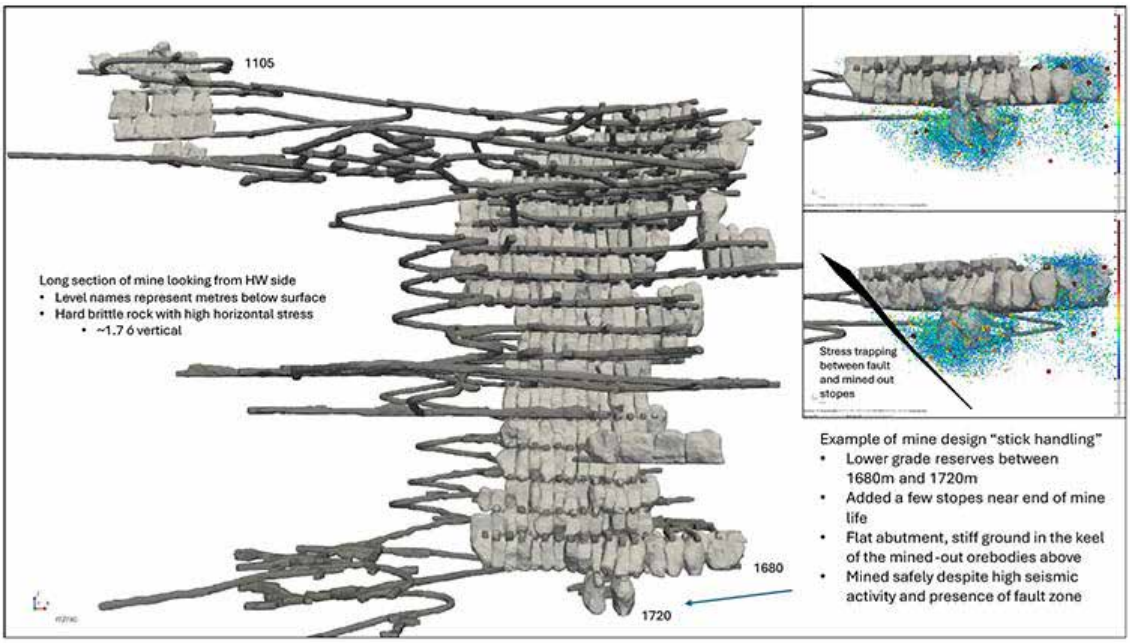

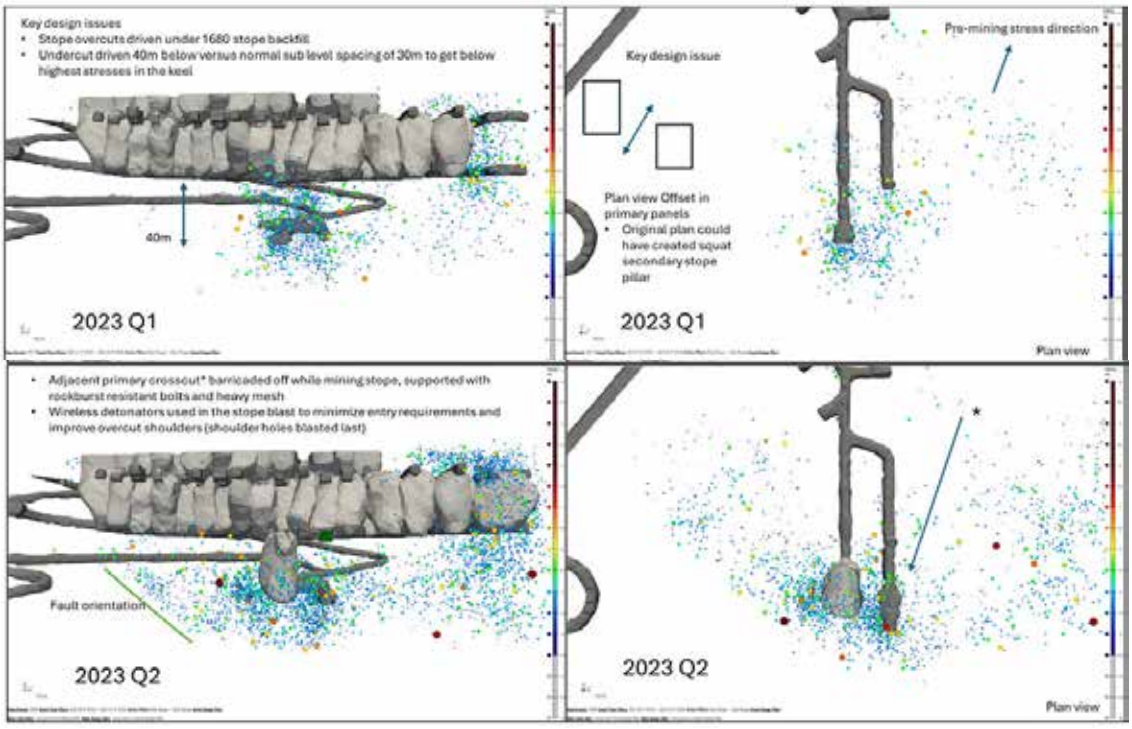

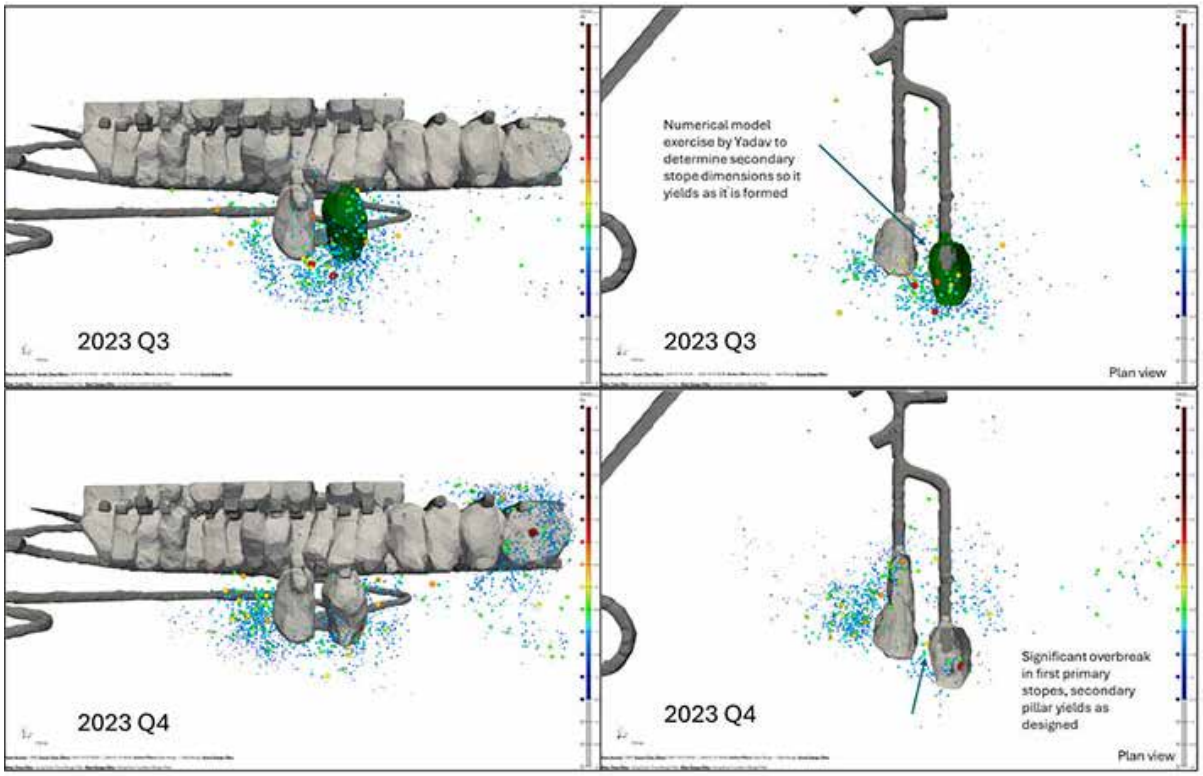
2023 Q3
Numerical model exercise by Yadav to determine secondary stope dimensions so it yields as it is formed
2023 Q3
Plan view
2023 Q4
2023 Q4
Significant overbreak in first primary stopes, secondary pillar yields as designed
Plan view

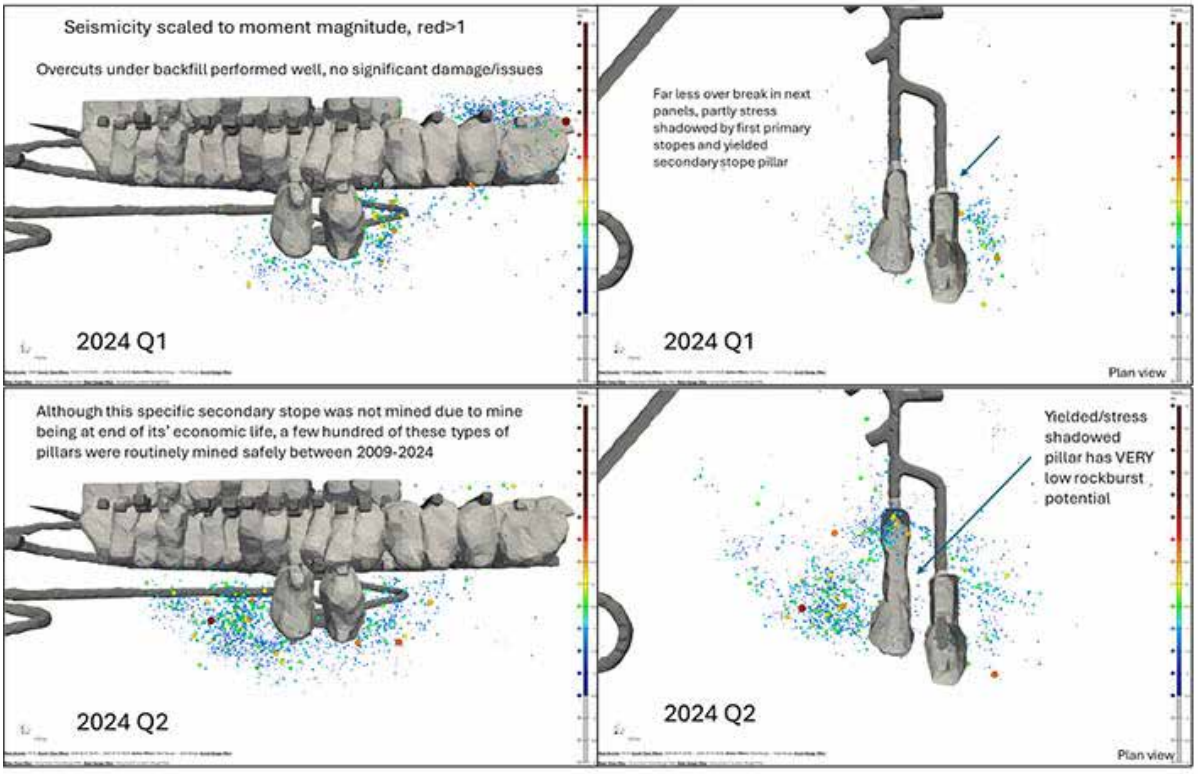
Seismicity scaled to moment magnitude, red>1
Overcuts under backfill performed well, no significant damage/issues
2024 Q1
Far less over break in next panels, partly stress shadowed by first primary stopes and yielded secondary stope pillar
2024 Q1
Plan view
Although this specific secondary stope was not mined due to mine being at end of its' economic life, a few hundred of these types of pillars were routinely mined safely between 2009-2024
2024 Q2
Yielded/stress shadowed pillar has VERY low rockburst potential
2024 Q2
Plan view

Application of the boundary element method for numerical modelling of the seismic hazard at Bambanani gold mine in South Africa

by J. Gerber[1,3], N. de Koker[1], Y Jooste[2]

Affiliation:
[1]Stellenbosch University, South Africa
[2]Harmony Gold Mine, South Africa
[3]Institute of Mine Seismology, South Africa

Correspondence to:
J. Gerber

Email:
Jacques.Gerber@IMSeismology.org

Dates:
Received: 14 Jul. 2025
Published: November 2025

How to cite:
Gerber, J., De Koker, N., Jooste, Y. 2025. Application of the boundary element method for numercial modelling of the seismic hazard at Bambanani gold mine in South Africa. *Journal of the Southern African Institute of Mining and Metallurgy*, vol. 125, no. 11, pp. 661–674

DOI ID:
https://doi.org/10.17159/2411-9717/875/2025

Abstract

This paper presents a novel application of the boundary element method for numerical modelling of the seismic activity and hazard that is associated with the shaft pillar extraction at Bambanani mine in South Africa. In the numerical model, the tabular mining excavations are represented by displacement discontinuity elements, and to accommodate crush, shear, and fault slip seismic events, the numerical model is populated with additional displacement discontinuity elements that represent modelled crush- and shear-type failures in the rockmass. Crush-type failures are evaluated by applying the limit equilibrium method and a Hoek-Brown strength criterion, and shear-type failures are evaluated by applying a Coulomb-friction strength criteria to Ortlepp-shear and geological features. In this paper, the modelling results are presented as time history analyses of modelled potency from 1 January 2010 to 30 June 2022 and normalised exceedance rates for different mining periods using an upper-truncated power law. The normalised exceedance rates of seismic events that have moment magnitude $Mw \geq 1.0$ are lowest for the initial mining period (26 events per year) and highest for the final mining period (218 events per year). The relative errors of the modelled potency and normalised exceedance rates are typically less than 10% or 15%, which suggests that the modelling methodology is appropriate for medium- and longer-term forecasting of seismic activity and hazard, as presented in this paper. Shorter-term forecasting is not considered in this paper.

Keywords

mine seismology, numerical modelling, boundary element method, seismic hazard

Introduction

Seismic activity at underground mines is typically associated with fault slip seismic events that occur on geological features and are similar to crustal earthquakes; shear events that occur on stress-induced shear fractures or shear ruptures, e.g., Ortlepp-shear features at the deep gold mines in South Africa (Van Aswegen, 2008), and crush events that occur as stress fracturing or strain bursting in the rockmass that surrounds the mining excavations (Malovichko, 2020; Van Aswegen, 2021a,b; Malovichko, 2022). From 1 January 2020 to 31 December 2024, the underground seismic systems monitored by the Institute of Mine Seismology (IMS) recorded approximately 1.8 million seismic events that have moment magnitude $-1.0 \leq M_w < 4.0$ at fourteen gold mines in the Witwatersrand Basin (Hanks, Kanamori, 1979; Handley, 2004; Tucker et al., 2016; Frimmel, 2019), including 180,834 events that have $M_w \geq 0.0$, 19,011 events that have $M_w \geq 1.0$, 1,017 events that have $M_w \geq 2.0$ and 17 events that have $M_w \geq 3.0$. The largest seismic event has moment magnitude $M_w = 3.4$ and occurred on 16 March 2020 in the Carletonville gold field and the second and third largest events have $M_w = 3.3$ and occurred on 10 February 2020 and 6 February 2022 in the Carletonville and Klerksdorp gold fields, respectively. Generally, the deep gold mines that extract the tabular orebodies in the Witwatersrand Basin are considered to have significantly higher seismic hazard and therefore higher risk of injuries and fatalities from seismic events than the shallower mines in other regions and countries that have comparably lower seismic hazard and risk. From 1 January 2020 to 31 December 2024, 3,119 injuries and 102 fatalities occurred in the South African gold mining industry (Mthenjane, 2025).

In crustal seismology, prediction of earthquakes is typically described as "extremely difficult" and "effectively impossible" (Kagan, 1997; Geller, 1997) and in mine seismology, short-term forecasting of seismic events using time history analyses is similarly described as "not sufficient" or "not viable" for mitigating the above-mentioned risk of injuries and fatalities Van Aswegen, 2003, 2005; Spottiswoode,

Numerical modelling of the seismic hazard at Bambanani gold mine in South Africa

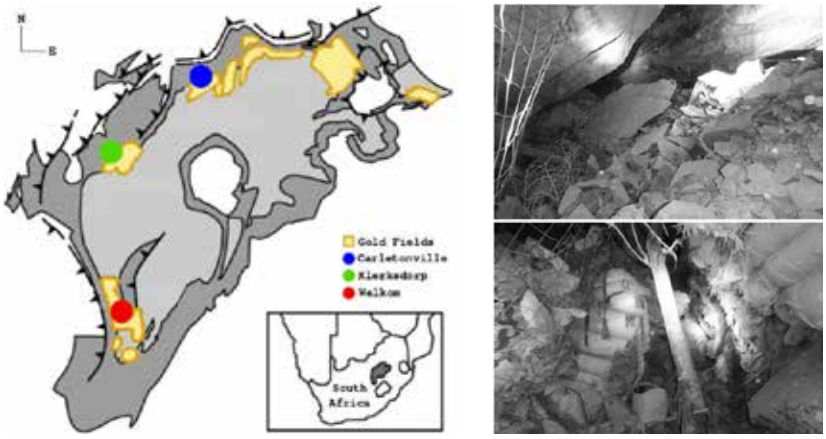

Figure 1—Schematic diagram of the Witwatersrand Basin in South Africa (left) and photographs of underground damage from a seismic event that occurred at Bambanani mine in the Welkom gold field (top and bottom right)

2009, 2010). Until seismic monitoring is considered to have predictive power (Kagan, 1999), numerical modelling applications are probably the primary defenses against the devastations of rockbursts, and therefore Salamon proposed the development of a modelling methodology that accommodates "realistic approximations of the source mechanisms" and facilitates "assessment of the relative hazardousness of various geological environments" (Salamon, 1993; Linkov, 1997, 2002, 2006, 2013; Linkov et al., 2015, 2016). This paper summarises the development of an appropriate and novel modelling methodology for medium- and longer-term forecasting of seismic activity and hazard and presents an application at a South African tabular orebody mine, i.e., the shaft pillar extraction at Bambanani mine in the Welkom gold field (Motsepe et al., 2021; Jooste, 2025). Figure 1 shows a schematic diagram of the Witwatersrand Basin (left) and photographs of underground damage at Bambanani mine (right). The gold fields in the Witwatersrand Basin are shown as yellow regions and the Carletonville, Klerksdorp, and Welkom gold fields are indicated by blue, green, and red dots, respectively (Jolley et al., 2007). The underground photographs correspond to a crush seismic event that has moment magnitude M_w = 1.6 and occurred on 11 October 2021 (Van der Wath et al., 2022).

Seismic monitoring

Source time and location

For a seismic event in this paper, the source time and location are calculated by minimising the travel time residual for the primary and secondary body waves (hereinafter referred to as P- and S-waves, respectively) recorded by a collection of seismic sensors (Salamon, Weibols, 1972; Gibowicz, Kijko, 1994b; Mendecki, Sciocatti, 1997; Mendecki et al., 1999b; Andersen et al., 2002):

$$\psi(t_0,\overline{w_0}) = \sum_{n=0}^{N_{GS}-1} \left|(t_{P,n} - t_0) - \frac{D(\overline{w_0})}{V_{P,n}}\right| + \left|(t_{S,n} - t_0) - \frac{D(\overline{w_0})}{V_{S,n}}\right| \quad [1]$$

where t_0 is the source time of the seismic event, $\overline{w_0}$ = $(w_{0,x},w_{0,y},w_{0,z})$) is the source location vector, $\psi(t_0, \overline{w_0})$ is the travel time residual, N_{GS} is the number of seismic sensors, $t_{P,n}$ is the arrival time of the P-wave recorded by the sensor with index $n < N_{GS}$, $t_{S,n}$ is the arrival time of the S-wave, ($t_{B}n$ - t_0), and ($t_{S,n}$ - t_0) is the travel time of the P- and S-wave respectively, $V_{P,n}$ and $V_{S,n}$ are the corresponding P- and S-wave velocities, and $D(\overline{w_0})$ is the distance from the source location to the sensor. The IMS seismic system at Bambanani mine consists of ten geophone sensors (Bredenkamp et al., 2013), and the average P- and S-wave velocities are approximately V_P = 5300 m/s and V_S = 3550 m/s, respectively.

Source size and scalar potency

In crustal seismology, the source size of a fault slip seismic event is typically expressed using scalar potency or moment, which are calculated by integrating the fault deformation over the slip surface, expressed in Equation 2 (Kanamori, 1977; King, 1978; Ben-Menahem, Singh, 1981; Ben-Zion, Zhu, 2002):

$$P = \iint_{A_0} u\,(x,y)\delta x \delta y$$
$$M = \frac{\gamma P}{2(1+\nu)} L = \sqrt[3]{\frac{3.5\gamma P}{2(1+\nu)\,\Delta\,\sigma}} \quad [2]$$

where P is the scalar potency of the fault slip event, $u(x,y)$ is the fault deformation on the slip surface, A_0 is the source area, M is the corresponding scalar moment, L is the average source length, γ is Young's Modulus, ν is Poisson's Ratio, and $\Delta\,\sigma$ is the average stress drop (Eshelby, 1957). For the Bambanani mine, Young's Modulus is γ = 70GPa, Poisson's Ratio is υ = 0.20, and the average stress drop is $\Delta\,\sigma$ =1MPa. Figure 2 shows a schematic diagram of a fault slip event. The fault deformation on slip surface is indicated by black arrows, the positive and negative subsurfaces are shown as red and blue regions, respectively, and the source area of the event is shown as a grey region.

In this paper, scalar potency is calculated by constructing the displacement spectra of the P- and S-waves recorded by the IMS seismic system at Bambanani mine (Aki, Richards, 1980; Gibowicz, Kijko, 1994a; Mendecki, Niewiadomski, 1997; Mendecki et al., 1999a):

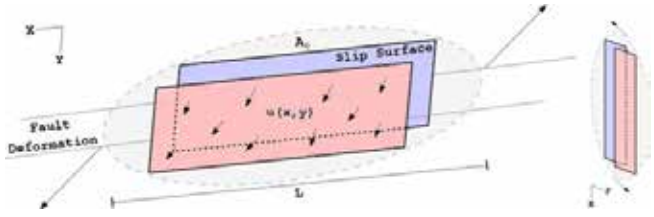

Figure 2—Schematic diagram of a fault slip seismic event. The fault deformation over the slip surface is indicated by black arrows, the subsurfaces are shown as red and blue regions and the source area is shown as a grey region

$$P = 2\pi V_S^2[R_P V_P^3 \Omega_P + R_S V_S^3 \Omega_S] \quad [3]$$

where V_P and V_S are the average P- and S-wave velocities, respectively, $R_P = 0.55$, and $R_S = 0.63$ are the corresponding radiation pattern factors, Ω_P and Ω_S are evaluated by fitting $\Omega(f) = \Omega_P/[1-(f/f_0)^{\gamma\eta}]^{\frac{1}{\gamma}}$ and $\Omega(f) = \Omega_S/[1-(f/f_0)^{\gamma\eta}]^{\frac{1}{\gamma}}$ to the displacement spectra of the P- and S-waves, Ω is the spectral amplitude, f is the spectral frequency, f_0 is the corner frequency, and γ and η are the spectral shape parameters (Brune, 1970; Boatwright, 1980).

Local magnitude and radiated energy

In mine seismology, the combined intensity of a seismic event is sometimes expressed using local magnitude, which is calculated by combining the logarithm of scalar potency as an indicator of the source size and the logarithm of radiated energy as an indicator of the body wave amplitudes (Butler, 1992; Burrows, Ebrahim-Trollope, 2004; Stankiewicz, Essrich, 2004; Mendecki, 2013):

$$m_L = m_P logP + m_E logE + m_0 \quad [4]$$

where m_L is the local magnitude of the seismic event, $logP$ is the logarithm of scalar potency, $logE$ is the logarithm of radiated energy, and m_P, m_E and m_0 are the local magnitude parameters. The local magnitude parameters for Bambanani mine are $m_P = 0.516$, $m_E = 0.344$, and $m_0 = -1.144$ (Butler, Van Aswegen, 1993; Stankiewicz, Essrich, 2004; Ebrahim-Trollope et al., 2013). For a seismic event in this paper, radiated energy and local magnitude are calculated by assuming a simple relationship between the logarithms of scalar potency and radiated energy ($logE = E_P logP + E_0$):

$$E = 10^{E_P logP + E_0}$$
$$m_L = (m_P + m_E E_P) logP + m_E E_0 + m_0 \quad [5]$$

where E is the radiated energy of the seismic event, and E_P and E_0 are the radiated energy parameters. The radiated energy parameters for Bambanani mine are $E_P = 1.0$, and $E_0 = 5.5$. Table 1 summarises the relationship between the logarithms of scalar potency and radiated energy, average source length, moment magnitude ($M_w = 0.667logP + 0.95$), and local magnitude ($m_L = 0.860logP + 0.748$).

Seismic activity and hazard

Seismic activity

In this paper, seismic events supplied by Harmony Gold Mining Company (Jooste, 2023) are considered for different mining periods that are associated with the shaft pillar extraction at Bambanani mine (hereinafter referred to as BAM_10-13, BAM_14-16, BAM_17-19, BAM_20-22, and BAM_ALL). BAM_10-13 spans 1,461 days or 4 years from 1 January 2010 to 31 December 2013 and contains 6207 seismic events that have scalar potency $logP \geq -2.0$ and local magnitude $m_L \geq -1.0$; BAM_14-16 spans 1,096 days or 3 years from 1 January 2014 to 31 December 2016 and contains 13290 seismic events; BAM_17-19 similarly spans 1,095 days from 1 January 2017 to 31 December 2019 and contains 13,714 seismic events; BAM_20-22 spans 943 days or 2.6 years from 1 January 2020 to 30 June 2022 and contains 12,368 seismic events; and BAM_ALL spans 4,595 days or 12.6 years from 1 January 2010 to 30 June 2022.

Figure 3 shows a representative plan of the seismic activity that is associated with the shaft pillar extraction at Bambanani mine. Potentially damaging (PD) seismic events that have scalar potency $logP \geq 0.0$ and local magnitude $m_L \geq 0.7$ are indicated by spheres that are sized by scalar potency and coloured according to the different mining periods such that the blue, green, yellow, and red spheres correspond to BAM_10-13, BAM_14-16, BAM_17-19, and BAM_20-22, respectively. The initial mining excavations of the shaft pillar extraction are shown as grey regions, and the final mining excavations are shown as blue, green, yellow, and red regions that similarly correspond to the mining periods. Some geological features in the rockmass are indicated by black dashed lines.

Figure 4 shows the cumulative number of seismic events recorded by the IMS seismic system at Bambanani mine with respect to calendar time (left) and volume extracted (right) such that the blue, green, yellow, and red lines correspond to BAM_10-13, BAM_14-16, BAM_17-19, and BAM_20-22 respectively. Significantly large (SL) seismic events that have scalar potency $logP \geq 1.0$ and local magnitude $m_L \geq 1.6$ are indicated by circles that are sized by scalar potency and similarly coloured according to the

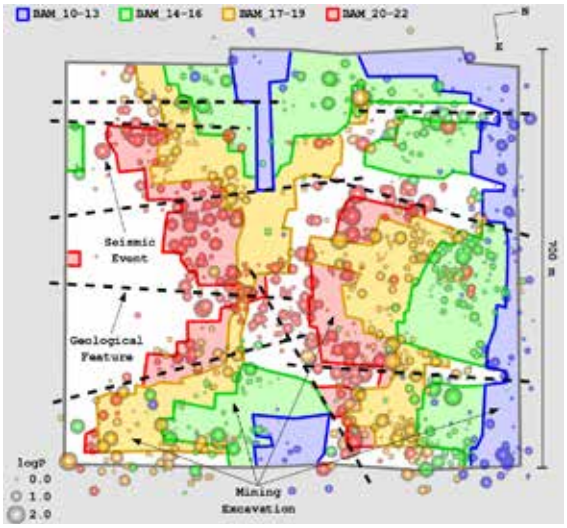

Figure 3—Representative plan of the seismic activity associated with the shaft pillar extraction at Bambanani mine. PD seismic events ($logP \geq 0.0$) are shown as spheres that are sized by scalar potency and coloured blue, green, yellow, and red according to the mining periods. The mining excavations are shown as grey, blue, green, yellow, and red regions. Some geological features in the rockmass are indicated by black dashed lines

Table 1

Relationship between the logarithms of scalar potency and radiated energy, average source length (γ = 70GPa, υ = 0.20, $\Delta\sigma$ = 1MPa), moment magnitude and local magnitude for Bambanani mine

$logP$	-3.0	-2.5	-2.0	-1.5	-1.0	-0.5	0.0	0.5	1.0	1.5	2.0	2.5	3.0	3.5	4.0
$logE$	2.5	3.0	3.5	4.0	4.5	5.0	5.5	6.0	6.5	7.0	7.5	8.0	8.5	9.0	9.5
$L[m]$	5	7	10	15	22	32	47	69	102	149	219	321	472	692	1016
M_w	-1.1	-0.7	-0.4	-0.1	0.3	0.6	1.0	1.3	1.6	2.0	2.3	2.6	3.0	3.3	3.6
m_L	-1.8	-1.4	-1.0	-0.5	-0.1	0.3	0.7	1.2	1.6	2.0	2.5	2.9	3.3	3.8	4.2

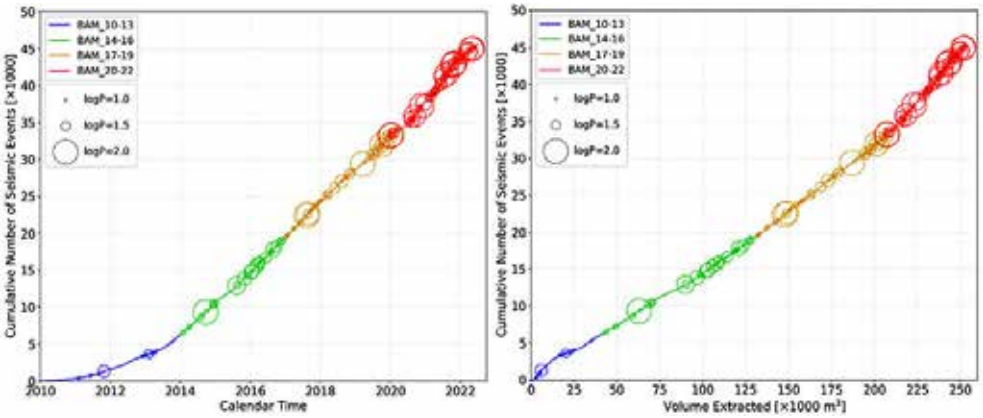

Figure 4—Cumulative number of seismic events with respect to calendar time (left) and volume extracted (right). The blue, green, yellow, and red lines correspond to the different mining periods at Bambanani mine. *SL* seismic events (*logP* ≥ 1.0) are indicated by similarly coloured circles that are sized by scalar potency

different mining periods of the shaft pillar extraction. BAM_10-13 contains 14 SL and 132 PD seismic events; BAM_14-16 contains 39 SL and 326 PD events including the largest event that has $logP$ = 2.3 and m_L = 2.7 and occurred on 19 September 2014; BAM_17-19 contains 60 SL and 379 PD events; and BAM_20-22 contains 97 SL and 392 PD events including the second and third largest events that have $logP$ = 2.2 and m_L = 2.6 and occurred on 22 October 2021 and 22 November 2020, respectively.

Seismic hazard

In mine seismology, seismic hazard is typically expressed as an exceedance probability (Pr), which is calculated by assuming that the source times of seismic events are Poissonian (Kijko, Funk, 1994; Du Toit, Mendecki, 2007) and the source sizes are represented by an upper-truncated power law (Gutenberg, Richter, 1944; Gibowicz, Kijko, 1994c; Burroughs, Tebbens, 2001, 2002; Christensen et al., 2002; Kagan, 2010; Kwiatek et al., 2010; Mendecki, 2012, 2016b):

$$Pr(\geq logQ) = 1 - exp[-N_e(\geq logQ)] \quad [6]$$

where Pr ($\geq logQ$) is the exceedance probability of a seismic event that has scalar potency, $logP \geq logQ$, $logQ$ is the logarithm of scalar potency that corresponds to the exceedance threshold, N_e is the expected number of events that is evaluated by fitting an upper-truncated power law N_e ($\geq logQ$) = $\alpha[10^{-\beta logQ} - 10^{-\beta logP_{max}}]$ to the recorded number of events, P_{max} is the maximum scalar potency of the next record-breaking (RB) seismic event, and α and β are the power-law parameters. In this paper, the maximum scalar potency is estimated using the trend of previous RB seismic events (Chandler, 1952; Robson, Whitlock, 1964; Cooke, 1979; Mendecki, 2016a), and for Bambanani mine, the maximum scalar potency is $logP_{max}$ = 2.5. The power-law parameters are $log\alpha$ = 3.15 and β = 0.765.

Figure 5 shows a comparison of the expected number of seismic events using the upper-truncated power law for BAM_ALL and the number of events recorded by the IMS seismic system at Bambanani mine. The expected number of seismic events that have scalar potency $logP \geq logQ$ is shown as a cyan line, and the recorded number of events that have $logP \geq logQ$ and $logP = logQ$ are, respectively, shown as magenta circles and grey squares that are sized by scalar potency. The number of SL and PD seismic events are appropriately represented by the upper-truncated power law, e.g., the expected number of events are N_e (≥ 1.0) = 225 and N_e (≥ 0.0) = 1395, respectively, the recorded number of events are N_r (≥ 1.0) = 230 and N_r (≥ 0.0) = 1357, respectively, and therefore the corresponding relative errors are $|N_e (\geq 1.0) - N_r (\geq 1.0)|/N_r$ (≥ 1.0) = 0.03 and $|N_e (\geq 0.0) - N_r (\geq 0.0)|/N_r$ (≥0.0) = 0.02, respectively.

In this paper, seismic hazard is expressed as a simple exceedance rate (Er), which is calculated by scaling the expected number of seismic events using the scalar potency for the different mining periods that are associated with the shaft pillar extraction, i.e., BAM_10-13, BAM_14-16, BAM_17-19, BAM_20-22, and BAM_ALL, and normalising the time span and volume extracted to some reference period:

$$\begin{aligned} Er_T(\geq logQ) &= \frac{T_{ref}}{T_{mp}} N_P(\geq logQ) \\ Er_V(\geq logQ) &= \frac{V_{ref}}{V_{mp}} N_P(\geq logQ) \\ N_P(\geq logQ) &= P_{mp} \frac{N_e(\geq logQ)}{P_{tot}} \\ &= P_{mp} \frac{\alpha}{P_{tot}} [10^{-\beta logQ} - 10^{-\beta logP_{max}}] \end{aligned} \quad [7]$$

where Er ($\geq logQ$) is the exceedance rate of a seismic event that has scalar potency $logP \geq logQ$, T_{mp} and T_{ref} is the time span for the mining period and reference period, respectively, V_{mp} and V_{ref}

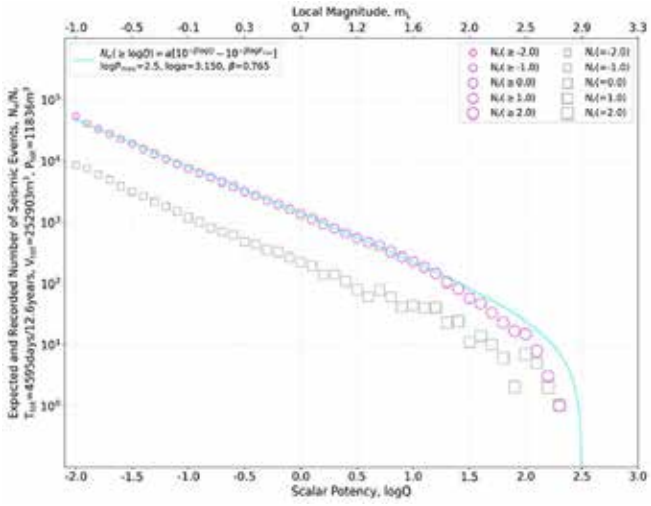

Figure 5—Comparison of the number of seismic events using the upper-truncated power law ($logP_{max}$ = 2.5, $log\alpha$ = 3.15, β = 0.765) and the number of seismic events recorded at Bambanani mine. The expected number of seismic events are shown as a cyan line ($logP \geq logQ$), and the recorded number of events are shown as magenta circles ($logP \geq logQ$) and grey squares ($logP \geq logQ$) that are sized by scalar potency

are the corresponding volume extracted, N_P (≥ *logP*) is the scaled number of seismic events using scalar potency, P_{mp} is the scalar potency for the mining period, and P_{tot} is the total scalar potency of seismic events recorded by the IMS seismic system at Bambanani mine. In this paper, the time span and volume extracted for the reference period is T_{ref} = 60days and V_{ref} = 3300m^3, respectively, and the total scalar potency for BAM_ALL is P_{tot} = 11836m^3. Table 2 summarises the scalar potency of seismic events, time span and volume extracted for the mining periods of the shaft pillar extraction at Bambanani Mine.

Figure 6 shows a comparison of the exceedance rates for the normalised time span (left) and normalised volume extracted (right) such that the blue, green, yellow, red, and black lines correspond to BAM_10-13, BAM_14-16, BAM_17-19, BAM_20-22, and BAM_ALL, respectively. The likelihood of a seismic event that has scalar potency *logP* ≥ *logQ* (similar to exceedance probability, *Pr* = 1 – *exp*[–Er]) is indicated by labelled grey regions and described as "unlikely", "possible", "likely", or "probable", i.e., Er_T/Er_V (≥ *logQ*)<0.2 is described as "unlikely", 0.2 ≤ Er_T/Er_V (≥ *logQ*)<2.0 is described as "possible", 2.0 ≤ Er_T/Er_V (≥ *logQ*)<10.0 is described as "likely", and Er_T/Er_V (≥ *logQ*)≥10.0 is described as "probable". The exceedance rates of PD and SL seismic events for the normalised volume extracted are lowest for BAM_10-13 and BAM_14-16, i.e., 8.3 ≤ Er_V (≥0.0) ≤ 12.0 and 1.3 ≤ Er_V (≥1.0)≤1.9, respectively; the exceedance rates are highest for BAM_20-22, i.e., Er_V (≥0.0) = 40.1 and Er_V (≥1.0) = 6.5, respectively; and the exceedance rates for BAM_17-19 are higher than those for BAM_10-13 and BAM_14-16 and lower than those for BAM_20-22, i.e., Er_V (≥0.0) = 17.5 and Er_V (≥1.0) = 2.8, respectively. The exceedance rates for the mining periods of the shaft pillar extraction suggest an increasing trend in the seismic hazard at Bambanani mine, particularly with respect to RB seismic events that have scalar potency *logP* ≥ 2.3 and local magnitude m_L ≥ 2.7 and are described as "unlikely" for the initial mining period and "possible" for the final mining period. The exceedance rates for the normalised time span suggest a similar increasing trend in the seismic hazard.

Numerical modelling

Boundary element method

In the South African gold mining industry, numerical modelling of underground mining excavations is typically performed by applying the Boundary Element Method (BEM) and solving the elasticity equations that correspond to displacement discontinuity (DD) or fictitious force (FF) elements (Salamon, 1964; Starfield, Crouch, 1973; Crouch, 1976a, 1976b; Banerjee, Butterfield, 1981; Crouch, Starfield, 1983; Brebbia, 1984; Napier, Stephansen, 1987; Ryder et al., 1999; Ryder, Malan, 2002). In this paper, the tabular mining excavations at Bambanani mine are approximated using planar surfaces and therefore represented by DD elements in the corresponding BEM model (hereinafter referred to as the DD-BEM model, non-tabular mining excavations are typically represented by FF elements). Figure 7 shows a schematic diagram of a DD element and DD vector $\overline{u} = (u_x, u_y, u_z)$ that represent planar deformation in the local co-ordinate system of the DD surface, i.e., u_x and u_y correspond to shear-type deformation in the XY plane (left and middle, sometimes referred to as ride in the X and Y direction, respectively, similar to fault deformation of a fault slip seismic event), and u_z corresponds to normal-type deformation along the Z axis (right, sometimes referred to as convergence). The planar deformation on the DD surface is indicated by black arrows and the positive and negative subsurfaces with respect to the orientation of the XY plane and Z axis are shown as yellow and green regions, respectively.

Table 2

Scalar potency of seismic events, time span, and volume extracted for the different mining periods that are associated with the shaft pillar extraction at Bambanani mine from 1 January 2010 to 30 June 2022

	BAM_10-13	BAM_14-16	BAM_17-19	BAM_20-22	BAM_ALL
Scalar Potency, P_{mp} [m^3]	880	2748	3438	4770	11836
Time Span, T_{mp} [days/years]	1461/4.0	1096/3.0	1095/3.0	943/2.6	4595/12.6
Volume Extracted, V_{mp} [m^3]	41103	89167	76321	46312	252903

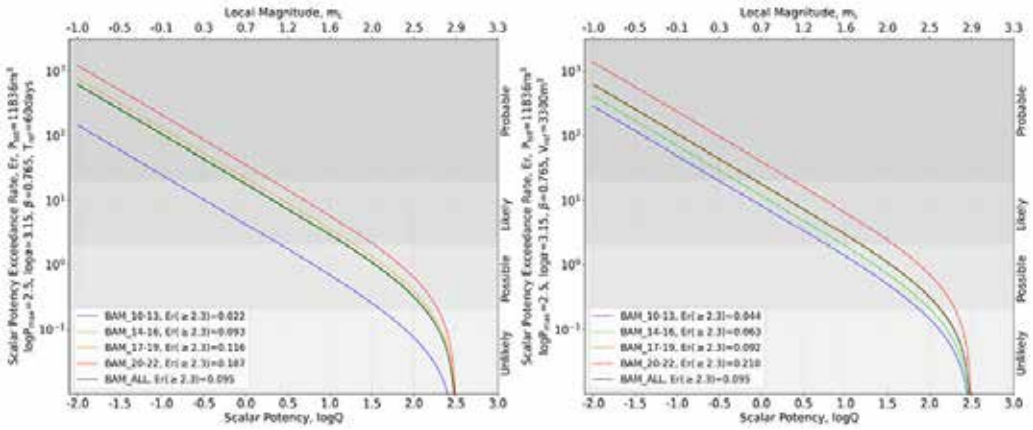

Figure 6—Comparison of the exceedance rates for the normalised time span (left) and normalised volume extracted (right). The blue, green, yellow, and red lines correspond to the mining periods at Bambanani mine. The likelihood of a seismic event that has scalar potency *logP* ≥ *logQ* is indicated by labelled grey regions

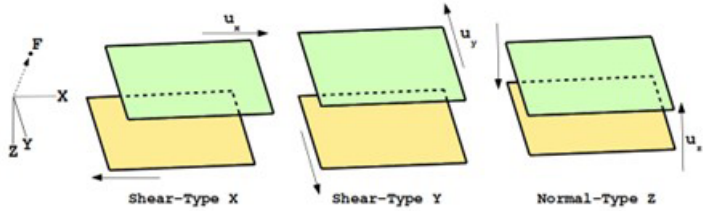

Figure 7—Schematic diagram of a DD element. The DD vector $\overline{u} = (u_x, u_y, u_z)$ represents shear- and normal-type deformation in the XY plane (left and middle) and along the Z axis (right). The planar deformation on the DD surface is indicated by black arrows, and the positive and negative subsurfaces are shown as yellow and green regions

In the DD-BEM model for Bambanani mine, the DD vectors are evaluated by solving the elasticity equations that correspond to a collection of DD elements and satisfy the virgin stress boundary conditions, and the combined stress field is constructed by calculating the induced stress kernels for a collection of points in the rockmass (hereinafter referred to as field points) and combining the induced stress field from the DD elements that represent the mining excavations and the virgin stress field:

$$S_{ij}^k = \begin{bmatrix} S_{xx} & S_{xy} & S_{xz} \\ S_{yx} & S_{yy} & S_{yx} \\ S_{zx} & S_{xy} & S_{zz} \end{bmatrix} = \sum_{k=0}^{N_{DE}-1} \sum \left[S_{ij,x}^{h\to k} u_{h,z} + S_{ij,y}^{h\to k} u_{h,y} + S_{ij,z}^{h\to k} u_{h,z} \right] + p_z^k v_{ij}^k$$

$$v_{ij}^k = \begin{bmatrix} v_{xx} & v_{xy} & v_{xz} \\ v_{yx} & v_{yy} & v_{yx} \\ v_{zx} & v_{zy} & v_{zz} \end{bmatrix} = \begin{bmatrix} 0.013494\,MPa/m & 0.0 & 0.0 \\ 0.0 & 0.013494\,MPa/m & 0.0 \\ 0.0 & 0.0 & 0.026988\,MPa/m \end{bmatrix} \quad [8]$$

where N_{DE} is the number of DD elements, N_{FP} is the number of field points, S_{ij}^k is the combined stress tensor for the field point with index $k < N_{FP}$ in the global co-ordinate system, $S_{ij,x}^{h\to k}$, $S_{ij,x}^{h\to k}$ and $S_{ij,z}^{h\to k}$ are the induced stress kernels for the DD element with index $h < N_{DE}$, $\overline{u}_h = (u_{h,x}, u_{h,y}, u_{h,z})$ is the corresponding DD vector that satisfies the virgin stress boundary condition $\overline{b}_h = -p_z^h v_{ij} n_h$, p_z^h and n_h are the depth and unit normal vector of the DD element, respectively, v_{ij} is the virgin stress tensor per unit depth and p_z^k is the depth of the field point. For Bambanani mine, the average depth is p_z = 2050m and the virgin stress tensor is $v_{zz} = \rho g = 0.026988\ MPa/m$ and $v_{xx} = v_{yy} = v_{zz}/2 = 0.013494\ MPa/m$, where $\rho = 2750k\ g/m^3$ is the density of the rockmass and g = 9.81 m/s² is gravitational acceleration. The normal- and shear-type stress for a field point that is associated with a planar surface in the DD-BEM model is calculated by transforming the combined stress tensor to a traction vector:

$$S_{nt}^k = \overline{S_{ct}^k} \cdot n_k \overline{S_{ct}^k} = S_{ij}^k n_k$$
$$S_{st}^k = \left| \overline{S_{ct}^k} - \left(\overline{S_{ct}} \cdot n_k \right) n_k \right| \quad [9]$$

where S_{nt}^k and S_{st}^k is the normal- and shear-type stress, respectively, $\overline{S_{ct}^k} = S_{ij}^k n_k$ is the combined traction vector for the field point with index $k < N_{FP}$, and n_k is the unit normal vector for the planar surface.

Modelled crush- and shear-type failures

Modelled crush-type failures

To accommodate crush seismic events at Bambanani mine, the DD-BEM model is populated with field points and additional DD elements that are constructed from the tabular orebody that surrounds the mining excavations and represent modelled crush-type failures in the rockmass. In this paper, the tabular orebody is approximated using planar surfaces (similar to tabular mining excavations) and the corresponding crush-type field points are evaluated using an excess normal stress (ENS) threshold, which is calculated by applying the limit equilibrium method (LEM) and a peak Hoek-Brown strength criterion (Hoek, Brown, 1980; Barron, 1984; Barron, Pen, 1992; Hoek, Marinos, 2007; Napier, Malan, 2007, 2011, 2012; Ilchev, 2013a, 2013b; Napier, Malan, 2014, 2018, 2021):

$$ENS = S_{nt}^k - \tau_{n0}$$
$$\tau_{n0} = S_{le} + \tau_{c0} \left[\frac{r_0}{\tau_{c0}} S_{le} + q_0 \right]^{\frac{1}{2}} \quad [10]$$

where τ_{n0} is the peak normal-type strength, S_{nt}^k is the normal-type stress for the crush-type field point and additional DD element with index $k < N_{FP}$, τ_{c0} is the peak uniaxial compressive strength of the rockmass, r_0 and q_0 are the peak Hoek-Brown strength parameters, and S_{le} is the transverse-type stress from the LEM. For a crush-type field point that exceeds the ENS threshold and therefore has $ENS > 0$, the boundary condition of the additional DD element is modified to accommodate the residual strength of the modelled crush-type failure and the corresponding crush-type deformation in the DD-BEM model for Bambanani mine (similar to convergence of mining excavations):

$$\overline{b}_k = -p_z^k v_{ij} n_k + \tau_{n1} n_k$$
$$\tau_{n1} = S_{le} + \tau_{c1} \left[\frac{r_1}{\tau_{c1}} S_{le} + q_1 \right]^{\frac{1}{2}} \quad [11]$$

where τ_{n1} is the residual normal-type strength, τ_{c1} is the residual uniaxial compressive strength, and r_1 and q_1 are the residual Hoek-Brown strength parameters. The DD vectors of the additional DD elements are iteratively evaluated by solving the elasticity equations that satisfy the residual strength boundary conditions until all crush-type field points have $ENS \le 0$. For the crush-type field points in the paper, the peak and residual uniaxial compressive strength of the rockmass is τ_{c0} = 200MPa and τ_{c1} = 20MPa, respectively, the peak Hoek-Brown strength parameters are r_0 = 4.0 and q_0 = 0.02, and the residual Hoek-Brown strength parameters r_1 = 1.5 and q_1 = 0.02 (Ryder, Jager, 2002).

Modelled shear-type failures

To accommodate shear and fault slip seismic events, the DD-BEM model for Bambanani mine is similarly populated with field points and additional DD elements that represent modelled shear-type failures in the rockmass and are evaluated using excess shear stress (ESS) thresholds, which are calculated by applying a simple Coulomb-friction strength criteria (Ryder, 1987; Napier, 1987; Spottiswoode, 1988; Ryder, 1988; Jager, Ryder, 1999a; Ryder et al., 2002):

$$ESS = S_{st}^k - \tau_{s0} \text{ or } S_{st}^k - \tau_{s1}$$
$$\tau_{s0} = S_{nt}^k \tan\phi_0 + C_0$$
$$\tau_{s1} = S_{nt}^k \tan\phi_1 + C_1 \quad [12]$$

where τ_{s0} is the peak shear-type strength for the peak ESS threshold, τ_{s1} is the residual shear-type strength for the residual ESS threshold, S_{st}^k is the shear-type stress for the shear-type field point and additional DD element with index $k < N_{FP}$, S_{nt}^k is the corresponding normal-type stress, ϕ_0 and C_0 are the peak friction angle and peak cohesion, respectively, and ϕ_1 and C_1 are the residual friction angle and residual cohesion, respectively. In this paper, the shear-type field points are constructed from the planar surfaces of Ortlepp-shear features that surround the mining excavations and correspond to the orientation of maximum ESS (Gay, Ortlepp, 1979; Ortlepp et al., 1997; Ortlepp, 2000; Ortlepp et al., 2005; Van Aswegen, Stander, 2012; Van Aswegen, 2013) and geological features that are approximated using additional planar surfaces that correspond to the digitised faults supplied by Harmony Gold Mining Company. For Ortlepp-shear features in this paper, the peak and residual friction angle is $\phi_0 = \phi_1 = 30°$ and the peak and residual cohesion is $C_{0c} = 20$MPa and $C_1 = 0$MPa, respectively, and for geological features in the rockmass, the peak friction angle is $\phi_0 = 25°$, the residual friction angle is $\phi_1 = 20°$, and the peak and residual cohesion is $C_0 = 10MPa$ and $C_1 = 0MPa$, respectively (Bieniawski, 1967; Byerlee, 1978; Jager, Ryder, 1999b; Ryder, 2002 James et al., 2007; Hofmann, Scheepers, 2011; Hofmann et al., 2013; Van Aswegen, 2020; Hofmann, 2024).

For a shear-type field point or modelled shear-type failure that exceeds the *ESS* thresholds in the DD-BEM model and therefore has peak *ESS* > 0 or residual ESS > 0, the DD vector of the additional DD element is iteratively modified to accommodate the corresponding shear-type deformation (similar to ride of mining excavations) until all shear-type field points have peak *ESS* ≤ 0 and all shear-type failures have residual *ESS* ≤ 0. Figure 8 shows the modelled shear-type failures that are associated with the different mining periods of the shaft pillar extraction at Bambanani mine, i.e., BAM_10-13, BAM_14-16, BAM_17-19, and BAM_20-22 (from top left to bottom right). The black-to-white contours indicate the cumulative shear-type deformation on the DD surfaces of the additional DD elements that represent the Ortlepp-shear and geological features in the DD-BEM model. The initial mining excavations are shown as grey regions and the final mining excavations are shown as blue, green, yellow, and red regions that correspond to BAM_10-13, BAM_14-16, BAM_17-19, and BAM_20-22, respectively.

Modelled potency and hazard

In the DD-BEM model for Bambanani mine, the planar size of a modelled crush- or shear-type failure is expressed using modelled potency, which is calculated by integrating the planar deformation over the DD surface of the additional DD element (similar to scalar potency of a fault slip seismic event):

$$P_k' = \iint_{A_k} [|\overline{u_k}(x,y) \cdot n_k| + |\overline{u_k}(x,y) - [\overline{u_k}(x,y) \cdot n_k] n_k|] \delta x \delta y = [|\overline{u_k} \cdot n_k| + |\overline{u_k} - [\overline{u_k} \cdot n_k] n_k|] A_k \quad [13]$$

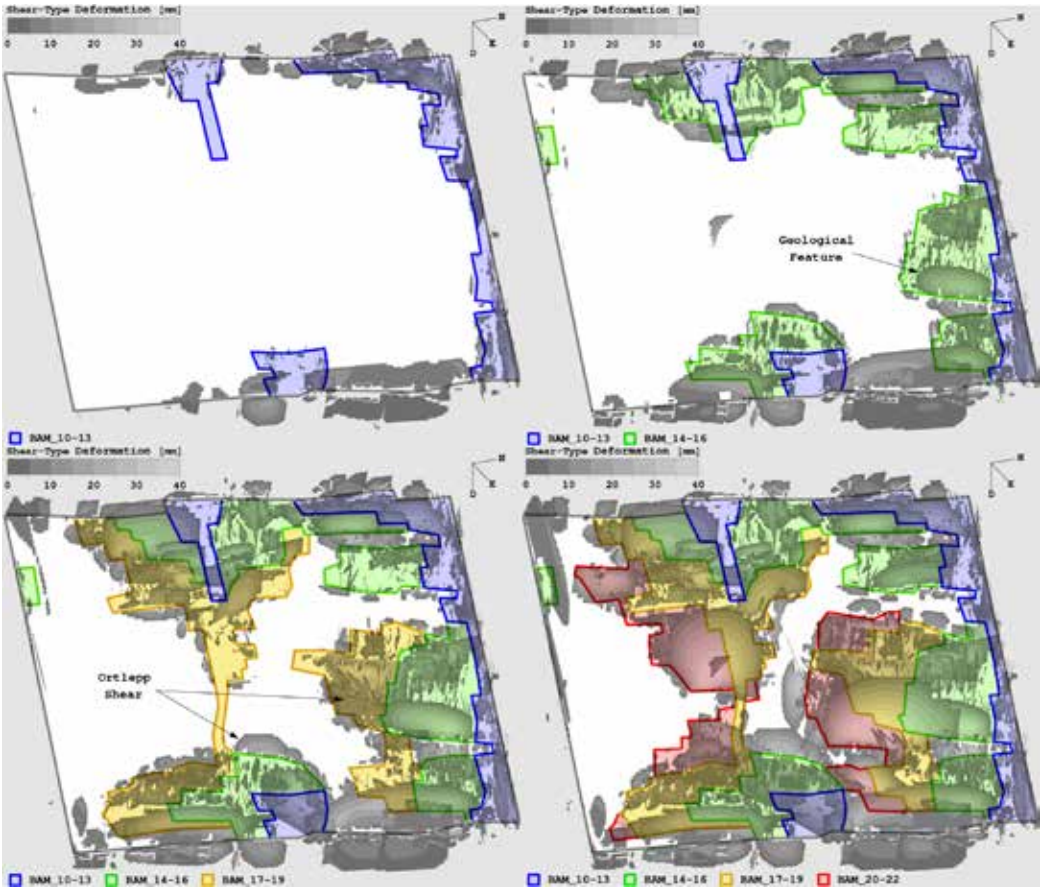

Figure 8—Modelled shear-type failures for the different mining periods of the shaft pillar extraction at Bambanani mine (from top left to bottom right). The cumulative shear-type deformation on the DD surfaces that represent shear-type failures is indicated by black-to-white contours. The initial mining excavations are shown as grey regions, and the final mining excavations are shown as blue, green, yellow, and red regions

where P'_k is the modelled potency of the additional DD element with index $k < N_{FP}$ that represents a modelled crush- or shear-type failure in the DD-BEM model, $\overline{u_k}(x,y) = \overline{u_k} = (u_{k,x}, u_{k,y}, u_{k,z})$ is the corresponding DD vector, n_k is the unit normal vector, and A_k is the planar area of the DD surface.

In this paper, the modelled hazard is expressed as an exceedance rate (Er'), which is calculated by scaling the expected number of seismic events using the modelled potency of the crush- and shear-type failures that exceed the ENS and ESS thresholds in the DD-BEM model for Bambanani mine and normalising the time span and volume extracted for the different mining periods of the shaft pillar extraction to some reference period (similar to the seismic hazard using scalar potency):

$$Er'_T(\geq logQ) = \frac{T_{ref}}{T_{mp}} N'_P(\geq logQ)\; Er'_V(\geq logQ) = \frac{V_{ref}}{V_{mp}} N'_P(\geq logQ)$$
$$N'_P(\geq logQ) = P'_{mp} \frac{N_e(\geq logQ)}{P_{tot}} = P'_{mp} \frac{\alpha}{P_{tot}} [10^{-\beta logP} - 10^{-\beta logP_{max}}] \quad [14]$$
$$P'_{mp} = \sum_{k=0}^{N_{FP}-1} [max(P'_{k+} - P'_{k-}, 0)]$$

where Er' ($\geq logQ$) is the exceedance rate of a seismic event that has scalar potency $logP \geq logQ$, T_{mp} is the time span for the mining period, T_{ref} = 60 days is the time span for the reference period, V_{mp} and V_{ref} = 3300m^3 are the corresponding volume extracted for the mining period and reference period, respectively, $N'_P(\geq logQ)$ is the scaled number of seismic events using the modelled potency of the crush- and shear-type failures, $N_e(\geq logQ) = \alpha[10^{-\beta logQ} - 10^{-\beta logP_{max}}]$ is the expected number of seismic events using the upper-truncated power law, P_{tot} = 11836 m^3 is the total scalar potency, P_{max} = 2.5 is the maximum scalar potency of the next RB seismic event, $log\alpha$ = 3.15 and β = 0.765 are the power-law parameters, P'_{mp} is the modelled potency for the mining period, N_{FP} is the number of field points, P'_{k+} is the final modelled potency of a crush- or shear-type failure that corresponds to the additional DD element with index $k < N_{FP}$, and P'_{k-} is the initial modelled potency.

Modelling results

In the DD-BEM model for Bambanani mine, the tabular mining excavations are subdivided according to a collection of digitised mining steps supplied by Harmony Gold Mining Company (Van Der Wath, 2023); the modelled potency of the crush- and shear-type failures is calculated for the corresponding mining steps; and the modelled hazard is calculated for the different mining periods that are associated with the shaft pillar extraction, i.e., BAM_10-13, BAM_14-16, BAM_17-19, BAM_20-22, and BAM_ALL. The DD-BEM model has 150 subdivided mining steps that correspond to the calendar months from 1 January 2010 to 30 June 2022, i.e., BAM_10-13 contains 48 mining steps that correspond to the calendar months from 1 January 2010 to 31 December 2013; BAM_14-16 and BAM_16-19 contain 36 mining steps from 1 January 2014 to 31 December 2016 and from 1 January 2017 to 31 December 2019, respectively; and BAM_19-22 contains 30 mining steps from 1 January 2020 to 30 June 2022. The tabular mining excavations at Bambanani mine typically strike northwards, dip eastwards at approximately 20° and are represented by 250 thousand DD elements that have 1 × 1 m, 2 × 2 m, 4 × 4 m, and 8 m × 8 m dimensions. To accommodate modelled crush-type failures, the tabular orebody that surrounds the mining excavations is represented by an additional 150 thousand DD elements that have 2 m × 2 m dimensions, and to accommodate modelled shear-type failures, the Ortlepp-shear and geological features are represented by an additional 400,000 DD elements that have 4 m × 4 m dimensions. The faults at Bambanani mine typically strike southwards and dip westwards at approximately 70°.

Figure 9 shows a comparison of the cumulative modelled potency and cumulative scalar potency with respect to calendar time (left) and volume extracted (right) such that the blue, green, yellow, and red lines correspond to BAM_10-13, BAM_14-16, BAM_17-19, and BAM_20-22, respectively. The solid lines indicate the cumulative modelled potency of the additional DD elements that represent modelled crush- and shear-type failures in the DD-BEM model, and the dashed lines indicate the cumulative scalar potency of seismic events recorded by the IMS seismic system at Bambanani mine. Table 3 summarises the modelled potency, scalar potency, time span, and volume extracted for the mining periods that are associated with the shaft pillar extraction. Figure 10 shows a comparison of the modelled potency and scalar potency exceedance rates for the normalised time span (left) and normalised volume extracted (right) such that the blue, green, yellow, red, and black lines correspond to BAM_10-13, BAM_14-16, BAM_17-19, BAM_20-22, and BAM_ALL, respectively. The solid lines indicate the exceedance rates using the modelled potency of the crush- and shear-type failures that exceed the ENS and ESS thresholds in the DD-BEM model for Bambanani mine, and the dashed lines indicate

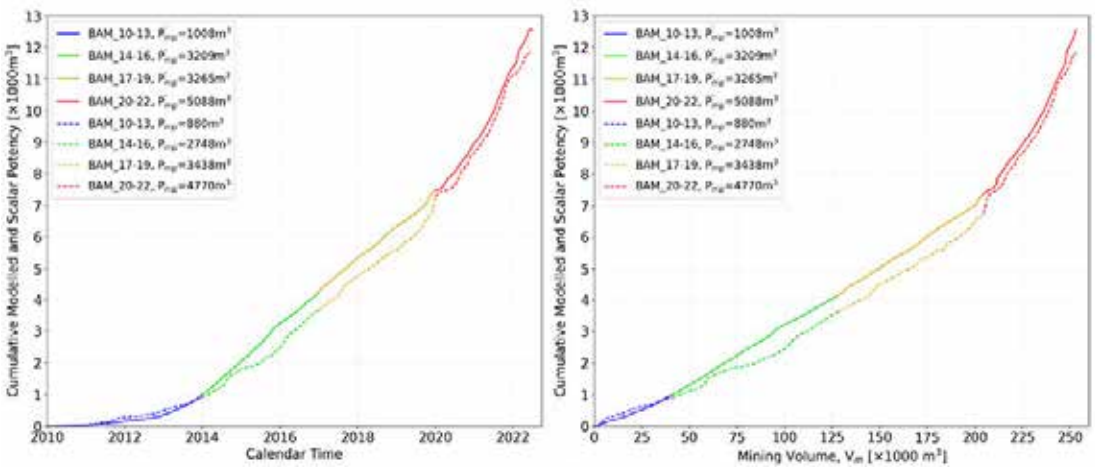

Figure 9—Comparison of cumulative modelled and scalar potency with respect to calendar months (left) and volume extracted (right). The solid lines indicate cumulative modelled potency, the dashed lines indicate cumulative scalar potency, and the lines are coloured according to the different mining periods at Bambanani mine

Table 3

Modelled potency, scalar potency, time span and volume extracted for the different mining periods associated with the shaft pillar extraction at Bambanani mine from 1 January 2010 to 30 June 2022

	BAM_10-13	BAM_14-16	BAM_17-19	BAM_20-22	BAM_ALL
Modelled Potency, P'_{mp} [m^3]	1008	3209	3265	5088	12570
Scalar Potency, P_{mp} [m^3]	880	2748	3438	4770	11836
Time Span, T_{mp} [days/years]	1461/4.0	1096/3.0	1095/3.0	943/2.6	4595/12.6
Volume Extracted, V_{mp} [m^3]	41103	89167	76321	46312	252903

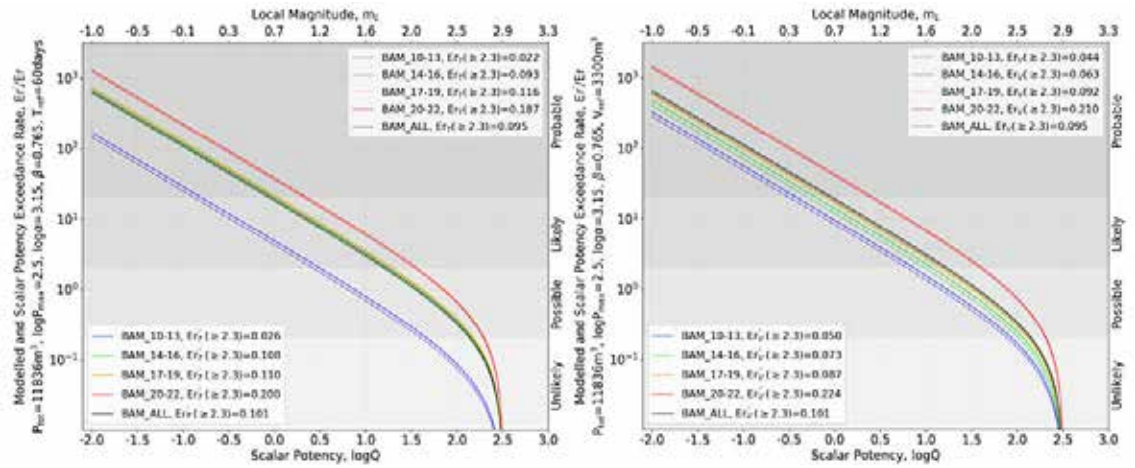

Figure 10—Comparison of the exceedance rates for the normalised time span (left) and normalised volume extracted (right). The solid and dashed lines indicate the exceedance rates using modelled potency and scalar potency, respectively. The lines are coloured according to the mining periods at Bambanani mine

the corresponding exceedance rates using the scalar potency of seismic events. The likelihood of a seismic event that has scalar potency $logP \geq logQ$, is indicated by labelled grey regions and described as "unlikely", "possible", "likely" or "probable", e.g., $0.2 \leq Er'_T/Er'_V (\geq logQ) < 2.0$ is described as "possible", and $Er'_T/Er'_V (\geq logQ) \geq 10.0$ is described as "probable".

The modelled hazard is a reasonably accurate estimation of the seismic hazard for the different mining periods of the shaft pillar extraction at Bamabanani mine. The modelled potency of the crush- and shear-type failures overestimates the scalar potency of seismic events for BAM-10-13, BAM_14-16, and BAM_20-22, i.e., the modelled potency is P'_{mp} = 1008m^3, 3209m^3, and 5088m^3, respectively; the scalar potency is P'_{mp} = 880m^3, 2748m^3, and 4770m^3, respectively; and the relative error is $[P'_{mp} - P_{mp}]/P'_{mp}$ = 0.12, 0.14, and 0.06, respectively. The modelled potency underestimates the scalar potency for BAM_17-19, i.e., the modelled potency is P'_{mp} = 3265m^3, the scalar potency is P_{mp} = 3438m^3, and the relative error $[P'_{mp} - P_{mp}]/P'_{mp}$ = –0.05. The modelled potency exceedance rates similarly overestimate and underestimate the scalar potency exceedance rates. The modelled potency exceedance rates of PD and SL seismic events are lowest for BAM_10-13, i.e., Er'_V (≥0.0) = 9.5 and Er'_V (≥1.0) = 1.5, respectively; the exceedance rates are highest for BAM_20-22, i.e., Er'_V (≥0.0) = 42.8 and Er'_V (≥1.0) = 6.9, respectively; and the exceedance rates for BAM_14-16 and BAM_17-19 are higher than those for BAM_10-13 and lower than those for BAM_20-22, i.e., $14.0 \leq Er'_V$ (≥0.0) ≤16.6 and $2.3 \leq Er'_V$ (≥1.0)≤2.7, respectively.

In the DD-BEM model for Bambanani mine, the spatial intensity of the modelled potency is expressed as a planar density, which is calculated by radially filtering the modelled crush- and shear-type failures that exceed the ENS and ESS thresholds according to a collection of grid points:

$$P^{l\prime}_{gd} = \sum_{k=0}^{N_{FP}-1} \chi(\overline{w_k})[max(P'_{k+} - P'_{k-}, 0)]$$

$$\chi(\overline{w_k}) = \left\{ \begin{matrix} 0 D(\overline{w_k}) > R \\ \frac{1}{\pi R^2} D(\overline{w_k}) \leq R \end{matrix} \right\} R = 100m \quad [15]$$

where N_{GP} is the number of grid points, $P^{l\prime}_{gp}$ is the planar density of the modelled potency for the grid point with index $l < N_{GP}$, N_{FP} is the number of field points, P'_{k+} is the final modelled potency of the additional DD element with index $k < N_{FP}$ that represents a modelled crush- or shear-type failure in the DD-BEM model, P'_{k-} is the initial modelled potency, $\overline{w_k} = (w_{k,x}, w_{k,y}, w_{k,z})$ is the corresponding DD location vector, $\chi(\overline{w_k})$ is the gridding factor, $D(\overline{w_k})$ is the distance from the additional DD element to the grid point, and R = 100 m is the gridding radius. The spatial intensity of the scalar potency is similarly calculated by radially filtering seismic events recorded by the IMS seismic system at Bambanani Mine:

$$P^{l}_{gp} = \sum_{n=0}^{N_{SE}-1} \chi(\overline{w_n}) P_n \quad [16]$$

where P^{l}_{gp} is the planar density of the scalar potency, N_{SE} is the number of seismic events, P_n is the scalar potency of the seismic event with index $n < N_{SE}$ and $\overline{w_n} = (w_{n,x}, w_{n,y}, w_{n,z})$ is the corresponding source location vector. Figure 11 shows the planar density of the modelled potency (left) and scalar potency (right) at Bambanani mine. The black-to-white contours indicate the planar density, and the "hotspots" in the spatial intensity that have planar density ($P^{l\prime}_{gp}/P^{l}_{gp} \geq 0.3$) are shown as cyan and magenta regions. Some geological features are indicated by black dashed lines.

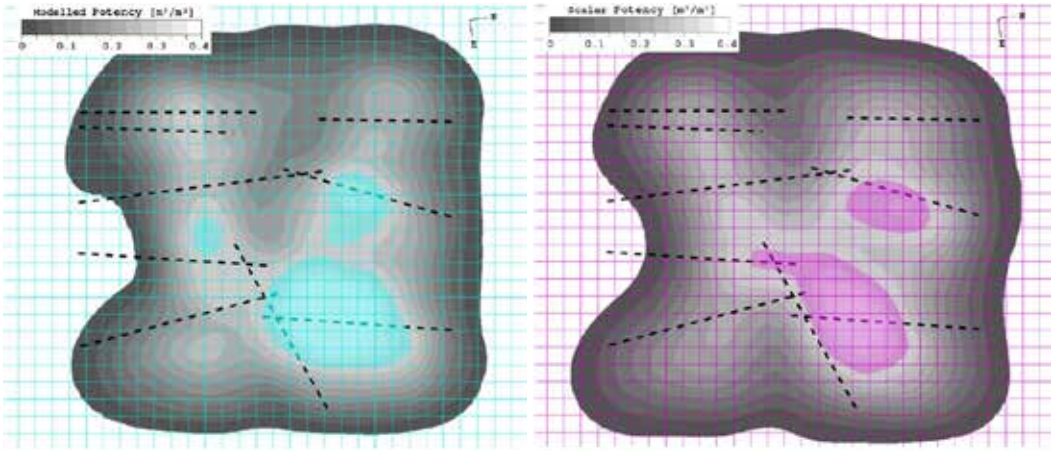

Figure 11—Planar density of the modelled potency (left) and scalar potency (right) at Bambanani mine. The planar density is indicated by black-to-white contours and the "hotspots" in the spatial intensity ($P^{lr}_{gp}/P^{l}_{gp} \geq 0.3$) are shown as cyan and magenta regions. Some geological features are indicated by black dashed lines

Comments

In this paper, the modelled potency and modelled hazard are presented for medium- and longer-term mining periods that are associated with the shaft pillar extraction at Bambanani mine, i.e., BAM_10-13, BAM_14-16, BAM_17-19, BAM_20-22, and BAM_ALL, and the modelling results suggest an increasing trend in the modelled hazard that is a reasonably accurate estimation of the seismic hazard. The modelled potency exceedance rates of RB seismic events for BAM_10-13, BAM_14-16, BAM_17-19, BAM_20-22, and BAM_ALL are Er'_V (≥2.3) = 0.050, 0.073, 0.087, 0.224, and 0.101, respectively, and the scalar potency exceedance rates are Er'_V (≥2.3) = 0.044, 0.063, 0.092, 0.210, and 0.095, respectively. The relative error is typically lower than 10% or 15%, e.g., $[Er'_V - Er_V]/Er'_V$ = 0.12, 0.14, -0.05, 0.06 and 0.06, respectively. The relative errors for shorter term mining periods are probably higher and not considered in this paper. The "hotspots" in the spatial intensity of the modelled potency are similar to those of the scalar potency. Generally, the modelling results suggest that the modelling methodology is appropriate for medium- and longer term forecasting of seismic activity and hazard, particularly for the comparison of different mining periods as presented in this paper. The modelling methodology is probably not appropriate for shorter term forecasting or prediction of seismic events.

References

Aki, K., Richards, P.G. 1980. Quantitative Seismology. Theory and Methods. W.H. Freeman and Company, San Francisco.

Andersen, L.M., Ryder, J.A., Goldbach, O.D. 2002. A Textbook on Rock Mechanics for Tabular Hard Rock Mines, chapter 5.3, seismology, location of seismic events, pp. 204–210.

Banerjee, P.K., Butterfield, R. Boundary element methods in engineering science. McGraw & Hill, 1981.

Barron, K. 1984. Analytical approach to the design of coal pillars. *CIM Bulletin,* vol. 77, no. 868, pp. 37–44. .

Barron, K., Pen, Y. 1992. A revised model for coal pillars. In *Proceedings of the Workshop on Coal Pillar Mechanics and Design*, vol. 9315, p. 144. United States, Department of the Interior, Bureau of Mines.

Ben-Menahem, A., Singh, S.J. 1981. Seismic Waves and Sources. Springer-Verlag, New York.

Ben-Zion, Y., Zhu, L. 2002. Potency-magnitude scaling relation for southern California earthquakes with 1.0<M<7.0. *Geophysical Journal International,* vol. 148, pp. F1–F5.

Bieniawski, Z.T. 1967. Mechanism of brittle fracture of rock: part 1 theory of the fracture process. In *International Journal of Rock Mechanics and Mining Sciences & Geomechanics Abstracts*, vol. 4, pp. 395–406. Elsevier.

Boatwright. J. 1980. A spectral theory for circular seismic sources; simple estimates of source dimension, dynamic stress drop, and radiated seismic energy. B*ulletin of the Seismological Society of America*, vol. 70, no. 1, pp. 1–27.

Brebbia, C.A. 1984. The Boundary Element Method for Engineers. 97807273020. Pentech Press, ISBN 0727302051

Bredenkamp, A.F.L., Goldswain, G., Green, M. 2013. 4.5Hz Geophone Sensors. Technical report, *Institute of Mine Seismology*.

Brune, J.N. 1970. Tectonic stress and the spectra of seismic shear waves from earthquakes. *Journal of Geophysical Research*, vol. 75, no. 26, pp. 4997–5009.

Burroughs, SM, Tebbens, S.F. 2002. The upper-truncated power law applied to earthquake cumulative frequency-magnitude distributions: Evidence for a time-independent scaling parameter. *Bulletin of the Seismological Society of America*, vol. 92, no. 8, pp. 2983–2993.

Burroughs, S.M., Tebbens, S.F. 2001. Upper-truncated power law distributions. *Fractals*, vol. 9, no. 02, pp. 209–222.

Burrows, D., Ebrahim-Trollope, R. 2004. Seismic magnitude and its application in the industry. In *SANIRE Symposium Proc, The Miners Guide Through the Earths Crust*,(J) Lass eds.), Potchefstroom, South Africa.

Butler, A.G. 1992. Magnitude evaluation for mining regions using the integrated seismic system. Technical report, ISS International.

Butler, A.G., van Aswegen, G. 1993. Ground velocity relationship based on a large sample of underground measurement in two south african mining regions. *Proceedings of the 3rd International Symposium on Rockbursts and Seismicity in Mines.*

Byerlee, J. 1978. Friction of rocks. Rock friction and earthquake prediction, pp. 615–626.

Cooke, P. 1979. Statistical inference for bounds of random variables. Biometrika, vol. 66, no. 2, pp. 367–374.

Christensen, K., Danon, L., Scanlon, T., Bak, P. 2002. Unified scaling law for earthquakes. *Proceedings of the National Academy of Sciences*, vol. 99(suppl_1), pp. 2509–2513.

Crouch, S.L. 1976a. nalysis of stress and displacements around underground excavations: an application of the displacement discontinuity method. Technical report, Department of Civil and Mineral Engineering, University of Minnesota.

Crouch, S.L. 1976b. Solution of plane elasticity problems by the displacement discontinuity method. *International Journal of Numerical Methods in Engineering*, vol. 10, pp. 301–343.

Crouch, S.L., Starfield, A.M. 1983. Boundary Element Methods in Solid Mechanics: With Applications in Rock Mechanics and Geological Engineering. Allen & Unwin, 1983. ISBN 004620010X, 9780046200107.

Dennison, R.J.G., van Aswegen, G. 1993. Stress Modelling and Seismicity on the Tanton Fault: A Case Study in a South African Gold Mine. In *Proceedings of the 3rd International Symposium on Rockbursts and Seismicity in Mines*, p. 327, Kingston, Ontario, Canada.

Dor, O., Reches, Z., van Aswegen, G. 2001. Fault zones associated with the matjhabeng earthquake, 1999, South Africa. In *5th International Symposium on Rockbursts and Seismicity in mines*, pp. 109–112.

Du Toit, C., Mendecki, A.J. 2007. Examples of time distribution of seismic events in mines. In IUGG Conference, Session on Induced Seismicity (SW006), Perugia.

Ebrahim-Trollope, R., Durrheim, R.J., Smith, G. 2013. Measuring the size of mining-induced earthquakes: a proposal. In *13th SAGA Biennial Conference and Exhibition*. European Association of Geoscientists & Engineers, pp. cp–378.

Eshelby, J.D. 1957. The determination of the elastic field of an ellipsoidal inclusion and related problems. *Proceedings of the Royal Society of London*, Series A, Mathematical and Physical Sciences, 241(1226):376–396, August 1957.

Frimmel, H.E. 2019. The witwatersrand basin and its gold deposits. The Archaean geology of the Kaapvaal craton, southern Africa, pp. 255–275.

Gay, N.C. Ortlepp, W.D. 1979. Anatomy of a mining-induced fault zone. *Geological Society of America Bulletin*, vol. 90, no. 1, pp. 47–58.

Geller, R.J. 1997. Earthquake prediction: a critical review. *Geophysical Journal International*, vol. 131, no. 3, pp. 425–450.

Gibowicz, S.J., Kijko, A. 1994a. An Introduction to Mining Seismology, chapter 11, seismic spectra and source parameters, pages 264–300.

Gibowicz, S.J., Kijko, A. 1994b. An Introduction to Mining Seismology, chapter 4, location of seismic events in mines , pages 48–77.

Gibowicz, S.J., Kijko, A. 1994c. An Introduction to Mining Seismology, chapter 12.3, Statistical Assessment of Seismic Hazard in Mines: Statistical Prediction, The Gutenberg-Richter Frequency-Magnitude Distribution, pp. 301–310.

Gutenberg, B., Richter, C.F. 1944. Frequency of earthquakes in california. *Bulletin of the Seismological Society of America*, vol. 34, no. 4, pp. 185–188.

Handley, J.R.F. 2004. Historic overview of the Witwatersrand Goldfields: A review of the discovery, geology, geophysics, development, mining, production and future of the Witwatersrand Goldfields as seen through a geological and financial association spanning 50 years.

Hanks, T.C. Kanamori, H. 1979. A moment magnitude scale. *Journal of Geophysical Research*, vol. 84, pp. 2348–2350.

Hoek, E., Brown, E. 1980. Empirical strength criterion for rock masses. *Journal of the Geotechnical Engineering Division*, ASCE, 106, 09. doi: 10.1061/AJGEB6.0001029

Hoek, E., Marinos, P. 2007. A brief history of the development of the hoek-brown failure criterion[j]. *Soils and Rocks*, 30, 05. doi: 10.28927/SR.302085

Hofmann, G., Scheepers, L. 2011. Simulating fault slip areas of mining induced seismic tremors using static boundary element numerical modelling. *Mining Technology*, vol. 120, pp. 53–64, 03 doi: 10.1179/037178411X12942393517291

Hofmann, G.F., Scheepers, L., Ogasawara, H. 2013. Loading conditions of geological faults in deep level tabular mines. In P*roc. 6th Int. Symp. In-Situ Rock Stress*. Sendai: Tohoku University, pp. 560–580.

Hofmann, G.F. 2024. Excess shear stress analysis of complex geological structures in underground mines. In *Deep Mining 2024: Proceedings of the 10th International Conference on Deep and High Stress Mining*, Australian Centre for Geomechanics. pp. 673–686.

Ilchev. A. 2013a. Comments on the implementation of the limit equilibrium method. Technical report. *Institute of Mine Seismology*.

Ilchev. A. 2013b. The limit equilibrium conjecture. Technical report, *Institute of Mine Seismology*.

Jager, A.J., Ryder, J.A. 1999a. A Handbook on Rock Engineering Practice for Tabular Hard Rock Mines, chapter 3.2.3, stoping layouts, excess shear stress, pp. 51–53.

Jager, A.J., Ryder, J.A. 1999b. A Handbook on Rock Engineering Practice for Tabular Hard Rock Mines, chapter 1.3.2, rock strength and friction properties, pages 13–14.

James, J.V., Rangasamy, T., Petho, S.P. 2007. Excess shear stress analysis of seimicity associated with dykes. In *Deep Mining 2007: Proceedings of the Fourth International Seminar on Deep and High Stress Mining*, pp. 21–30. Australian Centre for Geomechanics.

Jolley, S., Stuart, G., Freeman, S., Knipe, R., Kershaw, D., McAllister, E. 2007. Andrew Barnicoat, and R. Tucker. Progressive evolution of a late orogenic thrust system, from duplex development to extensional reactivation and disruption: Witwatersrand basin, south africa. *Geological Society*, London, Special Publications, 272:543–569, 05 2007. doi: 10.1144/GSL.SP.2007.272.01.28

Jooste. Y. 2025. A Numerical Modelling Methodology for Deep-Level Tabular Excavations using a Combined Bulking and Limit Equilibrium Constitutive Model, chapter 6, Monitoring during the Shaft Pillar Extraction at Bambanani Mine. PhD thesis, University of Pretoria.

Jooste. Y. 2023. Seismic events associated with the shaft pillar extraction at bambanani mine, supplied by harmony gold.

Kagan, Y.Y. 1997. Are earthquakes predictable? *Geophysical Journal International*, vol. 131, no. 3. pp. 505–525. https://academic.oup.com/gji/article/131/3/505/2140303

Kagan, Y.Y. 1999. Is earthquake seismology a hard, quantitative science? Seismicity Patterns, Their Statistical Significance and Physical Meaning, pp. 233–258.

Kagan, Y. 2010. Earthquake size distribution: Power-law with exponent 0.5? *Tectonophysics*, vol. 490, no. 1-2, pp. 103–114.

Kanamori, H. 1977. The energy release in great earthquakes. *Journal of Geophysical Research*, vol. 82, no. 20, pp. 2981–2987.

KN53463 Chandler. 1952. The distribution and frequency of record values. *Journal of the Royal Statistical Society: Series B* (Methodological), vol. 14, no. 2, pp. 220–228.

Kijko, A., Funk, C.W. 1994. The assessment of seismic hazards in mines. *Journal of the Southern African Institute of Mining and Metallurgy*, vol. 94, no. 7, pp. 179–185.

King, G.C.P. 1978. Geological faults, fractures, creep and strain. *Philosophical Transactions of the Royal Society of London. Series A, Mathematical and Physical Sciences*, 288(1350), pp. 197–212, February.

Kwiatek, G., Plenkers, K., Nakatani, M., Yabe, Y., Dresen, G., JAGUARS-Group. 2010. Frequency-magnitude characteristics down to magnitude-4.4 for induced seismicity recorded at mponeng gold mine, south africa. *Bulletin of the Seismological Society of America*, vol. 100, no. 3, pp. 1165–1173.

Linkov, A.M. 1997. New geomechanical approaches to develop quantitative seismicity. In *Rockbursts and seismicity in mines*, pp. 151–166.

Linkov, A.M. 2002. Integration of numerical modeling and seismic monitoring: general theory and first steps. In *Proceedings of the International Conference on New Developments in Rock Mechanics*, pp. 259–264.

Linkov, A.M. 2006. Numerical modeling of seismic and aseismic events in three dementional problems of rock mechanics. *Journal of Mining Science*, vol. 42, no. 1, pp. 1–14.

Linkov, A., Rybarska-Rusinek, L., Zoubkov, V. 2015. On comparison of simulated and observed seismicity. 07 2015.

Linkov, A., Rybarska-Rusinek, L., Zoubkov, V. 2016. Reasonable sets of input parameters and output distributions for simulation of seismicity. *International Journal of Rock Mechanics and Mining Sciences*, vol. 84, pp. 87–94, 04 2016. doi: 10.1016/j.ijrmms.2016.02.004

Linkov, A.M. 2013. Numerical modelling of seismicity: Theory and applications, Keynote lecture. In A. Malovichko and D. Malovichko, editors, *8th International Symposium on Rockbursts and Seismicity in Mines*, Russia, pp. 197–218.

Malovichko, D. 2020. Description of seismic sources in underground mines: Theory. *Bulletin of the Seismological Society of America*.

Malovichko, D. 2022. Utility of seismic source mechanisms in mining. In *Proceedings of the Tenth International Symposium on Rockbursts and Seismicity in Mines, Society for Mining, Metallurgy & Exploration*, Englewood, 2022.

McGarr, A., Bicknell, J., Sembera, E., Green, R.W.E. 1989. Analysis of exceptionally large tremors in two gold mining districts of south africa. *Seismicity in mines*, pp. 295–307.

Mendecki, A.J., Sciocatti, M. 1997. Seismic Monitoring in Mines, chapter 5, location of seismic events, pp. 87–107.

Mendecki, A.J., Niewiadomski, J. 1997. Seismic Monitoring in Mines, chapter 8, spectral analysis and seismic source parameters, pp. 144–158.

Mendecki, A.J., van Aswegen, G., Mountfort, P. 1999a. A Handbook on Rock Engineering Practice for Tabular HardRock Mines, chapter 9.4, a guide to routine seismic monitoring in mines, quantification of seismic sources, pp. 291–293.

Mendecki, A.J., van Aswegen, G., Mountfort, P. 1999b. A Handbook on Rock Engineering Practice for Tabular Hard Rock Mines, chapter 9.3, a guide to routine seismic monitoring in mines, location of seismic events, pages 290–291.

Mendecki, A.J. 2012. Size distribution of seismic events in mines. In *Proceedings of the Australian Earthquake Engineering Society 2012 Conference*, Queensland, pp. 1–20.

Mendecki, A.J. 2013.Mine Seismology: Glossary of Selected Terms. In *8th International Symposium on Rockbursts and Seismicity in Mines*, pp. 523–550, St Petersburg-Moscow, Russia.

Mendecki, A.J. 2016a. Mine Seismology Reference Book: Seismic Hazard, chapter 3, maximum event size. *Institute of Mine Seismology*, pp. 31–35. ISBN 978-0-9942943-0-2, www.imseismology.org/msrb/, 1 edition, May 2016a. http://www.imseismology.org/msrb/

Mendecki, A.J. 2016b. Mine Seismology Reference Book: Seismic Hazard, chapter 2, power laws and their utility. *Institute of Mine Seismology*, pp. 20–31. ISBN 978-0-9942943-0-2, www.imseismology.org/msrb/, 1 edition, May 2016b. URL http://www.imseismology.org/msrb/.

Motsepe, P.T., Motloba, J.M., Steenkamp, P.W., Lekubo, B.P, Mashego, H.E. 2021. Mineral resources and mineral reserves as at june 2021. Technical report, Harmony Gold, 2. https://www.har.co.za/21/download/HAR-RR21.pdf

Mthenjane, M. 2025. Minerals council south africa facts and figures pocket book 2024. https://www.mineralscouncil.org.za/component/jdownloads/?task=download.send&id=2390&catid=17&m=0&Itemid=119

Napier, J.A.L. 1987. The application of excess shear stress to the design of mine layouts. *Journal of the Southern African Institute of Mining and Metallurgy*, vol. 87, no. 12, pp. 397–405.

Napier, J.A.L., Stephansen, S.J. 1987. Analysis of deep-level mine design problems using the minsim-d boundary element program. In *Proceedings of the Twentieth International Symposium on the Application of Computers and Mathematics in the Mineral Industries.*, vol. 1, pages 3–19.

Napier, J.A.L., Malan, D.F. 2007. The computational analysis of shallow depth tabular mining problems. *Journal of the Southern African Institute of Mining and Metallurgy*, pp. 725–742.

Napier, J.A.L., Daniel Francois Malan. 2011. Numerical computation of average pillar stress and implications for pillar design.

Napier, J.A.L., Malan, D.F. 2012. Simulation of time-dependent crush pillar behaviour in tabular platinum mines. *Journal of the Southern African Institute of Mining and Metallurgy*, pp. 711–719.

Napier, J.A.L., Malan, D.F. 2014. A simplified model of local fracture processes to investigate the structural stability and design of large-scale tabular mine layouts. In *ARMA US Rock Mechanics/Geomechanics Symposium*, pp. ARMA–2014. ARMA.

Napier, J.A.L., Malan, D.F. 2018. Simulation of tabular mine face advance rates using a simplified fracture zone model. *International Journal of Rock Mechanics and Mining Sciences*. https://api.semanticscholar.org/CorpusID:134150957

Napier, J.A.L. Malan, D.F. 2021. A limit equilibrium model of tabular mine pillar failure. *Rock Mechanics and Rock Engineering*, vol. 54, pp. 71–89.

Ortlepp, W.D. 1997. Rock Fracture and Rockbursts: An Illustrative Study. Monograph series. *South African Institute of Mining and Metallurgy*. ISBN 9781874832676. https://books.google.co.za/books?id=tYQQAQAAMAAJ

Ortlepp, W.D. 2000. Study of rockburst source mechanism, gap 524 project. Technical report, *SIMRAC*, Johannesburg

Ortlepp, W., Armstrong, R., Ryder, J., OConnor, D. 2005. Fundamental study of micro-fracturing on the slip surface of mine-induced dynamic brittle shear zones. pp. 229–237, 01 2005. doi: 10.36487/ACG_repo/574_20

Ryder, J.A.E. 1987. xcess shear stress (ess): An engineering criterion for assessing unstable slip and associated rockburst hazards. In *ISRM Congress*, pages ISRM–6CONGRESS. ISRM.

Ryder, J.A. 1988. Excess shear stress in the assessment of geologically hazardous situations. *Journal of the Southern African Institute of Mining and Metallurgy*, vol. 88, pp. 27–39.

Ryder, J.A., Jager, A.J., Lightfoot, N. 1999. A Handbook on Rock Engineering Practice for Tabular Hard Rock Mines, chapter 11.3.5, numerical modelling, displacement discontinuity method, p. 337.

Ryder, J.A. 2002. A textbook on rock mechanics for tabular hard rock mines, chapter 2.6.2, mechanical properties of rock, shear properties of discontinuities, pp. 100–105.

Ryder, J.A., Malan, D.F. 2002. A textbook on rock mechanics for tabular hard rock mines, chapter 4.2.3, analytic solutions in elasticity, boundary element kernels, pp. 164–169.

Ryder, J.A., Jager, A.J. 2002. A textbook on rock mechanics for tabular hard rock mines, chapter 2.3.3, mechanical properties of rock, hoek-brown empirical strength criterion, pp. 68–70.

Ryder, J.A., York, G., Squelch, A.P. 2002. A textbook on rock mechanics for tabular hard rock mines, chapter 6.3, rockmechanics in the design of mining layouts, excess shear stress, pp. 255–267.

Robson, D.S., Whitlock, J.H. 1964. Estimation of a truncation point. *Biometrika*, vol. 51, no. 1/2, pp. 33–39.

Salamon, M.D.G. 1964. Elastic analysis of displacements and stresses induced by mining of seam or reef deposits – part iv: Inclined reef. *Journal of the Southern African Institute of Mining and Metallurgy*, vol. 65, pp. 319–338.

Salamon, M.D.G.,Weibols, G.A. 1972. Location of Seismic Events. Technical report, Chamber of Mines Research Organisation.

Salamon, M.D.G. 1993. Keynote address: Some applications of geomechanical modelling inrockburst and related research. In *3rd International Symposium on Rockbursts and Seismicity in mines*, pp. 297–309.

Starfield A.M., Crouch, S.L. 1973. Elastic analysis of single seam extraction. In *New Horizons in Rock Mechanics, American Society of Civil Engineers,* pp. 421–439.

Stankiewicz, T., Essrich, F. 2004. Standardised local magnitude scale for south african mines. Technical report, AngloGold Ashanti.

Spottiswoodet, S.M. 1988. Total seismicity, and the application of ess analysis to mine layouts. *Journal of the Southern African Institute of Mining and Metallurgy*, vol. 88, no. 4, pp. 109–116.

Spottiswoode, S.M. 2009. Is mine earthquake prediction possible. Rockbursts and Seismicity in Mines, Dalian, China.

Spottiswoode, S.M. 2010. Mine seismicity: Prediction or forecasting? *Journal of the South African Institute of Mining and Metallurgy*, vol. 110, no. 1, pp. 11–20.

Tucker, R.F., Viljoen, R.P., Viljoen, M.J. 2016. A review of the witwatersrand basin the worlds greatest goldfield. *Episodes*, vol. 39, no. 2, pp. 105–133.

van der Wath, S., Mohlatsane, J., Gerber, J.D. 2022. Seismic source mechanism characteristics observed during the bambanani mine shaft pillar extraction. Technical report, Association of Mine Managers South Africa.

Van Der Wath, S. 2023. Digitized mining steps and faults associated with the shaft pillar extraction at bambanani mine, supplied by harmony gold.

Van Aswegen, G. Ortlepp. 2008. Shears - dynamic brittle shears of South African gold mines. *Proc. 1st SHIRM Symposium*, 2, pp. 111–119, 01.

Van Aswegen, G. 2003. Towards best practice for routine seismic hazard assessment in mines. *The Southern African Institute of Mining and Metallurgy*.

Van Aswegen, G. 2005. Routine seismic hazard assessment in some south african mines. In *Controlling Seismic Risk: Sixth International Symposium on Rockburst and Seismicity in Mines Proceedings*, 9-11 March 2005, Australia, p. 437. Australian Centre for Geomechanics.

Van Aswegen, G. 2020. Fault stability in sa gold mines. In *Mechanics of Jointed and Faulted Rock*, pp. 717–725. CRC Press.

Van Aswegen, G., Stander, M. 2012. Origins of some fractures around tabular stopes in deep south african mines. *Journal of the Southern African Institute of Mining and Metallurgy*, vol. 112, no. 8, pp. 729–735.

Van Aswegen, G. 2013. Forensic rock mechanics, ortlepp shears and other mining induced structures. In *8th International Symposium Rockburst and Seismicity in Mines*, Saint-Petersburg, Moscow, pages 47–51.

Van Aswegen, G. 2021a. Forensic rock mechanics for the analysis of rockbursts and seismicity in mines, lecture series for south african rock mechanics practitioners, lecture 1, sections 6 and 7, nature of deformation controlled by rock characteristics and shear zones. https://www.sanire.co.za/images/fbfiles/GvA-webinar-20210707-f-lo-res-2.pdf

Van Aswegen. G. 2021b. Forensic rock mechanics for the analysis of rockbursts and seismicity in mines, lecture series for south african rock mechanics practitioners, lecture 2, section 4, rockburst nomenclature. https://www.sanire.co.za/images/fbfiles/GvA-20210721-A-fin-02082021.pdf

Sponsored Content

THE UNIVERSITY OF PRETORIA

Training architects of total mine solutions

Today's mining engineers are not merely on-site problem solvers, nor are they confined to the parameters of their discipline. Increasingly, qualified mining engineers are becoming the consulting engineers of the future. These are professionals who can design, plan and manage the entire lifespan of a mine or mining project, from exploration to rehabilitation, and everything in between. The new generation of mining engineers are architects of total mine solutions.

WHY DO MINING ENGINEERS MAKE EXCEPTIONAL CONSULTING ENGINEERS?

Mining engineers understand the complete mining life cycle. They can move effortlessly between technical details and big-picture strategy. From assessing mineral deposits and planning mine layouts, to coordinating machinery, safety protocols, environmental compliance and investment potential, they see and influence the entire process. This foundational knowledge, and the accompanying skills, expands beyond the confines of a mine itself. Clients in various industries increasingly need a turnkey solution to engineering problems. With expertise that spans technical, economic, legal and environmental considerations, mining engineers often become indispensable assets to multidisciplinary teams. For young professionals, a degree in mining engineering opens doors far beyond the mine site.

INNOVATION IS REDEFINING THE INDUSTRY

Modern mining is high-tech, with cutting-edge innovations that improve the safety, efficiency and environmental stewardship of industry players. Technologies for remote mining operations, virtual and extended reality (VR and XR), automation, artificial intelligence (AI) and sustainable practices are on the brink of changing the world as we know it, every day. However, these technologies require engineers who can think creatively, adapt quickly and combine technical expertise with visionary problem solving. This is exactly what mining engineers are trained to do.

The University of Pretoria's Department of Mining Engineering develops graduates who enjoy problem solving and critical thinking, who have an excellent grasp on the foundational knowledge of engineering, and who understand hands-on work as much as strategic planning.

SHORT COURSES THROUGH ENTERPRISES TRAINING SOLUTIONS

In collaboration with the University of Pretoria's Enterprises Training Solutions, a branch of Enterprises University of Pretoria, the lecturers and contract lecturers of the Department of Mining Engineering present a range of short courses for industry.

E | ENTERPRISES University of Pretoria

www.enterprises.up.ac.za
www.up.ac.za/mining-engineering

UNIVERSITEIT VAN PRETORIA
UNIVERSITY OF PRETORIA
YUNIBESITHI YA PRETORIA

Faculty of Engineering, Built Environment and Information Technology
Fakulteit Ingenieurswese, Bou-omgewing en Inligtingtegnologie / Lefapha la Boetšenere, Tikologo ya Kago le Theknolotši ya Tshedimošo

Make today matter
www.up.ac.za

NATIONAL & INTERNATIONAL ACTIVITIES

2026

3-4 March 2026 — Tailings 2026—Where to Now?
Indaba Hotel, Spa and Conference Centre, Fourways
Contact: Gugu Charlie
Tel: 011 538-0238
E-mail: gugu@saimm.co.za
Website: http://www.saimm.co.za

13-14 April 2026 — SANCOT Symposium 2026
Unlocking Africa's Potential: Advances in Tunnelling in Civil Engineering and Mining
Southern Sun Rosebank
Contact: Gugu Charlie
Tel: 011 538-0238
E-mail: gugu@saimm.co.za
Website: http://www.saimm.co.za

12 May 2026 — Re-Imagining Diversity and Inclusion Showcase 2026
Southern Sun Rosebank
Contact: Gugu Charlie
Tel: 011 538-0238
E-mail: gugu@saimm.co.za
Website: http://www.saimm.co.za

26-28 May 2026 — SAIMM Pyrometallurgy International Conference 2026
Foundation of Competitiveness and Sustainability
CSIR International Convention Centre, South Africa
Contact: Gugu Charlie
Tel: 011 538-0238
E-mail: gugu@saimm.co.za
Website: http://www.saimm.co.za

24-25 June 2026 — Global Best Practices in Thickener and Dewatering Operations for Low-Grade and Complex Deposits Conference 2026
Mintek, Randburg, Johannesburg
Contact: Gugu Charlie
Tel: 011 538-0238
E-mail: gugu@saimm.co.za
Website: http://www.saimm.co.za

18-20 August 2026 — CAVING 2026
Ulaanbaatar, Mongolia
Website: https://www.acgcaving.com/

18-21 August 2026 — SAIMM Uranium Conference 2026
Swakopmund Hotel and Entertainment Centre, Swakopmund, Namibia
Contact: Gugu Charlie
Tel: 011 538-0238
E-mail: gugu@saimm.co.za
Website: http://www.saimm.co.za

22-25 September 2026 — XIX International Society for Mine Surveying Congress 2026
Century City, Cape Town
Contact: Gugu Charlie
Tel: 011 538-0238
E-mail: gugu@saimm.co.za
Website: http://www.saimm.co.za

29-30 September 2026 — 7TH Young Professionals Conference 2026
Mintek, Randburg, Johannesburg
Contact: Gugu Charlie
Tel: 011 538-0238
E-mail: gugu@saimm.co.za
Website: http://www.saimm.co.za

18-22 October 2026 — XXXII International Mineral Processing Congress 2026
Cape Town, South Africa
Contact: Camielah Jardine
Tel: 011 538-0237
E-mail: camielah@saimm.co.za
Website: http://www.saimm.co.za

4-6 November 2026 — Southern African Mine Water Conference 2026
Let's Connect
Mintek, Randburg, Johannesburg
Contact: Gugu Charlie
Tel: 011 538-0238
E-mail: gugu@saimm.co.za
Website: http://www.saimm.co.za

Company affiliates

The following organizations have been admitted to the Institute as Company Affiliates

acQuire Technology Solutions
AECI Mining Chemicals, a division of AECI Mining Ltd
African Pegmatite
Allied Furnace Consultants
AMIRA International Africa (Pty) Ltd
Anglo American Platinum Corporation
Anglogold Ashanti Ltd
Anton Paar Southern Africa
Arcus Gibb (Pty) Ltd
Becker Mining (Pty) Ltd
Bluhm Burton Engineering Pty Ltd
BSI Group South Africa
Buraaq mining Services (Pty) Ltd
Caledonia Mining South Africa
Carbocraft (Pty) Ltd
Castle Lead Works
CIGroup ACE Pty Ltd
DDP Specialty Products South Africa (Pty) Ltd
Digby Wells and Associates
E2 Test
EHL Consulting Engineers (Pty) Ltd
EKATO South Africa
Elbroc Mining Products (Pty) Ltd
Elderberry Trading
Epiroc South Africa (Pty) Ltd
Ex Mente Technologies (Pty) Ltd
Exxaro Resources Limited
FLSmidth Minerals (Pty) Ltd
GHH Mining Machines (Pty) Ltd
Geobrugg Southern Africa (Pty) Ltd
Glencore
Gravitas Minerals (Pty) Ltd
Hatch (Pty) Ltd
Herrenknecht AG
Impala Platinum Holdings Limited
IMS Engineering (Pty) Ltd
Ingwenya Mineral Processing
Ivanhoe Mines SA
M84 Geotech Pty Ltd
Malvern Panalytical (Pty) Ltd
Maptek (Pty) Ltd
Mech-Industries (Pty) Ltd
Micromine Africa (Pty) Ltd
Minearc South Africa (Pty) Ltd
Minerals Council of South Africa
MineRP Holding (Pty) Ltd
Mining Projection Concepts (Pty) Ltd
Mintek
MLB Investments CC
Modular Mining Systems Africa (Pty) Ltd
Murray & Roberts Cementation (Pty) Ltd
Optron (Pty) Ltd
Paterson & Cooke Consulting Engineers (Pty) Ltd
Pump and Abrasion Technologies (Pty) Ltd
Redpath Mining (South Africa) (Pty) Ltd
Rosond (Pty) Ltd
Roytec Global (Pty) Ltd
Rustenburg Platinum Mines Limited - Union
Salene Mining (Pty) Ltd
Schauenburg (Pty) Ltd
Sebotka (Pty) Ltd
SENET (Pty) Ltd
Sibanye Gold Limited
Solenis
Sound Mining Solution (Pty) Ltd
SRK Consulting SA (Pty) Ltd
Sulzer Pumps (South Africa) (Pty) Ltd
Tomra (Pty) Ltd
Trans-Caledon Tunnel Authority
Ukwazi Mining Solutions (Pty) Ltd
VBKOM Consulting Engineers
Weir Minerals Africa
Zutari (Pty) Ltd

Our Services

Technical Consulting

- Open Pit Slope Design
- Open Pit to Underground transition
- Underground Mine Design
- Excavation Support Design Analysis
- Pillar Optimisation

Site Ivestigation

- Forensic FOG Investigation
- Raisebore Shaft Stability Analysis
- Sinkhole/Subsidence Investigation

Professional Consulting

- Advanced Inelastic Numerical Modelling
- Governance Auditing
- Rock Engineering Studies (BFS / FS / PFS)
- System Implementation (TARP, etc.)

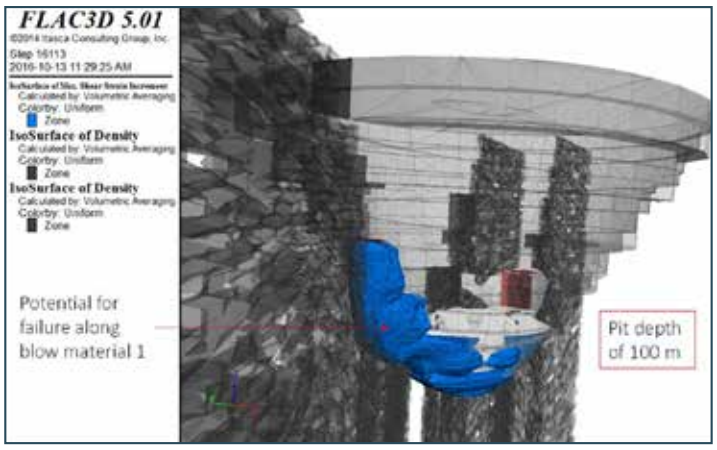

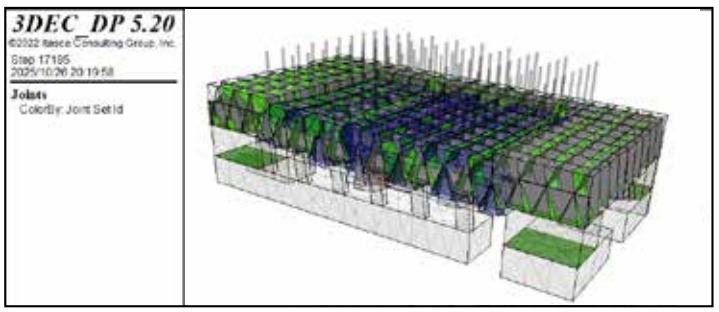

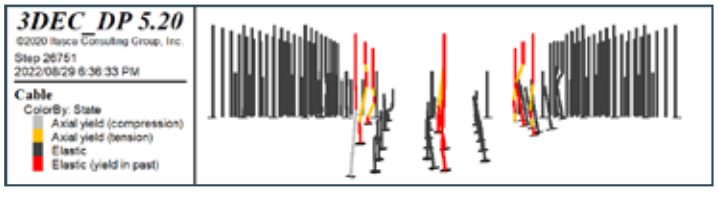

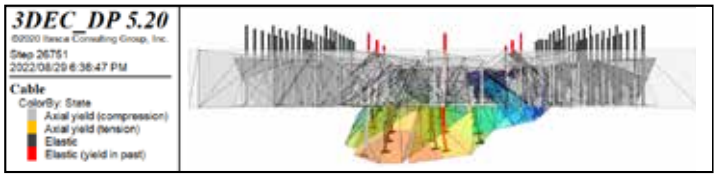

www.mlbconsulting.co.za | +27 84 826 1528
admin@mlbconsulting.co.za

MLB CONSULTING

ECSA and SACNASP Validated CPD Activity Credits = 0.1 per hour attended

South African National Committee on Tunnelling

SANCOT SYMPOSIUM 2026

13-14 APRIL 2026
SOUTHERN SUN ROSEBANK, JOHANNESBURG

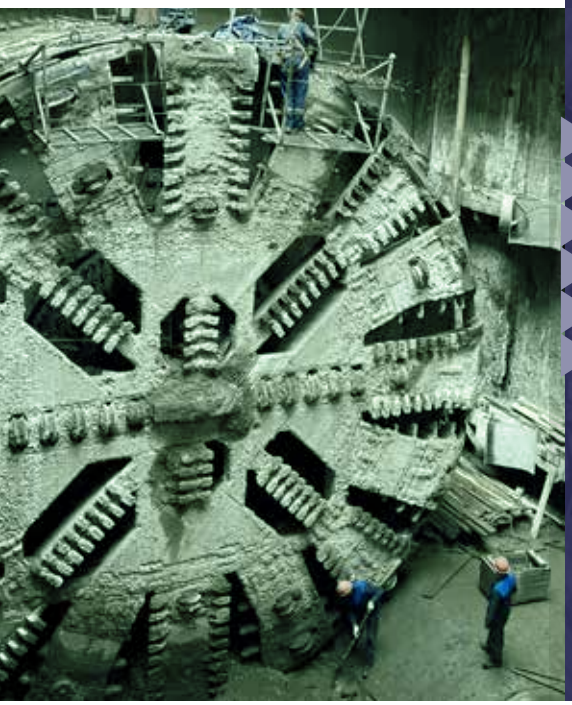

Unlocking Africa's Potential: Advances in Tunnelling in Civil Engineering and Mining

BACKGROUND

With the continued pace of urbanisation, economic and population growth, the availability of space for necessary infrastructure in the urban environment is a major challenge.
This, in conjunction with climate change and a focus on reducing impact on the environment, are the key factors driving the necessity and relevance of tunnelling.
Tunnels are increasingly seen as a means to providing sustainable, safe and reliable transport, electricity, gas, water, sewage facilities and extraction of raw materials.
Whilst the public and private sectors come to terms with the high capital expenditure required for tunnel construction, we live in an age of continued technological development and the application of these technologies presents an opportunity to better and more cost-effectively design, construct, and monitor tunnels. Furthermore, it is imperative that tunnelling consultants and contractors keep up to date with rapidly changing tunnelling technologies in order to remain viable in a competitive industry.

THEME

This conference concentrates on advances in the tunnelling industry, current best practice and how technology has improved tunnelling design, construction, supervision and monitoring.

FOR FURTHER INFORMATION CONTACT:

Gugu Charlie
Conferences and Events Coordinator
E-mail: gugu@saimm.co.za

Tel: +27 11 538-0238
Web: www.saimm.co.za

SAIMM
THE SOUTHERN AFRICAN INSTITUTE OF MINING AND METALLURGY